Hull girder failure of a container ship and of a bulk carrier under combined global and local loads

Patrick Stykuc

Master Thesis

presented in partial fulfillment
of the requirements for the double degree:
“Advanced Master in Naval Architecture” conferred by University of Liege
"Master of Sciences in Applied Mechanics, specialization in Hydrodynamics, Energetics and Propulsion” conferred by Ecole Centrale de Nantes

developed at University of Rostock
in the framework of the

“EMSHIP”

Supervisor: Prof. Patrick Kaeding, University of Rostock

Reviewer: Prof. Philippe Rigo, University of Liege

Rostock, February 2013

ABSTRACT

Hull girder failure of a container ship and of a bulk carrier under combined global and local loads

By **Patrick Stykuc**

Nowadays, the ships strength can be very well estimated using developed methods and available tools. To ensure the safety of construction is reached the classification society rules should be followed. To estimate hull ultimate bending capacity by means of ultimate bending moment Smith's method is used. Although it is well working it was formulated in the seventies of the twentieth century and nowadays the bigger accuracy would be desired. This work is an analysis of ultimate bending moment using advanced modeling tools. The models of a bulk carrier and of a container vessel will be built in Ansys Workbench program. Two midship part of two hulls will be modeled respecting all scantlings of constructions members. The crucial part of the hull will show fined mesh to achieve the desired level of accuracy. Ship's loading will include hogging bending moment as well as local loads from water pressure and cargo loading condition. The influence of the initial imperfections on the results also will be checked. The progressive collapse analysis will be performed using LS-Dyna solver. Obtained results will be compared with results from Germanischer Lloyd program Poseidon which uses Smith's method. The comparison could give a better insight in the safety margin used in estimating hull girder bending capacity to ensure its safety.

ACKNOWLEDGEMENTS

This thesis was developed in the frame of the European Master Course in “Integrated Advanced Ship Design” named “EMSHIP” for “European Education in Advanced Ship Design”, Ref.: 159652-1-2009-1-BE-ERA MUNDUS-EMMC.

Significant part of this work was performed in Germanischer Lloyd in Hamburg in Research and Rule development department. Necessary materials as well as access to professional software were provided by Germanischer Lloyd.
Special thanks to Dipl. Ing. Ionel Darie who as a supervisor gave a lot of help on different parts of this thesis. Thanks to all other employees in Germanischer Lloyd in Hamburg, not mentioned here, who had helped with working on this thesis.

Part of the calculations were done using resources provided by the University of Rostock.
Special thanks to the Professor Patrick Kaeding as a supervisor from the side of University of Rostock.

TABLE OF CONTENTS

Declaration of Authorship

I declare that this thesis and the work presented in it are my own and has been generated by me as the result of my own original research.

Where I have consulted the published work of others, this is always clearly attributed.

Where I have quoted from the work of others, the source is always given. With the exception of such quotations, this thesis is entirely my own work.

I have acknowledged all main sources of help.

Where the thesis is based on work done by myself jointly with others, I have made clear exactly what was done by others and what I have contributed myself.

This thesis contains no material that has been submitted previously, in whole or in part, for the award of any other academic degree or diploma.

I cede copyright of the thesis in favour of the University of Rostock

Date: Signature

TABLE OF SYMBOLS

Symbol	Definition equation	Unit	Name
a	-	m	Smaller breadth of plate panel
a	-	m	Spacing of stiffeners
$\vec{a}$	$\frac{\overrightarrow{dV}}{ds}$	$\frac{m}{s^2}$	Acceleration
α	-	-	Column slenderness
A	-	m^2	Section area
A_f	$b_f \cdot t_f$	m^2	Flange area
A_w	$h_w \cdot t_w$	m^2	Web area
b	-	m	Larger breadth of plate panel
b_e	-	m	Effective width of plating
b_f	-	mm	Flange breadth
β	-	-	Plate slenderness
B	-	m	Breadth (moulded) of the vessel
B_{max}	-	m	Breadth maximum
c	-	-	Coefficient
c_B, δ	-	-	Block coefficient
d	-	m	Diameter
D	$\gamma \cdot V$	t	Displacement
E	-	MPa	Young's modulus,
ε	-	-	Elongation
F	-	N	Force
g	-	$\frac{m}{s^2}$	Gravity acceleration
h_{db}	-	m	Height of double bottom
h_w	-	mm	Web height
H	-	m	Depth
H_{md}	-	m	Depth to main deck
k	$\frac{R_{eH}}{235}$	-	Material factor for steel
K	-	-	Buckling factor
l	-	m	Unsupported length of stiffener
l_K	-	m	Effective supporting length

I_x, I_y	-	cm^4	Moments of inertia of the longitudinal or transverse stiffener including effective width of plating
L	-	m	Calculated length of the ship
LCB	-	m	Longitudinal center of buoyancy
LCG	-	m	The longitudinal center of gravity
$L_{o.a.}$, L_c	-	m	Total length of the vessel
L_{pp}	-	m	The length between perpendiculars of the ship
L_{wl}	-	m	Waterline length
λ	-	-	Reference degree of slenderness
m	-	t	Weight
M	-	Nm	Bending moment
M	-	t	Ship's weight
M_S	-	t	Light ship
M_X	-	$t \cdot m$	Static moment of weight to the plane oyz
M_Z	-	$t \cdot m$	Static moment of weight to the plane oxy
N	-	N	Axial force
N_e	-	kW	Effective main engine power
p	-	kN/m^2	Applicable design load
P	-	N	Force
P_N	-	t	Deadweight
R	-	m	Radius
R	-	m	Radius of gyration
R	-	Mm	Range
R_{eH}	-	MPa	Yield strength
R_m	-	MPa	Tensile strength
R_p	-	MPa	Proof stress
S	-	-	Safety factor
S	-	m^3	Static moment
σ	-	MPa	Stress
σe	-	MPa	Reference stress
σp	-	MPa	Permissible stress
σx	-	MPa	Membrane stress in x-direction
σy	-	Mpa	Membrane stress in y-direction

t	-	mm	Plate thickness
t	-	s	Time
t'	-	mm	Required rule thickness excluding t_K
t_f	-	mm	Flange thickness
t_A	-	mm	Plate thickness as built
t_K	-	mm	Corrosion addition
t_w	-	mm	Web thickness
T	-	N	Shear force
T	-	m	Draft
T_s	-	m	Draft (scantlings)
TCB	-	m	Transverse position of the center of buoyancy
T_F	-	m	Fore draft
T_A	-	m	Aft draft
τ	-	MPa	Shear stress in the x-y plane
U	-	m	Perimeter
v	$\frac{ds}{dt}$	knots	Ship's speed
ν	-	-	Poison coefficient
V	-	m^3	Underwater hull volume
VCB	-	m	Vertical position of the center of buoyancy
VCG	-	m	Vertical coordinate of center of gravity
w_o	-	mm	Assumed imperfection
W	-	m^3	Rule deck or bottom section modulus
W	-	m^3	Section modulus of the stiffener
W(a)	-	m^3	Actual deck or bottom section modulus
x, y, z	-	-	Hull axis system
x_G	-	m	Longitudinal coordinate of center of gravity
y_G	-	m	Horizontal coordinate of center of gravity
z_G	-	m	Height of center of gravity
ρ	-	$\frac{t}{m^3}$	Sea water density

1. INTRODUCTION

Subject of this master thesis was given by the classification society Germanischer Lloyd in Hamburg. All the calculations and modeling were performed during the internship in Germanischer Lloyd. The topic of the thesis covers the area of the ultimate strength of the hull girder. The full subject of the thesis is

“Hull girder failure of a container ship and of a bulk carrier under combined global and local loads”

The task of the thesis is to build a model of the ship and using chosen techniques analyze the problem of ultimate strength. Results from the FE analysis will be compared with results obtained using classical approach. The scope of the work includes the pure vertical bending moment acting on the ship in hogging condition as well as the case with local loads included into calculations. The main aim is to compare the obtained results with ones from the class society software Poseidon and to analyze the influence of the additional loads. In addition the imperfections of the structure will be modeled and their influence on the results will be checked.

The example of analysis of bulk carrier. The global vertical bending moment in hogging condition is present. The influence of the alternate loading in the cargo holds and the water pressure is also included.

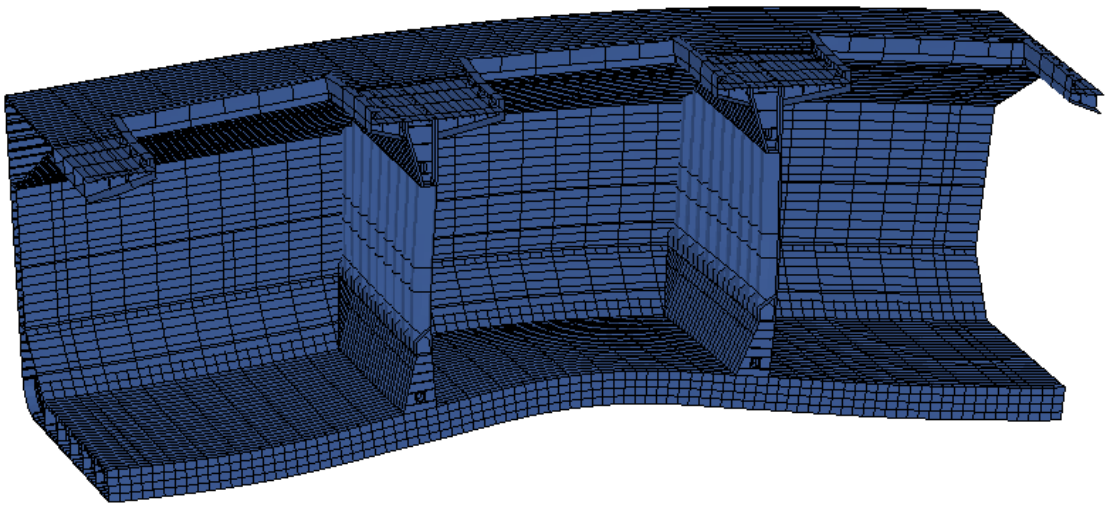

Figure 1 Bulk carrier model under influence of global and local loads

The example of the model of the container ship done by Germanischer Lloyd. Hull bending moment in hogging condition is acting and local loads from containers as well as water pressure are applied.

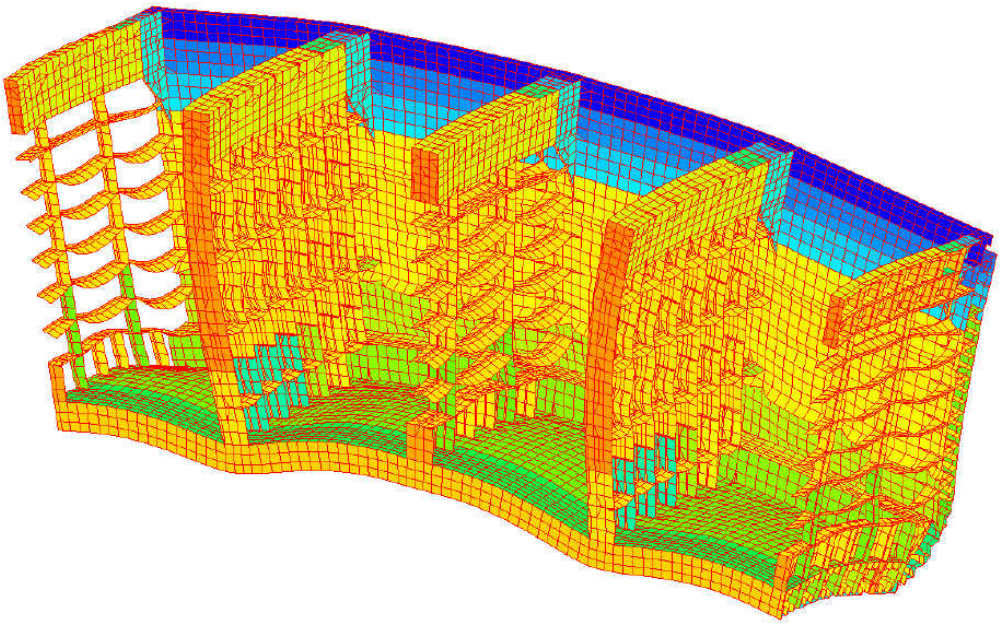

Figure 2 Container ship model under influence of global and local loads

1.1 Analyzed ships

The calculations were performed for the ships characterized by the big size, yet characteristic for their class. The main parameters of the chosen ships are given.

1.1.1 Capesize bulk carrier

Capesize ships are cargo ships originally too large to transit the Suez Canal (i.e., larger than both Panamax and Suezmax vessels). To travel between oceans, such vessels used to have to pass either the Cape of Good Hope or Cape Horn. In effect Capesize reads as "unlimited". When the Suez was deepened, the definition of Suezmax changed. Some ships previously unable to transit the canal and deemed Capesize, changed categories.

Capesize vessels are typically above 150,000 long tons deadweight (DWT), and ships in this class include bulk carriers transporting coal, ore, and other commodity raw materials. The term "Capesize" is most commonly used to describe bulk carriers rather than tankers. A standard Capesize bulker is around 175,000 DWT, although larger ships (normally dedicated to ore transportation) have been built, up to 400,000 DWT. The large dimensions and deep drafts of such vessels mean that only the largest deep water terminals can accommodate them.

Capesize ships are commonly used in transportation of coal, iron ore and commodity raw materials. Because of this fact, they are often termed as bulk carriers rather than tankers. In the subcategory of capesize vessels include the very large ore carriers (VLOC) and very large bulk carriers (VLBC) of above 200,000 DWT. These vessels are mainly designed to carry iron ore. According to estimates, 93% cargo of capesize bulkers comprises iron ore and coal. While a standard capesize vessel is around 175,000 DWT, bulkers up to 400,000 DWT or even more have been built in recent times to meet the growing demand for bulk ore transportation carriers.

The main parameters of the analyzed ship are shown below:

Table 1 Bulk carrier main parameters

Length between perpendiculars	Lpp	282,80	[m]
Length at the waterline at T	Lwl	287,46	[m]
Breadth	B	46,50	[m]
Depth	H	24,20	[m]
Draugth	T	17,0	[m]
Deadweight	P_N	177400	[t]
Number of cargo holds		9	[-]

Ship has double bottom and double sides. Hull is built from high tensile steel 355 MPa.
Example of the Capesize bulk carrier model in Poseidon is shown in the Fig. 3.

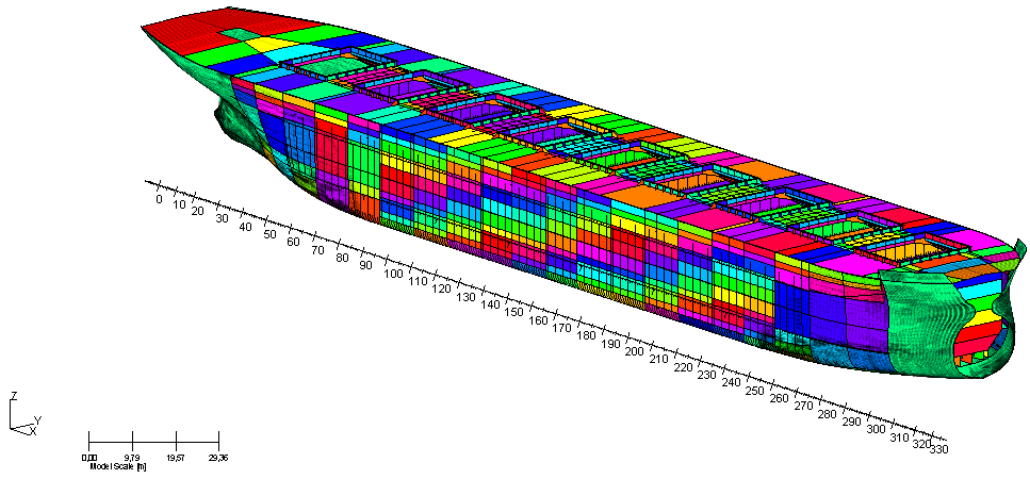

Figure 3 Bulk Carrier model in Poseidon software

1.1.2 New Panamax Container ship

New Panamax (NPX) refers to ships designed to fit exactly in the locks of the expanded Panama Canal, expected to open in 2014, and which confers capacity of about 14,000 TEU. Like its Panamax counterparts, New Panamax ships will compose a specific ship class able to effectively service the Americas and the Caribbean, either from Europe or from Asia.

Ships of such class are characterized by length up to 366 meters, breadth up to 49 meters, draft up to 15,2 meters and containers capacity between 10000 and 14500 TEU.

Increase of the container capacity was also possible by new design arrangement of the superstructure which now was localized amidships. It allows to increase the high of the container's stocks without decreasing the visibility from the navigation room.

Analyzed ship has the following main parameters.

Table 2 Container ship main parameters

Length between perpendiculars	Lpp	349,50	[m]
Length at the waterline at T	Lwl	356,40	[m]
Breadth	B	51,20	[m]
Depth	H	29,90	[m]
Draugth	T	16,00	[m]
Deadweight (nr of containers)	P_N	14000	[TEU]

Example of New Panamax Container ship from Poseidon is shown below.

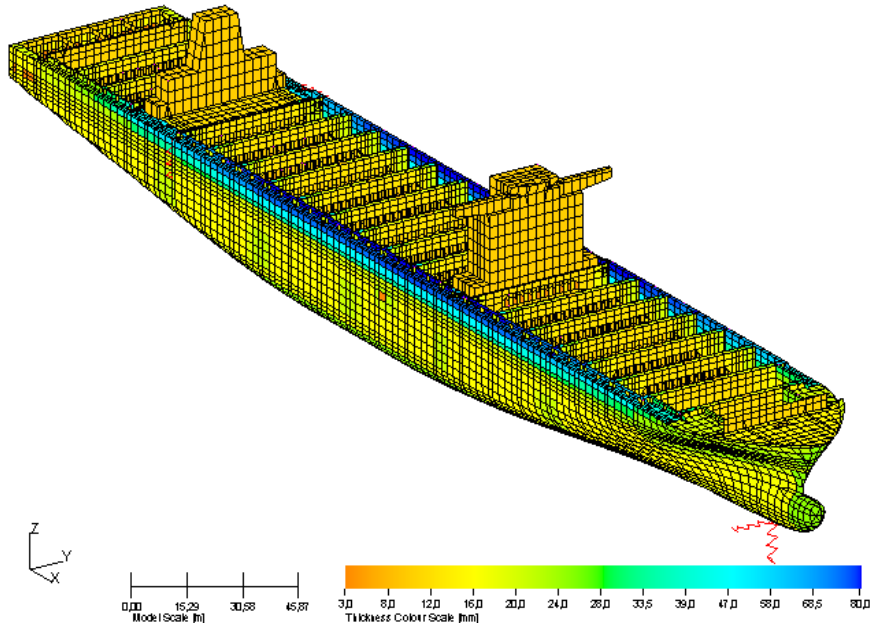

Figure 4 Container ship model in Poseidon software

Hull construction has double bottom and double sides and is characterized by very thick plates on the main deck. Most structural elements are from high tensile steel 315 MPa. Main deck plates are from steel 390 MPa.

1.2 Work plan

The master thesis is governed by the work plan divided into several steps.

For the bulk carrier:

1. Generation of the bulk carrier model in Ansys, Design Modeler
2. Generation of the mesh in Ansys, Mechanical
3. Calculation of the ultimate strength for pure vertical bending moment
4. Checking the mesh convergence for the three different mesh densities
5. Modeling imperfections on the bulk carrier model in LS-Dyna Prepost
6. Calculation of the ultimate strength for pure vertical bending moment with influence of imperfections
7. Calculation of the ultimate strength for the pure vertical bending moment in Poseidon using GL rules
8. Calculation of the ultimate strength for the set of loading conditions with varying wave height

For the container ship:

1. Generation of the container ship model in Ansys, Design Modeler
2. Generation of the mesh in Ansys, Mechanical
3. Calculation of the ultimate strength for pure vertical bending moment
4. Checking the mesh convergence for the three different mesh densities
5. Modeling imperfections on the bulk carrier model in LS-Dyna Prepost
6. Calculation of the ultimate strength for pure vertical bending moment with influence of imperfections
7. Calculation of the ultimate strength for the pure vertical bending moment in Poseidon using GL rules
8. Evaluation of FE results and comparison with ultimate hull girder strength assessment implemented in GL rules

2. METHODS FOR ULTIMATE STRENGTH ASSESMENT

The ultimate strength introduction as well as the general description of progressive collapse methodology are written based on “Ship structural design” – Owen F.Hughes and on “Ultimate Limit State Design of Steel Plated Structures” – J.K.Paik, A.K.Thayamballi respectively.

A ship hull in the intact condition will sustain applied loads smaller than the design loads, and in normal sea and loading conditions it will not suffer any structural damages such as buckling and collapse except for possible localized yielding. However, the loads acting on the hull are uncertain due to rough seas or unusual loading/unloading of cargo. In these cases applied loads may exceed design loads and the hull may collapse globally. Furthermore, since aging ships may have suffered structural damage due to corrosion and fatigue and their structural resistance may have weakened, the hull may collapse under applied loads even smaller than design loads.

As applied loads increase, structural members of the hull will buckle in compression and yield in tension. The hull can normally carry further loading beyond the onset of member buckling or yielding, but the structural effectiveness of failed members decreases or can even become negative and their internal stress will be redistributed to adjacent intact members. The most highly compressed member will collapse first and the stiffness of the overall hull decreases gradually. Buckling and collapse of structural members will occur progressively until the ultimate limit state is reached. When the structural safety of a ship’s hull is considered, the ultimate overall hull strength should be evaluated. It is also necessary to derive a simple expression for calculation of the hull ultimate strength so that it can be used as a design equation or failure function in reliability analysis.

Classification societies have provided their own design criteria for structural scantlings, which are usually based on first yielding and elastic buckling with a simple correction for plasticity. These expressions are often far from true ultimate state limit. It should be noted that the calculated value of the ultimate strength will not be a deterministic but a probabilistic value and it will depend on uncertainties associated with material properties and calculation assumptions. However, these uncertainties are much less than those associated with the traditional linear elastic calculations. To get an acceptable margin of safety against overall hull collapse, the hull ultimate strength provides a more reasonable criterion than the conventional elastic buckling or first yield criteria.

2.1 Progressive collapse method general methodology

A progressive collapse analysis is to be used to calculate the ultimate vertical bending moments of a ship's transverse section. The procedure is to be based on a simplified incremental-iterative approach where the capacities are defined as the peaks of the resulting moment-curvature curve (M-χ) in hogging (positive) and sagging (negative) conditions, i.e. χ is the hull girder curvature [1/m].

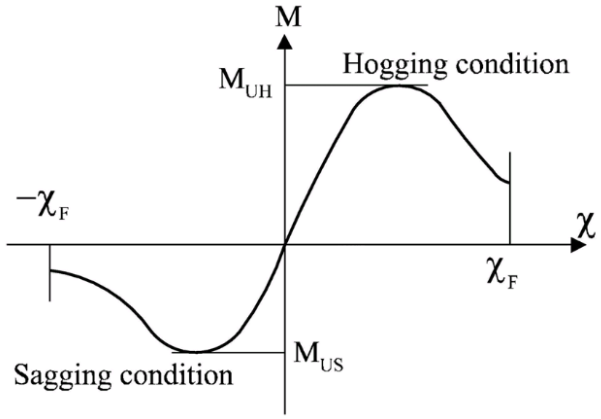

Figure 5 Example of moment-curvature curve

Each step of the incremental procedure is represented by the calculation of the bending moment Mi which acts on the hull transverse section as the effect of an imposed curvature χ i. For each step, the value χ i is to be obtained by summing an increment of curvature Δχ to the value relevant to the previous step χ i-1.This increment of curvature corresponds to an increment of the rotation angle of the hull girder transverse section around its horizontal neutral axis. This rotation increment induces axial strains ε in each hull structural element, whose value depends on the position of the element. In hogging condition, the structural elements above the neutral axis are lengthened, while the elements below the neutral axis are shortened. Vice-versa in sagging condition. The stress σ induced in each structural element by the strain ε is to be obtained from the load-end shortening curve σ-ε of the element, which takes into account the behaviour of the element in the non-linear elasto-plastic domain.

The distribution of the stresses induced in all the elements composing the hull transverse section determines, for each step, a variation of the neutral axis position, since the relationship σ-ε is non-linear. The new position of the neutral axis relevant to the step considered is to be obtained by means of an iterative process, imposing the equilibrium among the stresses acting in all the hull elements.

Once the position of the neutral axis is known and the relevant stress distribution in the section structural elements is obtained, the bending moment of the section Mi around the new position of the neutral axis, which corresponds to the curvature χi imposed in the step considered, is to be obtained by summing the contribution given by each element stress.

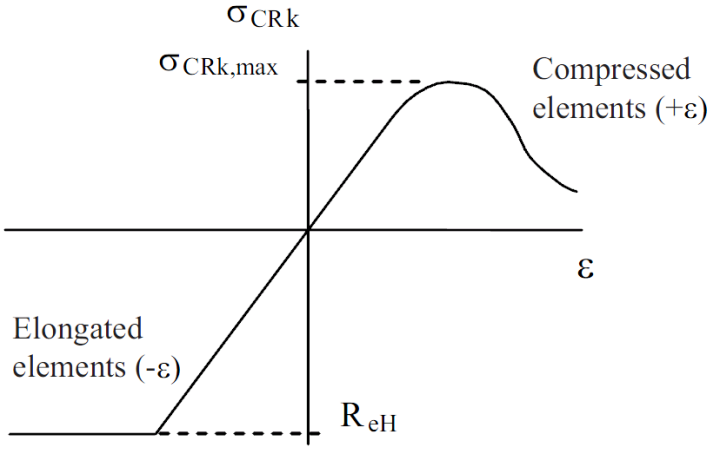

Figure 6 Typical average stress - average strain curve

Checking criteria

It is to be checked that the hull girder ultimate bending capacity at any hull transverse section is in compliance with the following formula:

$$M \leq \frac{MU}{\gamma R} \qquad \textbf{(2-1)}$$

where:

MU : Ultimate bending moment capacity of the hull transverse section considered, calculated with net offered scantlings based on gross offered thickness reduced by 0,5 t_C, in kN.m:

MU = MUH in hogging conditions

MU = MUS in sagging conditions

t_C – corrosion addition

2.2 Ultimate strength in the rules - Smith's method

The ultimate strength calculation procedure applied in the Poseidon software is described in the Rules of Germanischer Lloyd 2012 Sea going ships - Hull Structures. The description and methodology of this approach is presented below.

2.2.1 In extreme conditions, larger loads than referred to in may occur. Therefore, dimensioning of longitudinal structures is to be verified by proving the ultimate capacity according to 2.2.2 and 2.2.3. The calculations are to include those structural elements contributing to the hull girder longitudinal strength and are to be based on gross scantlings.
The following safety factors are to be assumed:

$\gamma_R = 1{,}20$

$\gamma_{WV} = 1{,}20$

2.2.2 Ultimate vertical bending moment

$$\left| M_{SW} + \frac{\gamma_{WV} \cdot M_{WV}}{c_s} \right| \leq \left| \frac{M_U}{\gamma_R} \right| \quad \textbf{(2-2)}$$

$$\left| M_{SWf} + \frac{0{,}8 \cdot \gamma_{WV} \cdot M_{WV}}{c_s} \right| \leq \left| \frac{M_{Uf}}{\gamma_R} \right| \quad \textbf{(2-3)}$$

M_{SWf} = maximum vertical still water bending moment in flooded conditions [kNm]. For a transverse section under consideration, the most severe levels of vertical still water bending moments are to be selected from those cases of flooding used in the damage stability calculations.

c_s = stress factor

M_U = ultimate vertical bending moments of the ship's transverse section in the hogging ($M_{U,H}$) and sagging ($M_{U,S}$) conditions [kNm]. See 2.2.2.1.

M_{Uf} = ultimate vertical bending moments of the ship's damaged transverse section in the hogging ($M_{Uf,H}$) and sagging ($M_{Uf,S}$) conditions [kNm]. If no assumptions regarding the extent of damage are prescribed, $M_{Uf} = \kappa_{dM} \cdot M_U$, where κ_{dM} is a reduction factor for the ultimate moments in damaged conditions (κ_{dM} δ 1). The reduction factor κ_{dM} equals 1 unless a smaller value is specified by the owner or shipyard.

2.2.2.1 Progressive collapse analysis

A progressive collapse analysis is to be used to calculate the ultimate vertical bending moments of a ship's transverse section. The procedure is to be based on a simplified incremental-iterative approach where the capacities are defined as the peaks of the resulting moment-curvature curve (M-χ) in hogging (positive) and sagging (negative) conditions, i.e. χ is the hull girder curvature [1/m]. See Figure 7

The main steps to be used in the incremental-iterative approach are summarised as follows:

Step 1 The ship's transverse section is to be divided into plate-stiffener combinations (see 2.2.2.2.2 (a)) and hard corners (see 2.2.2.2.2(b)).

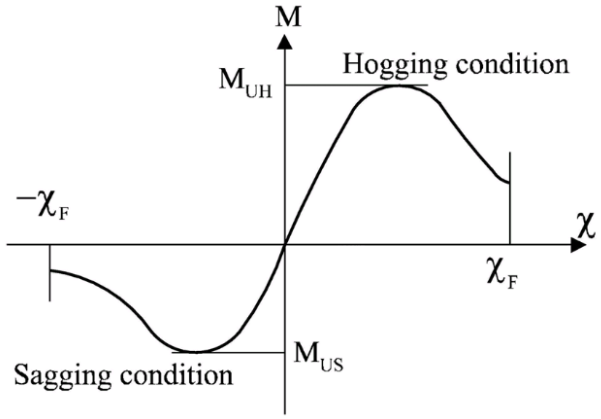

Figure 7 Moment-curvature curve

Step 2 The average stress – average strain relationships

σ_{CRk}-ε for all structural elements (i.e. stiffener plate combinations and hard corners) are to be defined, where the subscript k refers to the modes 0, 1, 2, 3 or 4, as applicable (see 2.2.2.2).

Step 3 The initial and incremental value of curvature $\Delta\chi$ is to be defined by the following formula:

$$\Delta x = \frac{0{,}05\frac{R_{eH}}{E}}{z_D - z_{NA,e}} \quad \textbf{(2-4)}$$

z_D = z co-ordinate of strength deck at side [m]

$z_{NA,e}$ = z co-ordinate of elastic neutral axis for the ship's transverse section [m]

Step 4 For the value of curvature, $\chi_j = \chi_{j-1} + \Delta\chi$, the average strain $\varepsilon_{Ei,j} = \chi_j z_i$ and corresponding average stress $\sigma_{i,j}$ is to be defined for each structural element i (see 2.2.2.2). For structural elements under tension, $\sigma_{i,j} = \sigma_{CR0}$ (see 2.2.2.2.1). For plate-stiffener combinations under compression, $\sigma_{i,j}$ = minimum $[\sigma_{CR1}, \sigma_{CR2}, \sigma_{CR3}]$ (see 2.2.2.2.2 (a)). For hard corners under compression, $\sigma_{i,j} = \sigma_{CR4}$ (see 2.2.2.2.2 (b)).

z_i = z co-ordinate of i_{th} structural element [m] relative to basis,

Step 5 For the value of curvature, $\chi_j = \chi_{j-1} + \Delta\chi$, the height of the neutral axis $z_{NA,j}$ is to be determined iteratively through force equilibrium over the ship's transverse section:

$$\sum_{i=1}^{m} A_i \sigma_{i,j} = \sum_{i=1}^{n} A_i \sigma_{i,j} \quad \textbf{(2-5)}$$

m is the number of structural elements located above $z_{NA,j}$ n is the number of structural elements located below $z_{NA,j}$

A_i = cross-sectional area of i_{th} plate-stiffener combination or hard corner

Step 6 For the value of curvature, $\chi_j = \chi_{j-1} + \Delta\chi$, the corresponding bending moment is to be calculated by summing the contributions of all structural elements within the ship's transverse section:

$$M_{U,j} = \sum \sigma_{i,j} A_i (z_{NA,j} - z_i) \quad \textbf{(2-6)}$$

Steps 4 through 6 are to be repeated for increasing increments of curvature until the peaks in the M-χ curve are well defined. The ultimate vertical bending moments $M_{U,H}$ and $M_{U,S}$ are to be taken as the peak values of the M-χ curve.

2.2.2.2 Average stress - average strain curves

A typical average stress – average strain curve σ_{CRk}-ε for a structural element within a ship's transverse section is shown in Figure 8, where the subscript k refers to the modes 0, 1, 2, 3 or 4, as applicable.

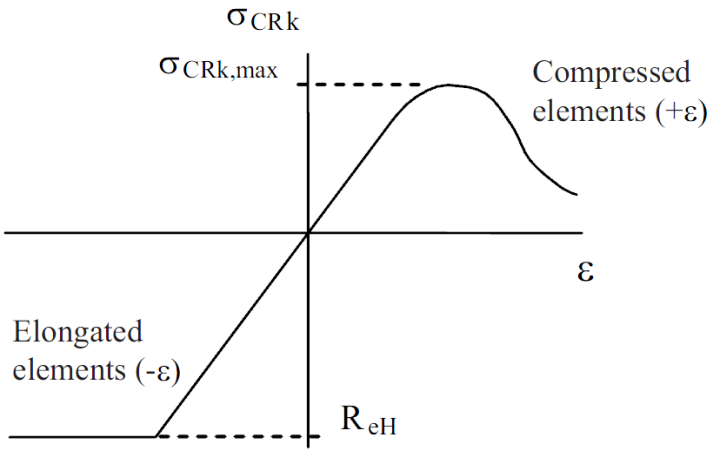

Figure 8 Typical average stress – average strain curve

2.2.2.2.1 Negative strain (σ_{CR0}-ε)

The portion of the curve corresponding to negative strain (i.e. tension) is in every case to be based on elasto-plastic behaviour (i.e. material yielding) according to the following:

$$\sigma_{CR0} = \Phi R_{eH} \left[\frac{N}{mm^2}\right] \quad \textbf{(2-7)}$$

Φ = edge function

= –1 for ε < –1

= ε for –1 ≤ ε ≤ 0

∑ = relative strain

= εE/ εY

ε E = element strain

ε Y = strain at yield stress in the element

= R eH /E

2.2.2.2.2 Positive strain

The portion of the curve corresponding to positive strain (i.e. compression) is to be based on some mode of collapse behaviour (i.e. buckling) for two types of structural elements; (a) plate-stiffener combinations and (b) hard corners. See Figure 9.

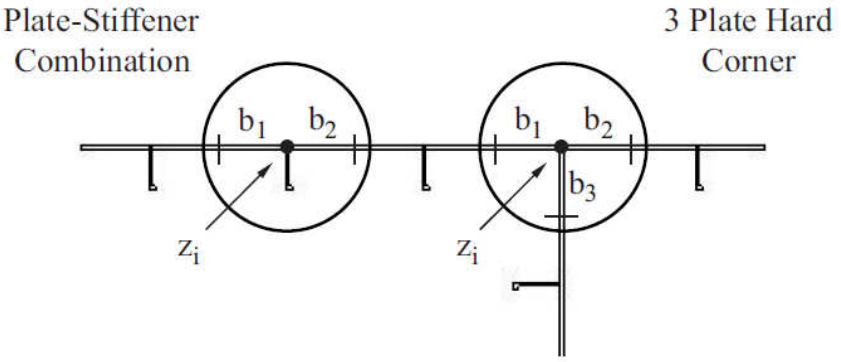

Figure 9 Structural elements

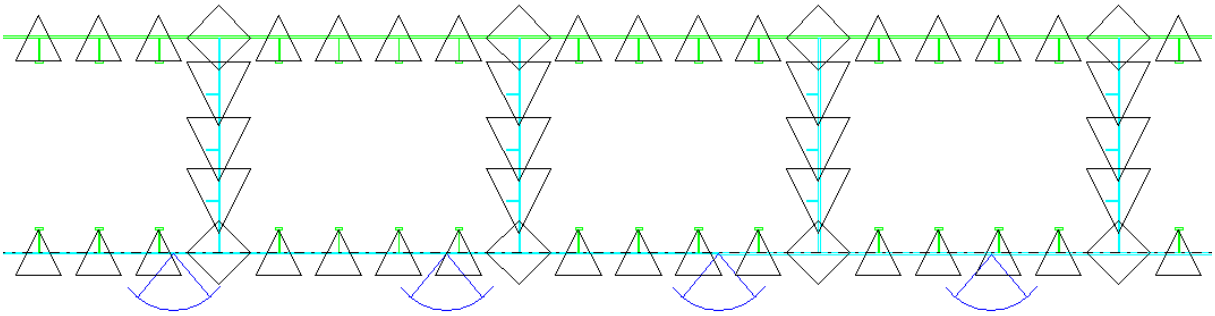

Figure 10 Plate-stiffener combinations and hard corners in Poseidon software

(a) Plate-stiffener combinations

(σ_{CR1}-ε, σ_{CR2}-ε, σ_{CR3}-ε)

Plate-stiffener combinations are comprised of a single stiffener together with the attached plating from adjacent plate fields. Under positive strain, three average stress – average strain curves are to be defined for each plate stiffener combination based on beam column buckling (σ_{CR1}-ε), torsional buckling (σ_{CR2}-ε) and web/flange local buckling (σ_{CR3}-ε).

(i) Beam column buckling σ_{CR1}-ε

The positive strain portion of the average stress – average strain curve σ_{CR1}-∑ based on beam column buckling of plate-stiffener combinations is described according to the following:

$$\sigma_{CR1} = \Phi R_{eH} \kappa_{BC} \frac{A_{Stif} + \frac{b_{m,1} t_1}{2} + \frac{b_{m,2} t_2}{2}}{A_{Stif} + \frac{b_1 t_1}{2} + \frac{b_2 t_2}{2}} \quad \textbf{(2-8)}$$

Φ = edge function

= ε for $0 \leq \sum \leq 1$

= 1 for ε > 1

κ_{BC} = reduction factor

= 1 for $\lambda_K \leq 0{,}2$

$= \frac{1}{k_D + \sqrt{k_D^2 - \lambda_K^2}}$ for $\lambda_K > 0{,}2$

$$\lambda_K = \sqrt{\frac{\varepsilon_E a^2 A_x}{\pi^2 I_x} \cdot 10^{-4}} \quad \textbf{(2-9)}$$

$k_D = (1 + 0{,}21\,(\lambda_K - 0{,}2) + \lambda_K^2) / 2$

a = length of stiffener [mm]

A_x = sectional area of stiffener with attached shell plating of breadth ($b_{m,1}/2 + b_{m,2}/2$) [mm^2]

I_x = moment of inertia of stiffener with attached shell plating of breadth ($b_{m,1}/2 + b_{m,2}/2$) [cm^4]

$b_{m,1}$, $b_{m,2}$ = effective widths of single plate fields on sides 1 and 2 of stiffener [mm], where the reference degree of slenderness is to be defined as

$$\lambda = \sqrt{\frac{\varepsilon_E}{0{,}9\left(\frac{t}{b}\right)^2 K}} \quad \textbf{(2-10)}$$

b_1, b_2 = breadths of single plate fields on sides 1 and 2 of stiffener [mm]

t_1, t_2 = thicknesses of single plate fields on sides 1 and 2 of stiffener [mm]

A_{Stif} = sectional area of the stiffener without attached plating [mm^2]

(ii) Torsional buckling σ_{CR2}-ε

The positive strain portion of the average stress – average strain curve σ_{CR2}-ε based on torsional buckling of plate-stiffener combinations is described according to the following:

$$\sigma_{CR2} = \Phi R_{eH} \frac{A_{Stif}\,\kappa_T + \frac{b_{m,1} t_1}{2} + \frac{b_{m,2} t_2}{2}}{A_{Stif} + \frac{b_1 t_1}{2} + \frac{b_2 t_2}{2}} \quad \textbf{(2-11)}$$

κ_T = reduction factor

(iii) Web/flange local buckling σ_{CR3}-ε

The positive strain portion of the average stress – average strain curve σ_{CR3}-ε based on web/flange local buckling of plate-stiffener combinations is described according to the following:

$$\sigma_{CR3} = \Phi R_{eH} \frac{h_{w,m}t_w + b_{f,m}t_f + \frac{b_{m,1}t_1}{2} + \frac{b_{m,2}t_2}{2}}{h_w t_w + b_f t_f + \frac{b_1 t_1}{2} + \frac{b_2 t_2}{2}} \quad \textbf{(2-12)}$$

$h_{w,m}$, $b_{f,m}$ = effective width of web/flange plating [mm]

h_w = web height [mm]

t_w = web thickness [mm]

b_f = flange breadth, where applicable [mm]

t_f = flange thickness, where applicable [mm]

(b) Hard corners (σ_{CR4}-ε)

Hard corners are sturdy structural elements comprised of plates not lying in the same plane. Bilge strakes (i.e. one curved plate), sheer strake-deck stringer connections (i.e. two plane plates) and bulkhead-deck connections (i.e. three plane plates) are typical hard corners. Under positive strain, single average stress – average strain curves are to be defined for hard corners based on plate buckling (σ_{CR4}-ε).

(i) Plate buckling σ_{CR4}-ε

$$\sigma_{CR4} = \Phi R_{eH} \frac{\sum_{i=1}^{n} b_{m,i}t_i}{\sum_{i=1}^{n} b_i t_i} \quad \textbf{(2-13)}$$

$b_{m,i}$ = effective widths of single plate fields [mm]

b_i = breadth of single plate fields [mm]

t_i = thickness of single plate fields [mm]

n = number of plates comprising hard corner

2.2.3 Ultimate vertical shear force

$$\left| Q_{SW} + \frac{\gamma_{WV} \cdot Q_{WV}}{c_s} \right| \leq \left| \frac{Q_U}{\gamma_R} \right| \quad \textbf{(2-14)}$$

$$\left| Q_{SWf} + \frac{0{,}8 \cdot \gamma_{WV} \cdot Q_{WV}}{c_s} \right| \leq \left| \frac{Q_{Uf}}{\gamma_R} \right| \quad \textbf{(2-15)}$$

Q_{SWf} = maximum vertical still water shear force in flooded conditions [kN]. For a transverse section under consideration, the most severe levels of vertical still water shear forces are to be selected from those cases of flooding used in the damage stability calculations.

c_s = stress factor

Q_U = ultimate vertical shear force of the ship's transverse section [kN]

$$= \frac{1}{1000\sqrt{3}} \cdot \sum_{i=1}^{q} \kappa_{\tau i} \cdot b_i t_i \cdot R_{eH,i} \quad \textbf{(2-16)}$$

q = number of shear force transmitting plate fields (in general, these are only the vertical plate fields of the ship's transverse section, e.g. shell and longitudinal bulkhead plate fields)

$\kappa_{\tau i}$ = reduction factor of the i_{th} plate field

b_i = breadth of the i_{th} plate field [mm]

t_i = thickness of the i_{th} plate field [mm]

Q_{Uf} = ultimate vertical shear force of the ship's undamaged transverse section [kN]. If no assumptions regarding the extent of damage are prescribed, $Q_{Uf} = \kappa_{dM} \cdot Q_U$, where κ_{dM} is a reduction factor for the ultimate force in damaged conditions ($\kappa_{dM} \leq 1$).

3. BULK CARRIER – FINITE ELEMENT MODEL

3.1 Methodology

In order to perform progressive collapse analysis desirable extent of the ship's hull is treated as a beam. Supported on one end and with applied moment in terms of rotation on the other end. The value of rotation is incrementally growing to the value that ensures collapse of the structure. The rotation is defined at the level of neutral axis of the cross section and all the points on this section follow the rotation movement.

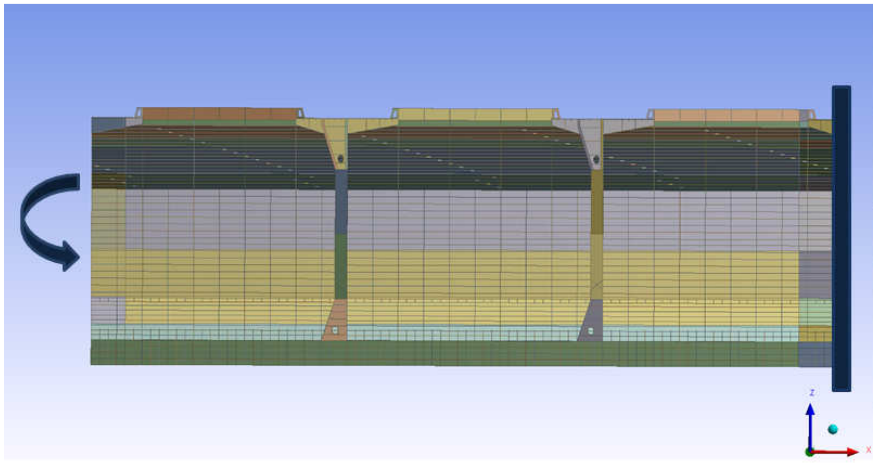

Figure 11 Beam model methodology

Area where collapse is expected should be meshed with higher level of accuracy. Outside this region the coarse mesh can be applied. It is desirable due to reduction of the total mesh size and the computation time required to analyze the problem.

To represent the material properties of the steel the model with applied hardening is used. After steel reaches the yield point the stress - strain curve changes its shape to model the realistic behaviour of material. At the fore and aft extremities the pure elastic material is used.

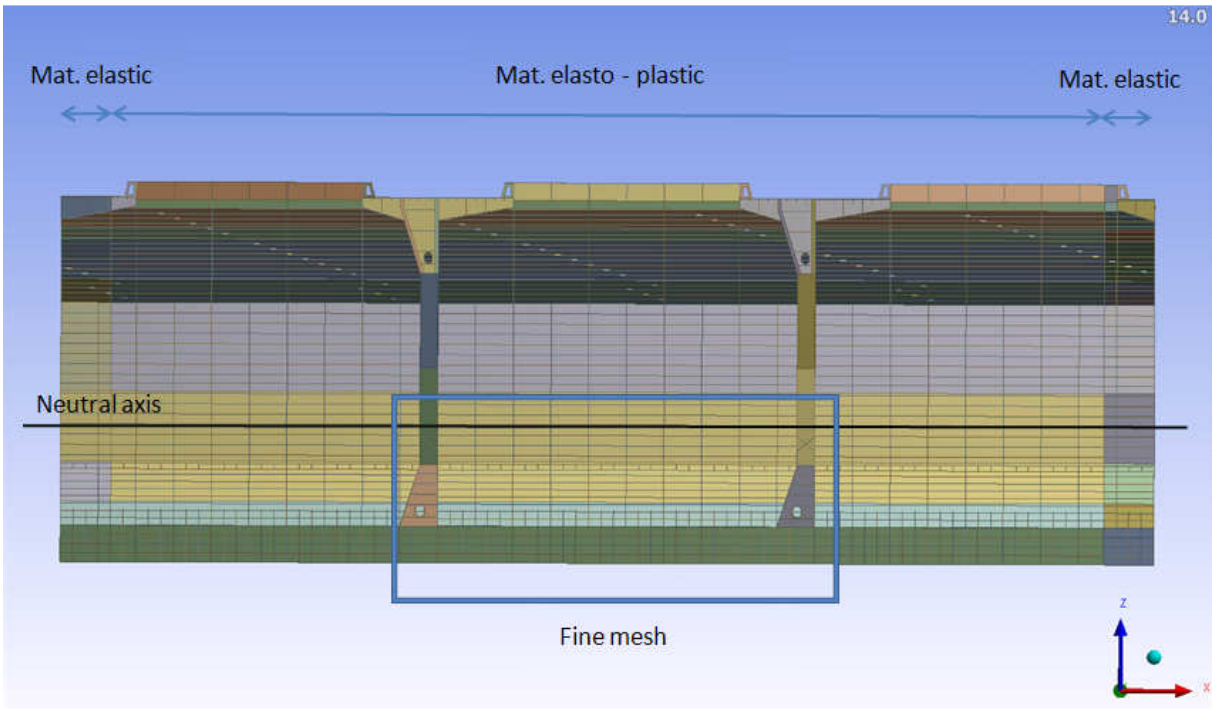

Figure 12 Material type assignment on the bulk carrier model

3.1.1 Used software

To perform modeling and analysis different programs will be used. First part of the work will be construction modeling using Ansys Workbench. It will allow to model crucial part of the ship's hull respecting scantlings of all construction members. Modeling will be performed in Static Structural module.

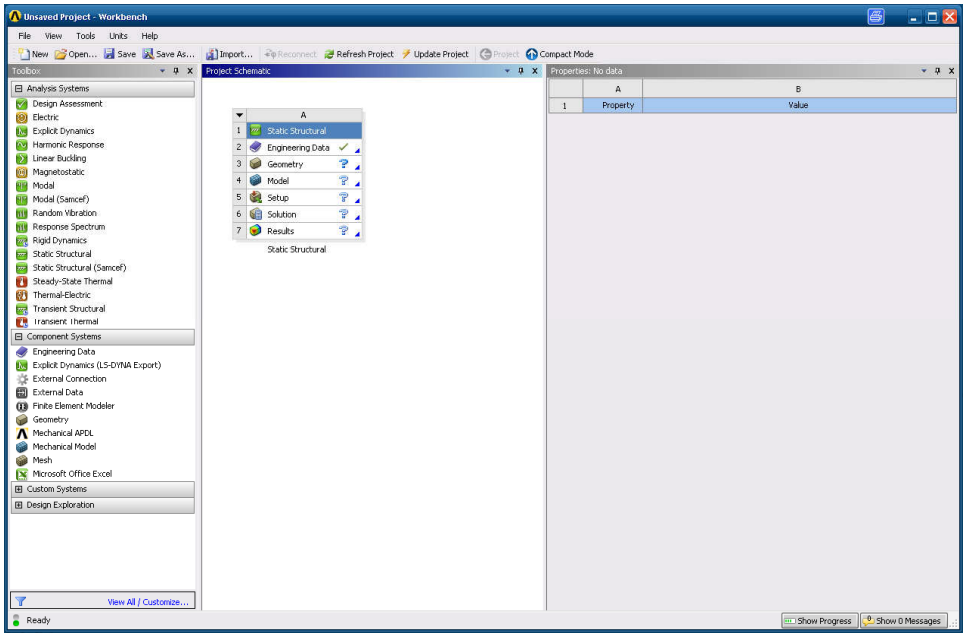

Figure 13 Example of window In Ansys Workbench 14.0 software

After modeling the construction a mesh with desired level of accuracy will be created in the same program. After creating the mesh model will be analyzed in Ansys Classic using LS-Dyna solver. Obtained results for ultimate bending moment will be compared with results from Poseidon program.

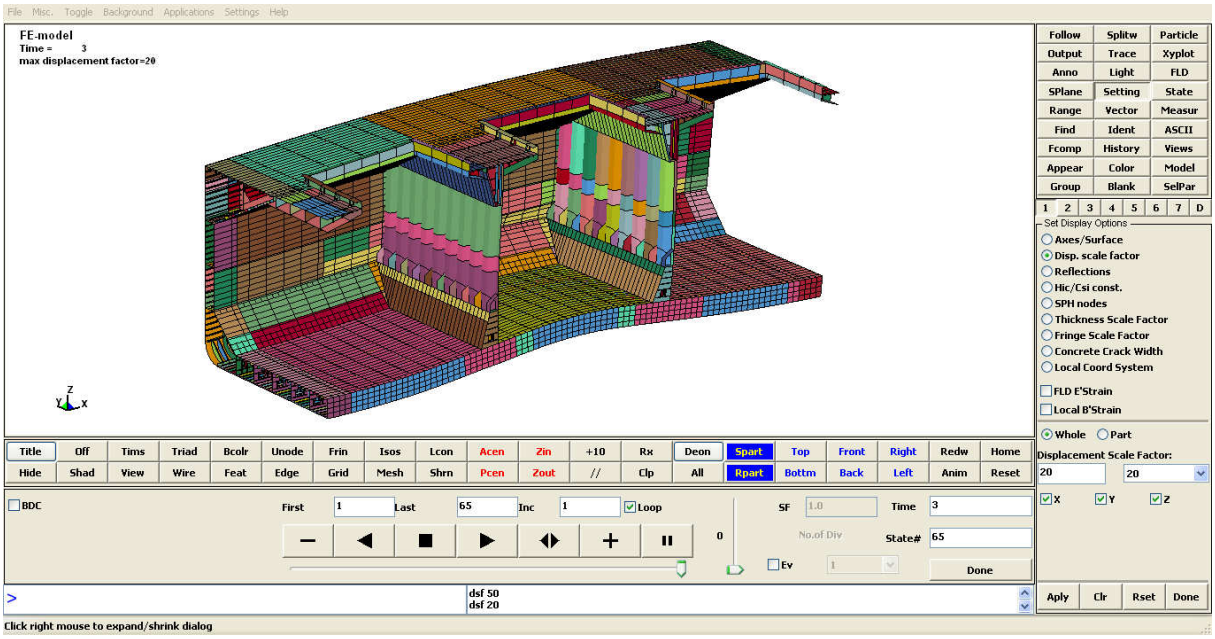

Figure 14 Example of window In LS-Dyna software

3.1.2 Model extent

Since the global vertical bending moment is considered chosen part of the ship is located amidships. From the distribution of global moment for the alternate loading condition it is found that the maximum value of the moment is for the cargo hold nr 6. It's fore bulkhead is located at the midship section of the ship. To include the influence of the alternate loading condition the adjacent cargo holds are taken into consideration as well. Therefore FE model of the bulk carrier include three cargo holds 5, 6 and 7. To reduce the size of the model, construction was represent from centre line to the side of the ship.

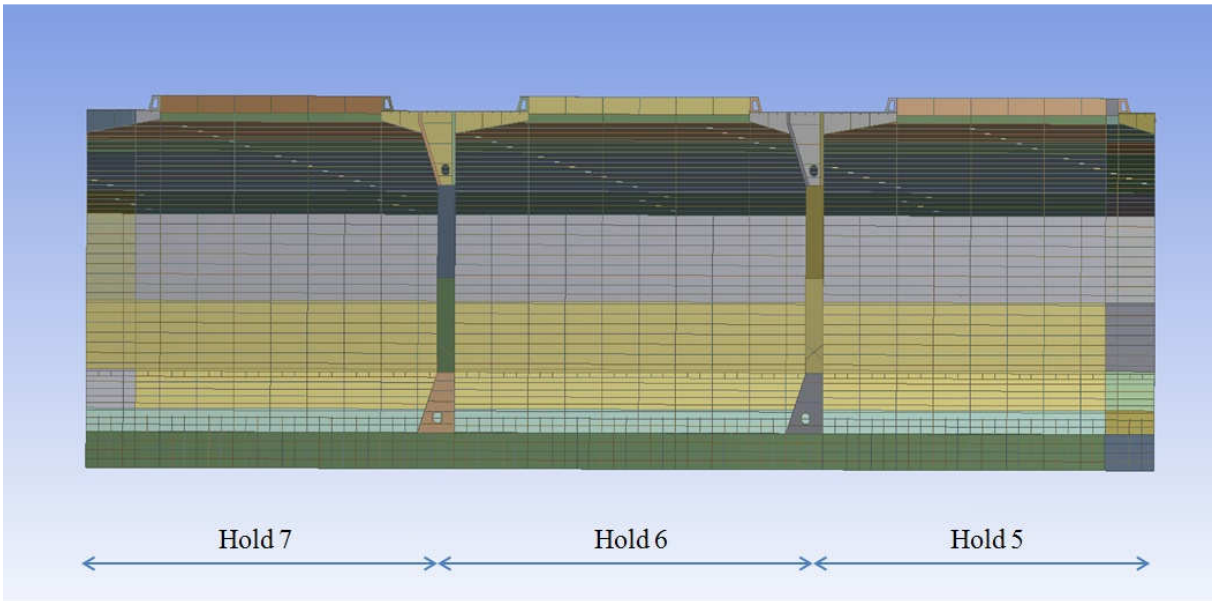

Figure 15 Bulk carrier model extent

3.1.3 Modelling of panel using shell elements

The model is done using shell elements therefore all structural members should follow the rules for the scantlings of the shell elements. The shell element models should be made in the mid-plane of plate and stiffeners. Therefore the dimensions of equivalent shell elements should be chosen according to the picture below:

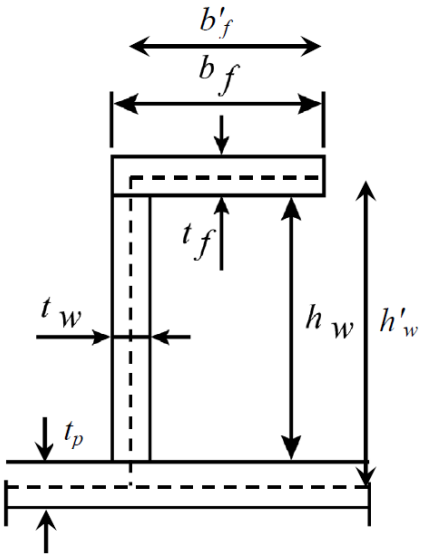

Figure 16 Equivalent stiffener dimensions using shell elements

Where:

$$h'_w = h_w + \frac{t_p}{2} + \frac{t_f}{2} \quad \textbf{(3-1)}$$

$$b_f' = b_f + \frac{t_w}{2} \quad \textbf{(3-2)}$$

3.1.4 Bulb profiles as equivalent angle profiles

In the construction of the bulk carrier many stiffeners were designed as bulb profiles. For the modeling, the equivalent angle profiles had to be found. It was done according to the procedure from the Common Structural Rules for Bulk Carriers, Chapter 3, Section 6, /1/.

$$h_w = h_w' + \frac{h_w'}{9{,}2} + 2 \quad \textbf{(3-3)}$$

$$b_f = \alpha\left(t_w' + \frac{h_w'}{6{,}7} - 2\right) \quad \textbf{(3-4)}$$

$$t_f = \frac{h_w'}{9{,}2} - 2 \quad \textbf{(3-5)}$$

where:

$w\,h'$, $w\,t'$: Height and net thickness of a bulb section, in mm, as shown in Figure 18.

α : Coefficient equal to:

$$\alpha = 1{,}1 + \frac{(120 - h_w')^2}{3000} \quad \text{for } h_w' \leq 120 \quad \textbf{(3-6)}$$

$$\alpha = 1{,}0 \quad \text{for } h_w' > 120 \quad \textbf{(3-7)}$$

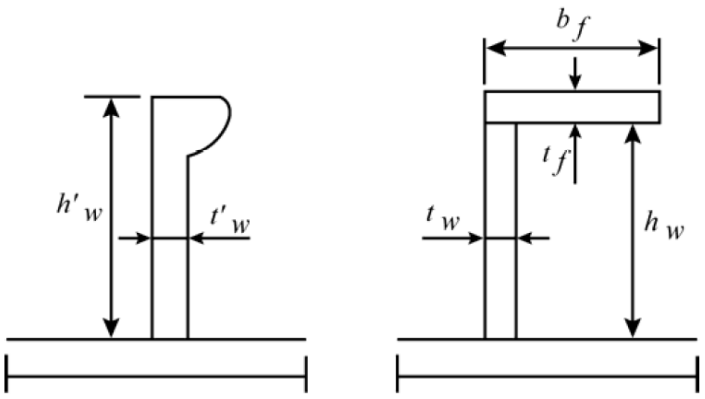

Figure 17 Dimensions of stiffeners

According to the procedure above the following bulb profiles included in the construction drawings were replaced by equivalent angle profiles

Table 3 Equivalent angle profiles

Previous bulb profile GHOST 30810	Equivalent angle profile
HP200x10	L180,3x10/37,9x19,7
HP220x10	L198,1x10/40,8x21,9
HP260x10	L233,7x10/46,8x26,3

3.1.5 Material properties

For the bulk carrier the material used for all structural elements is high tensile steel 355 Re. In the model a bi-linear material is applied with included strain hardening effect. Material properties are given below:

Young's modulus, E [N/mm2] 206 000

Poisson ratio, ν 0,3

Yield stress [N/mm2] 355

Strain hardening parameter, E_T [N/mm2] 1000

At the fore and aft part of the model pure elastic material is used.

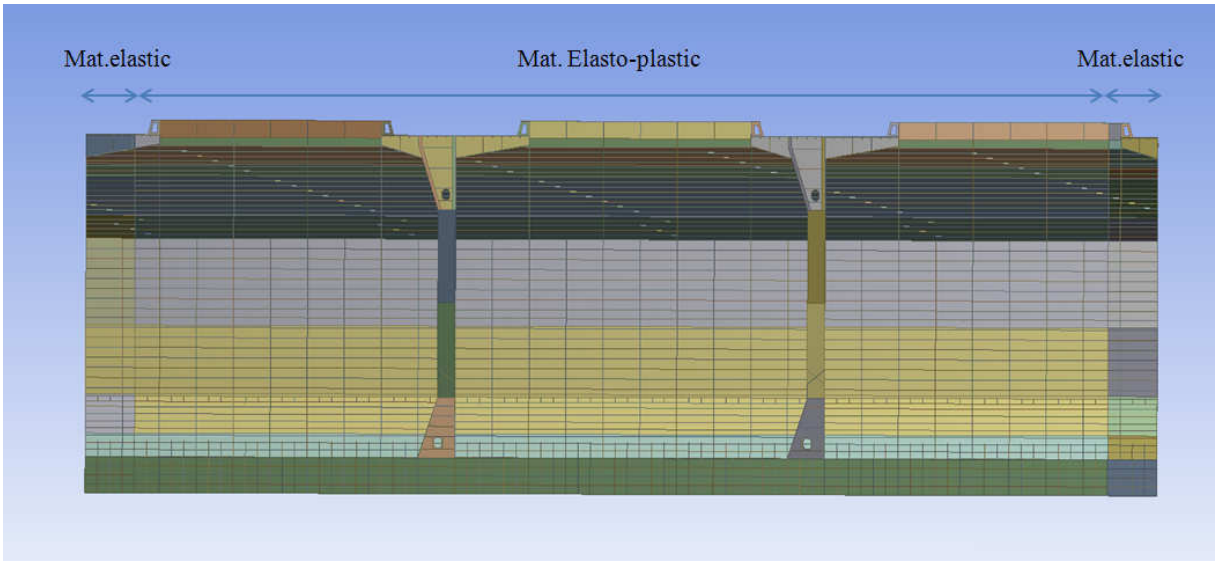

Figure 18 Material type assignment on the bulk carrier model

Stress – strain curve for both elasto-plastic and pure elastic material is given below.

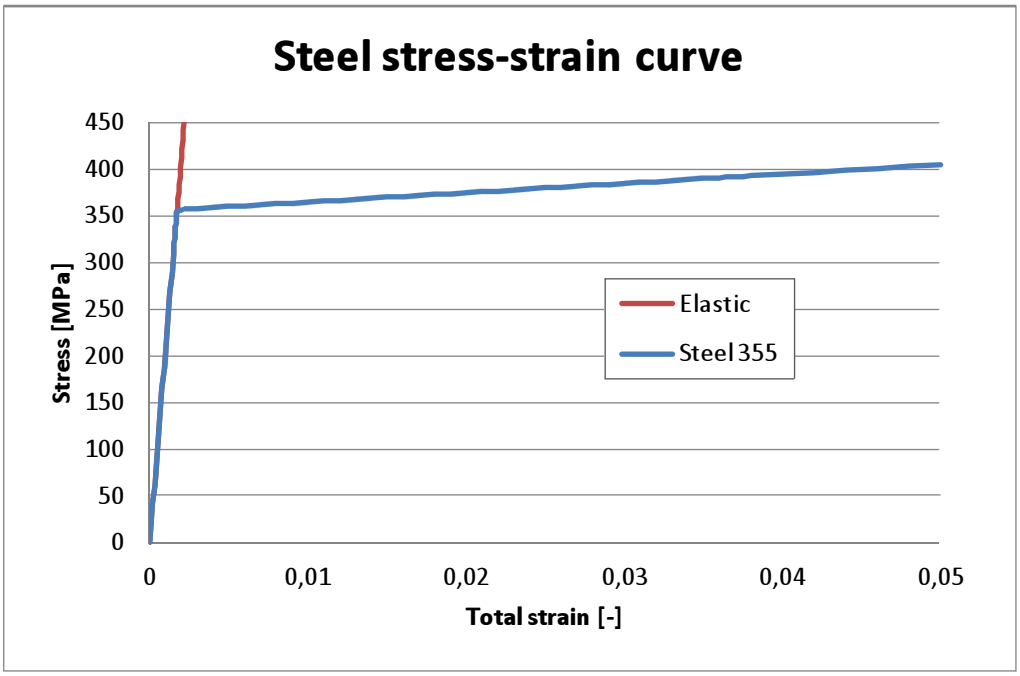

Figure 19 Steel properties

At the aft and fore and of the model pure elastic material is used.

3.1.6 Coordinate system

The model is developed in a right hand Cartesian coordinate system with x- and y-axis in the plane of the ship's outer bottom and z-axis perpendicular to this. The x-axis is directed along the ship's center line towards the fore end of the ship. The y – axis is oriented to the port side of the ship. The z – axis is oriented up. The beginning of the coordinate system is located at the aft perpendicular. Therefore the coordinates of all the elements are the same as in the reality. It allows directly mapping the pressure field on the model in respect to the acceleration on the different locations on the ship. A model is shown in Figure 20 for illustration.

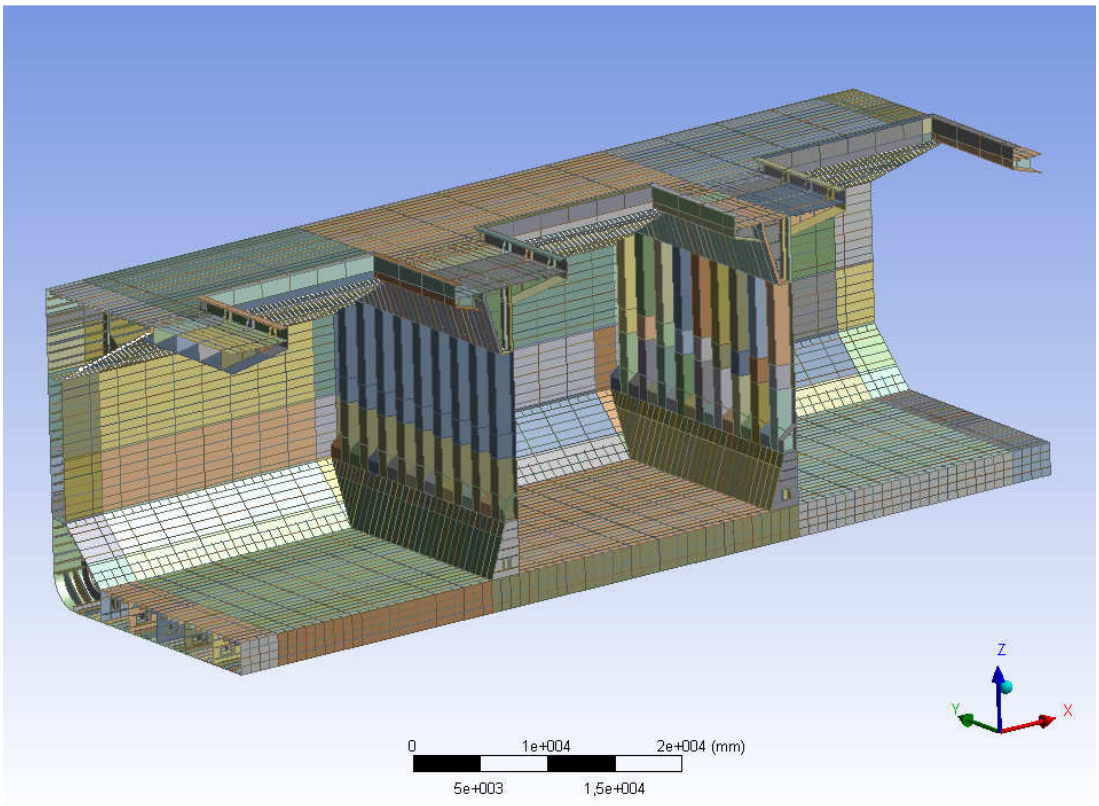

Figure 20 Coordinate system

3.1.7 Boundary conditions

To perform the calculations for the pure vertical bending moment acting on the construction, a set of boundary conditions was introduced. The fore end of the model was fixed in all six degrees of freedom i.e. three translations and three rotations. It was done by constrain all the nodes on the fore end section of the model. The picture is shown below.

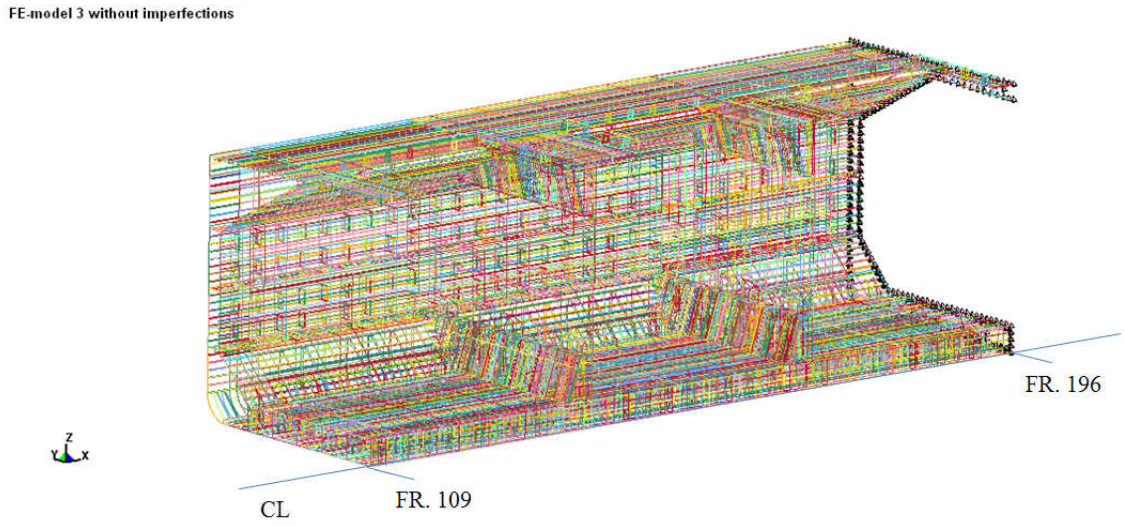

Figure 21 Boundary condition on bulk carrier model - fixed end

In the centre line the symmetry condition was applied with following set of parameters.

Table 4 Symmetry condition in the center line parameters

	x	y	z
Translation	free	fixed	free
	ox	oy	oz
Rotation	fixed	free	fixed

The picture is shown below.

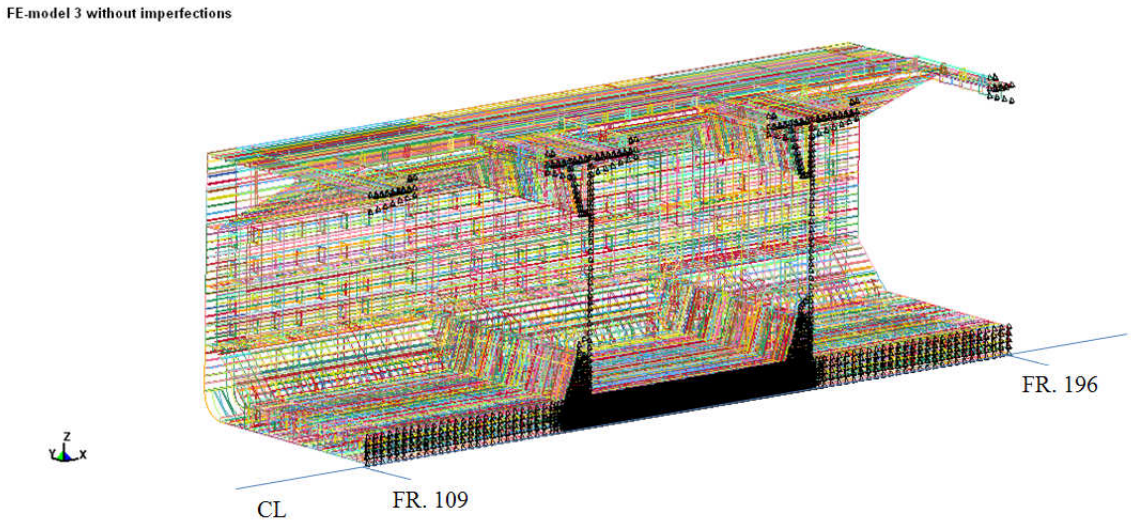

Figure 22 Boundary condition – symmetry condition in ship's center line

To realize the rotation at the aft end of the model the coupling between the section and the rotation point was applied. By this all the nodes at the first section follow the rotation given at the rotation node. The picture of the coupling at the aft end is shown below.

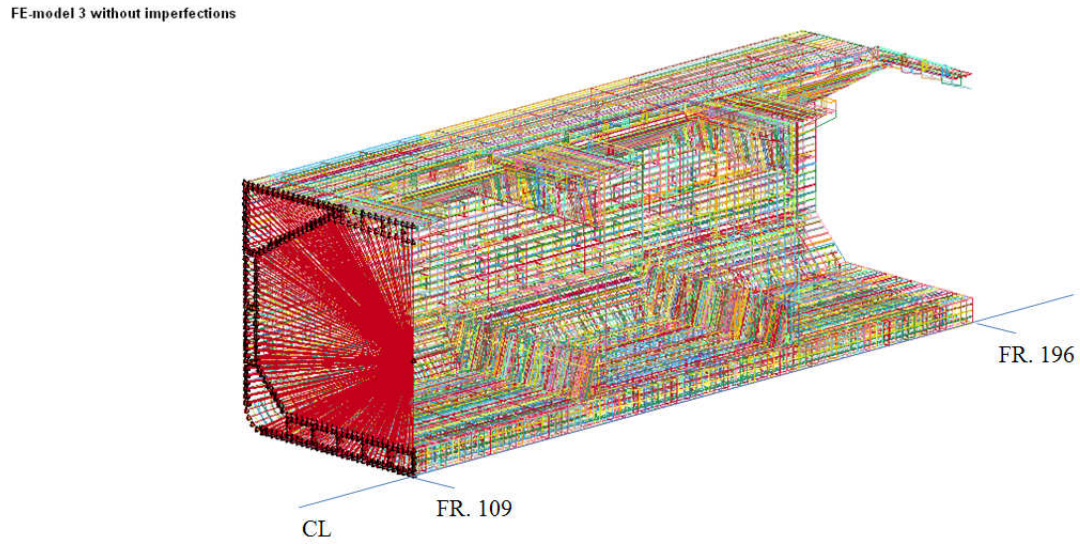

Figure 23 Boundary condition on bulk carrier model – coupling on the aft end section

3.1.8 Loading

In case of pure vertical bending moment the only load acting on the structure is the global bending moment applied by means of rotation at one end. The maximum value of rotation as well as increment is defined as the input parameter in the solver.

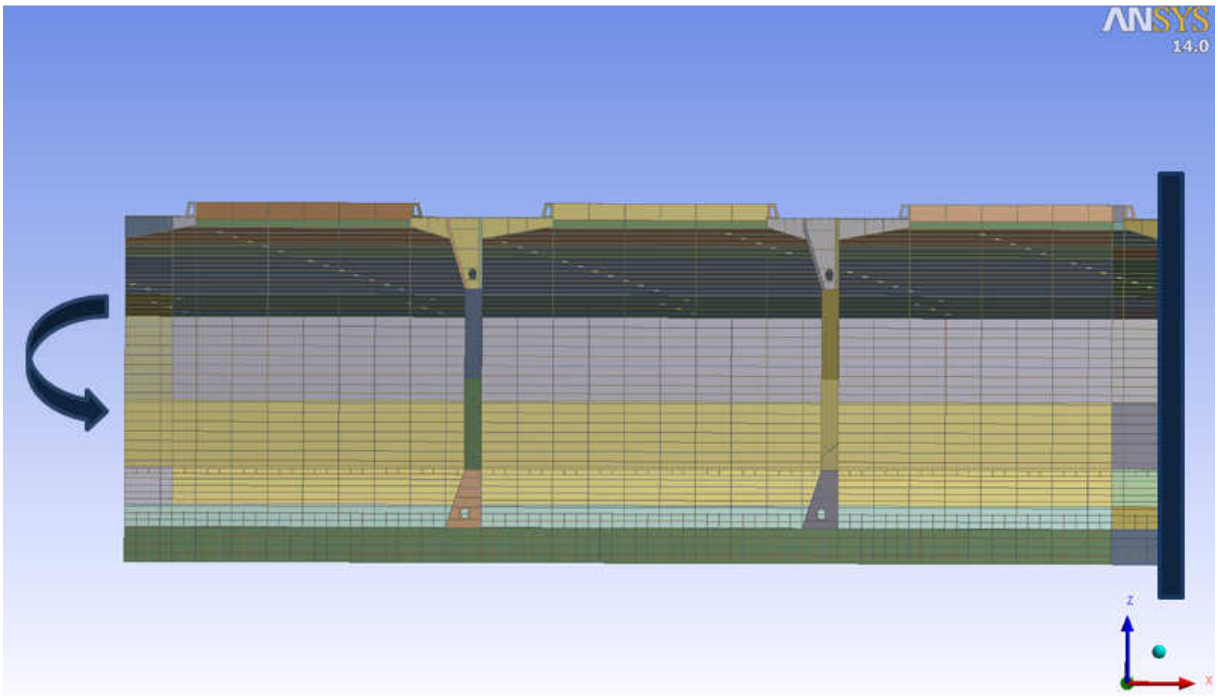

Figure 24 Beam model methodology

The rotation is given at the rotation node that is located at the level of neutral axis. The rotation node is shown below.

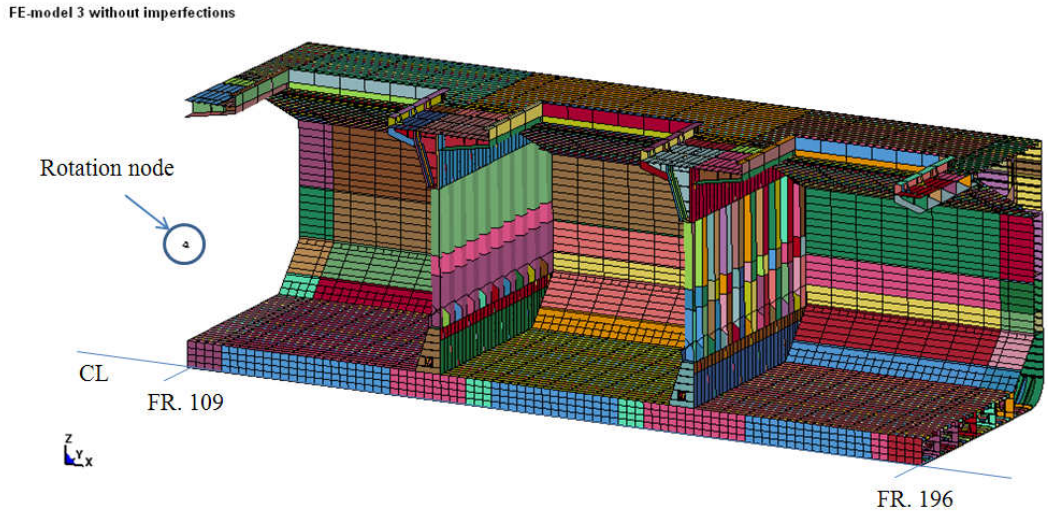

Figure 25 Rotation node

To execute the generation of the moment the aft end of the model is coupled with this rotation node. The coupling is shown below.

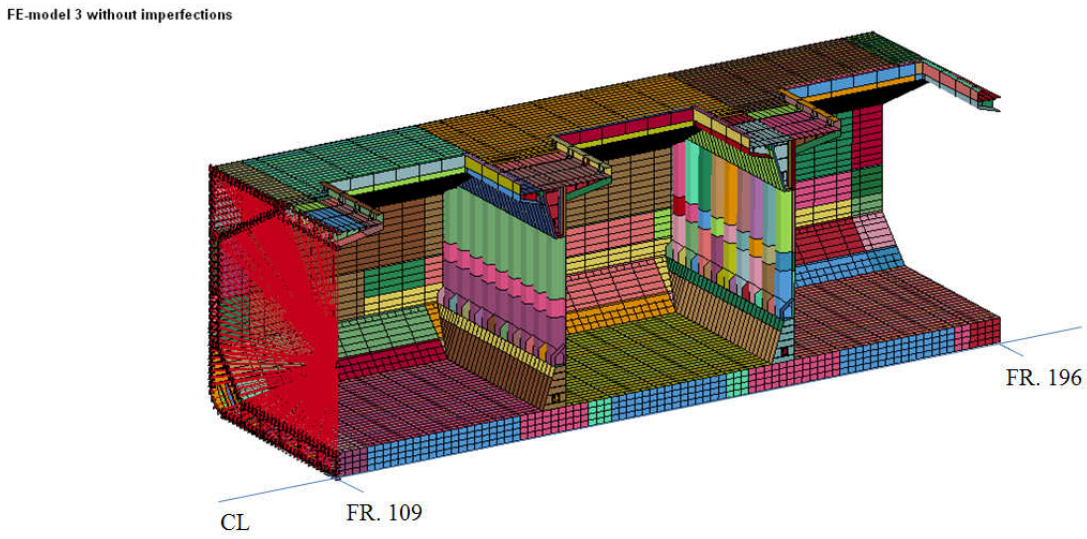

Figure 26 Coupling at the aft end section

3.1.9 Reading planes

The results of the ultimate moment are written for three different locations. Since the value of the moment is constant the results should be the same in all three points. It is to check that the procedure is done correctly.

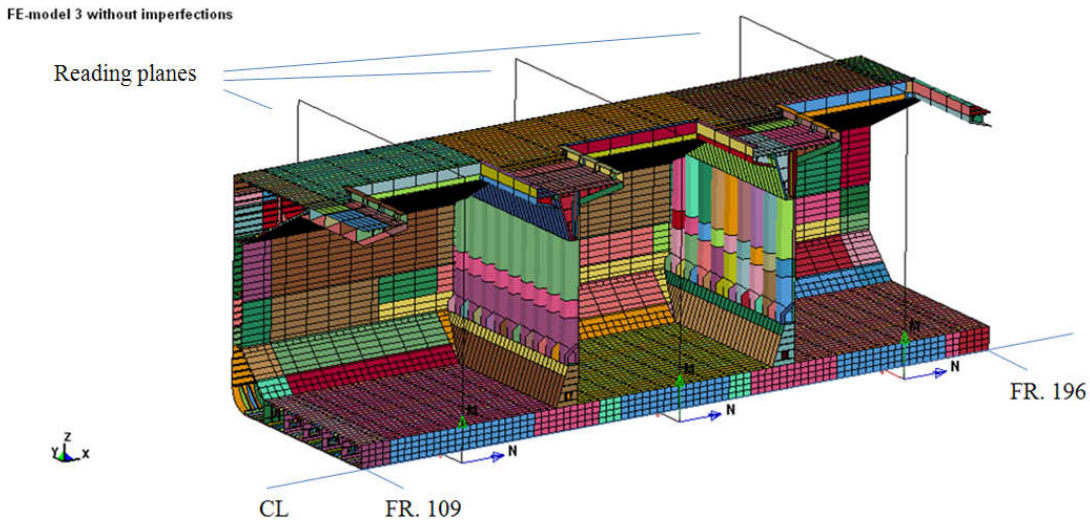

Figure 27 Results reading planes

3.1.10 Solver used

All the analysis were run using the LS-Dyna Program Manager with implicit solver. Implicit solvers are properly applied to static, quasi-static, and dynamic problems with a low frequency content. The advantage of the implicit solver is that the number of load or time steps are typically significantly fewer than would be used in an explicit calculation.

An incremental-iterative numerical algorithm is implemented is LS-Dyna. The method is stable for wide range of nonlinear problems that involve finite strain and arbitrarily large rotations. Accuracy consideration usually limits the load increment or time step size since an inaccurate solution will ultimately not converge.

To obtain the solution at load increment n+1 given the solution at load increment n, linearized equations of the form shown below are assembled.

$$K_t(x^n)\Delta u_0 = P(x^n)^{n+1} - F(x^n) \quad \textbf{(3-8)}$$

Where:

K – Positive-definite tangent stiffness matrix

Δu – Desired increment in displacements

$P(x^n)^{n+1}$ – External load vector at n+1 based on geometry at time n

$F(x^n)$ – Stress divergence vector at time n

The displacement vector is updated:

$$x_1^{n+1} = x^n + s_0\Delta u_0 \quad \textbf{(3-9)}$$

And equilibrium iterations begin:

$$K_{tj}\Delta u_i = P(x_i^{n+1})^{n+1} - F(x_i^{n+1}) = Q_i^{n+1} \quad \textbf{(3-10)}$$

Where the subscripts *i* denotes the iterate and *j*<*i* and s_0 is a parameter between 0 and 1. After each iteration, convergence is checked. Convergence is assumed if the conditions

$$\frac{\|\Delta u_i\|}{u_{max} < \varepsilon_d} \quad \textbf{(3-11)}$$

And

$$\frac{|\Delta u_i^t Q_i|}{|\Delta u_0^t Q_0|} < \varepsilon_e \quad \textbf{(3-12)}$$

are satisfied.

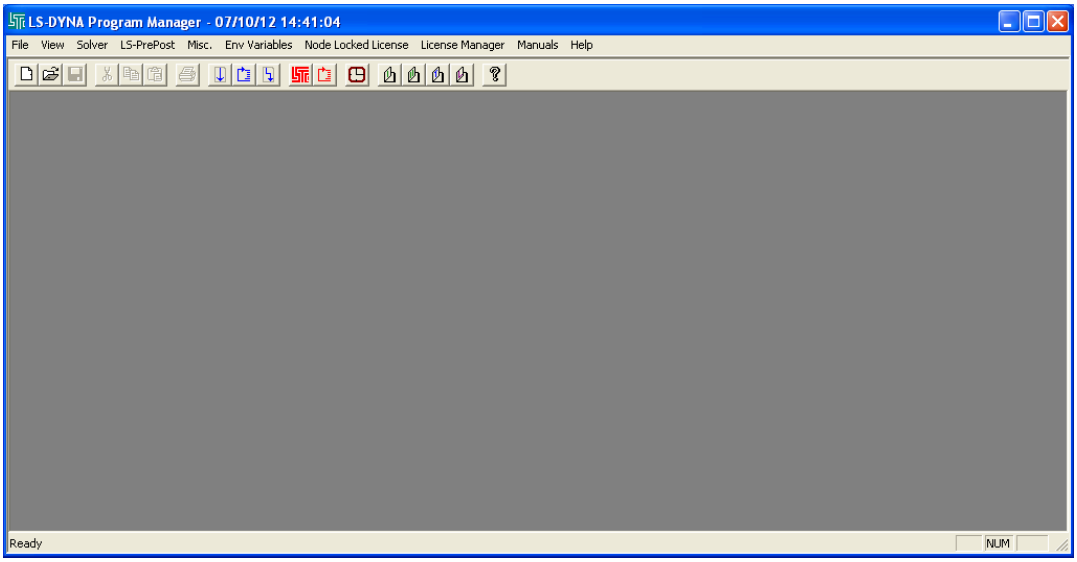

Figure 28 LS-Dyna solver window

The solver requires previously written text file with defined calculation parameters. Example of the calculation input file is shown below.

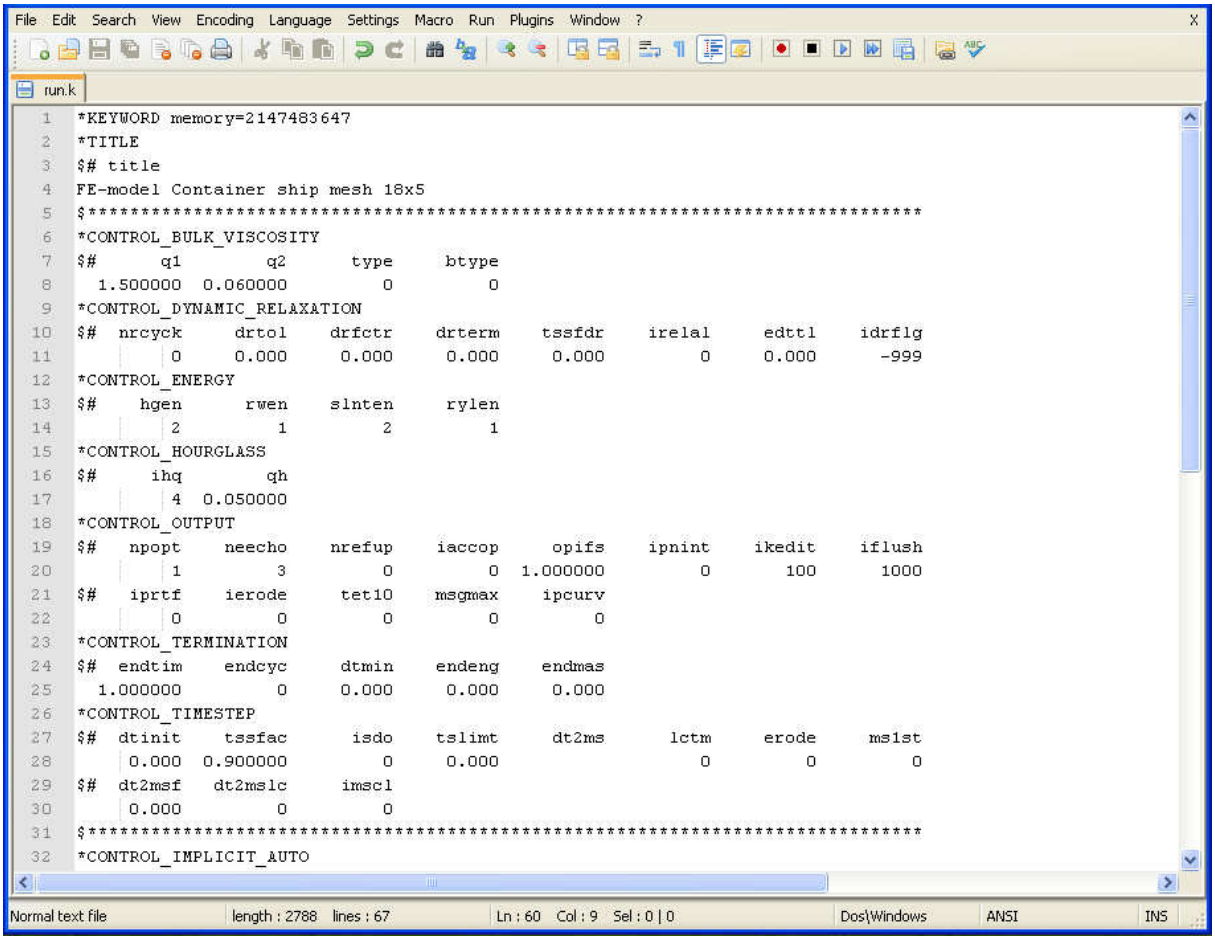

Figure 29 Example of LS-Dyna input file

3.2 Structure modeling

The bulk carrier geometry was modelled in Ansys Workbench 14.0 in Design Modeller. All the elements are as shell elements with constant thickness in all directions. The main aim was to follow the given construction drawings with as much of details as possible. All the longitudinal and transversal structural members were modelled including man holes and local stiffenings. Since longitudinal stiffeners were originally a HP profiles a necessary calculations were done and finally the equivalent angle profiles were introduced to the model.

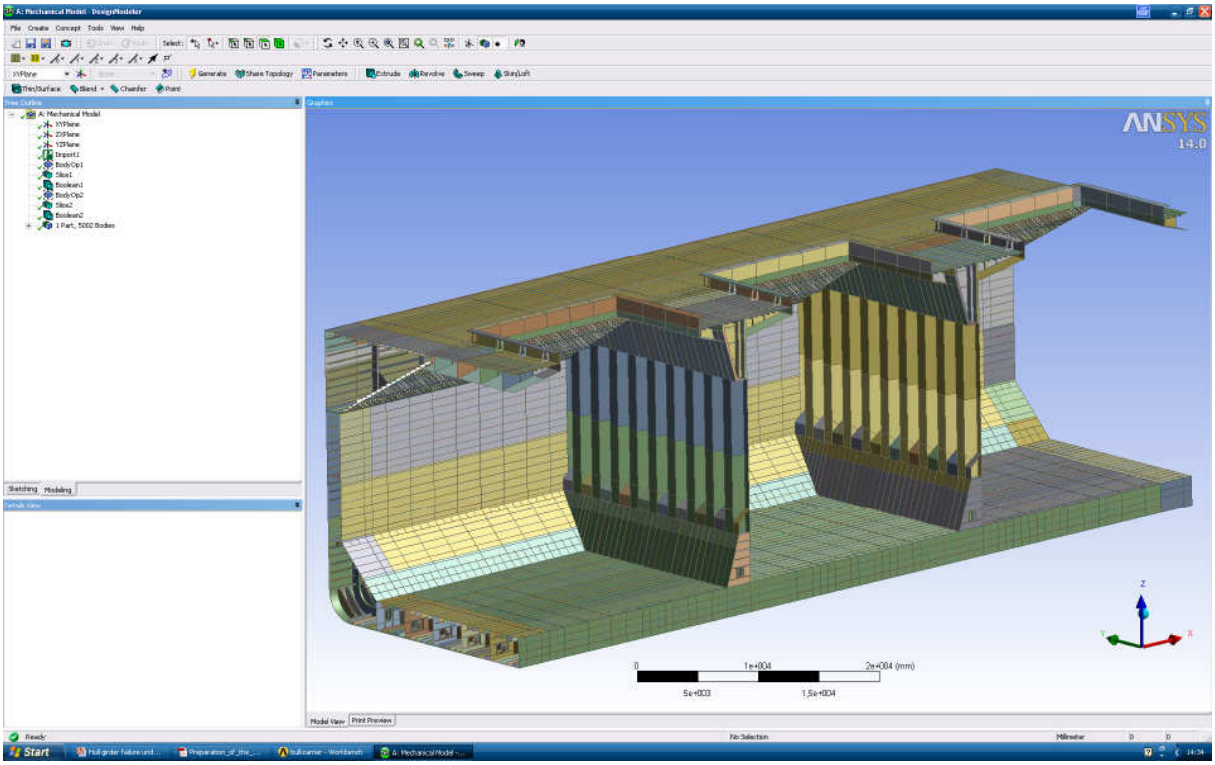

Figure 30 Example window of the model in Ansys Workbench, Design Modeller

Construction details in the way of the bulkhead are shown below.

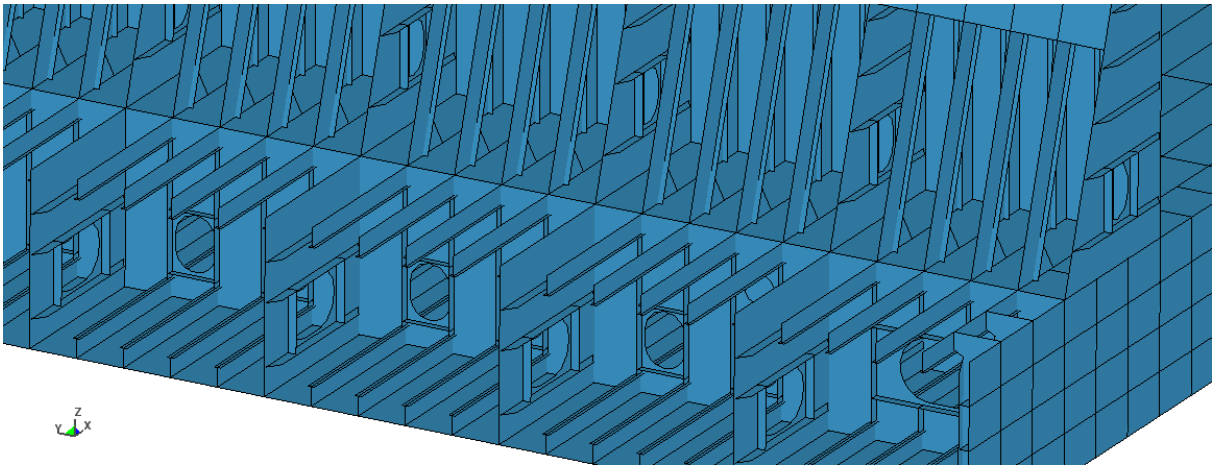

Figure 31 Structural details of the bulk carrier model

3.3 Mesh

Mesh generation was done in accordance to a set of requirements. All structural members such as plates, stiffeners web and flanges are modeled using shell elements. The majority of the elements are four nodes elements (quadrilaterals), however some triangular elements were created in more complex areas.

3.3.1 Mesh density requirements

The generated mesh should be accurate enough to give results independent on the mesh density. The mesh parameters should be chosen to show the local stress patterns and deformations especially to include buckling effects on plates and stiffeners. The parameters of the mesh depends on the geometrical proportions of the elements, loads combinations, local complexity of structure and elements used.
The following mesh density should be applied:

- Plate: Six elements in the transverse directions between stiffeners. The number of elements in the axial direction should be selected so that the elements are nearly square, i.e. the typical element length for plate elements should be set to *s*/6, where *s* is the stiffener spacing.
- Stiffener web: Minimum three elements across the web height. The number of elements should be selected so that the elements are as close to square-shaped as possible.
- Stiffener flange: One element across the stiffener flange for angle- and bulb profiles and two elements for T profiles.

3.3.2 Mesh generation

The general mesh parameter could be divided into two groups, the fine mesh and the coarse mesh. In the part of the model where high accuracy of the results is desirable the fine mesh was applied. It includes the hold nr 6 region for double bottom elements including shell, the bilge area and the sides up to the level of the neutral axis. For all other regions coarse mesh was applied. Using fine mesh only in the crucial part of the model allowed to save on the model size and the computation time needed to obtain the results.

Since the mesh parameters were specially chosen, in many areas the mesh quality had to be more manually controlled. In reality it means that for example the number of divisions on many elements had to be given separately. The other important aspect was the complexity of the structure that required more careful treatment of the mesh. Especially where many elements are crossing such as in the bilge or bulkhead area.

The fine mesh on the shell in the hold nr 6 area and coarse mesh around is shown in the picture below.

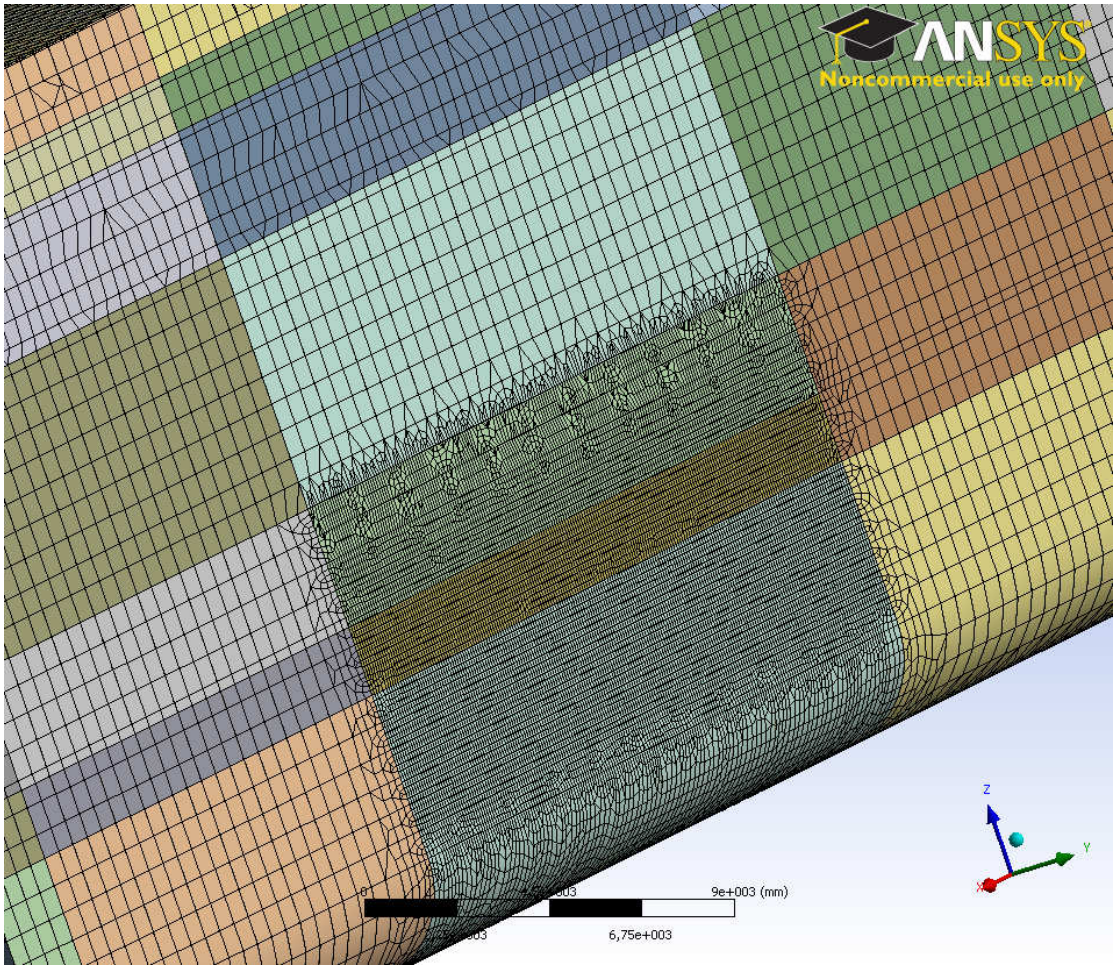

Figure 32 Fine mesh generated on the outer shell

Fine mesh on the inner bottom and inner side area with coarse mesh on the other elements including main deck area.

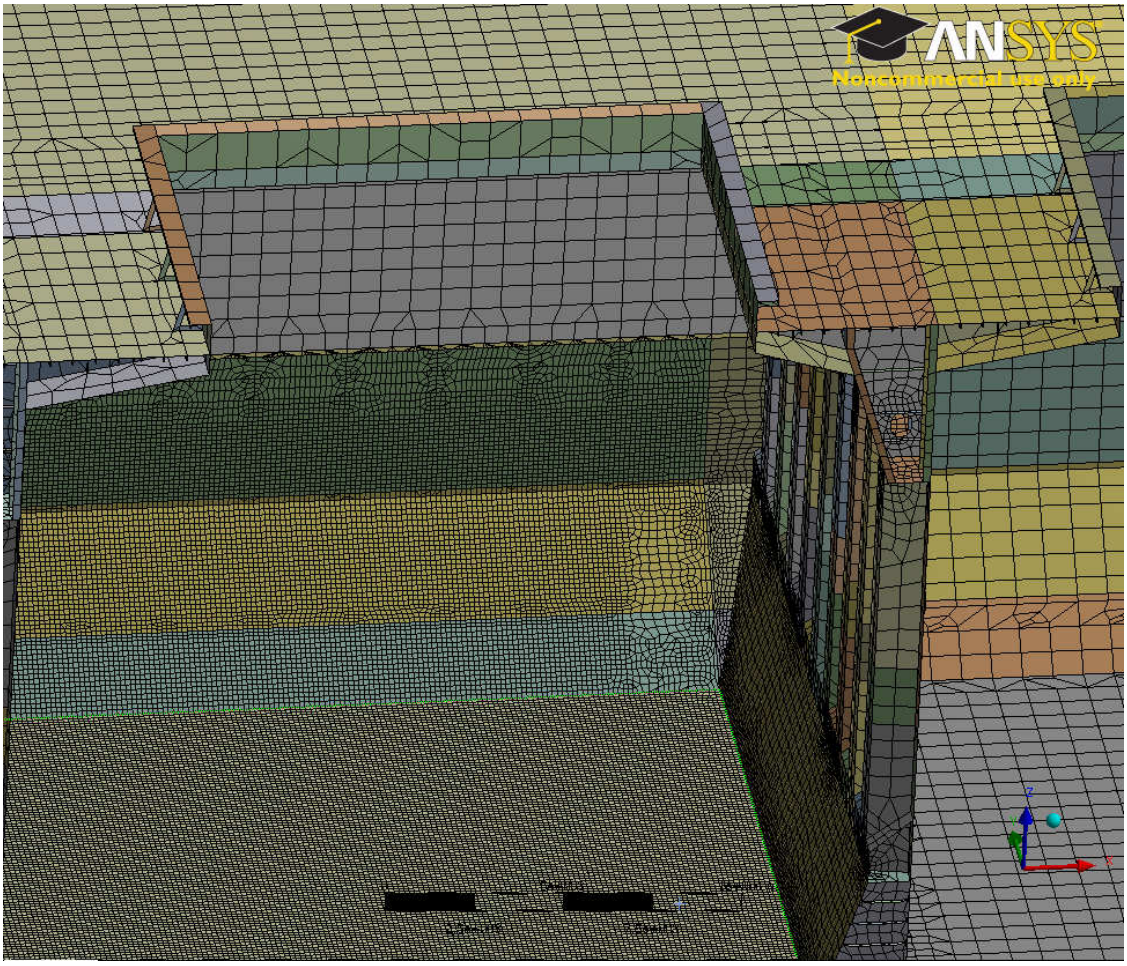

Figure 33 Example of the mesh generated on the bulk carrier model

3.4 Study on the mesh convergence

To ensure that the quality of the mesh has no higher influence on the obtained results the mesh convergence study was performed. Three following mesh densities were checked with increasing number of elements between frames and longitudinal stiffeners. All analyzed mesh densities meet the requirements for the mesh quality.

The following mesh models were studied:

- Mesh 1 – 8 elements between main frames, 2 elements between longitudinal stiffeners, the size of the element 350 mm,
- Mesh 2 – 9 elements between main frames, 3 elements between longitudinal stiffeners, the size of the element 300 mm,
- Mesh 3 – 18 elements between main frames, 5 elements between longitudinal stiffeners, the size of the element 140 mm,

3.4.1 Mesh 1 (8x2)

Picture below shows the mesh generated on the inner bottom structures.

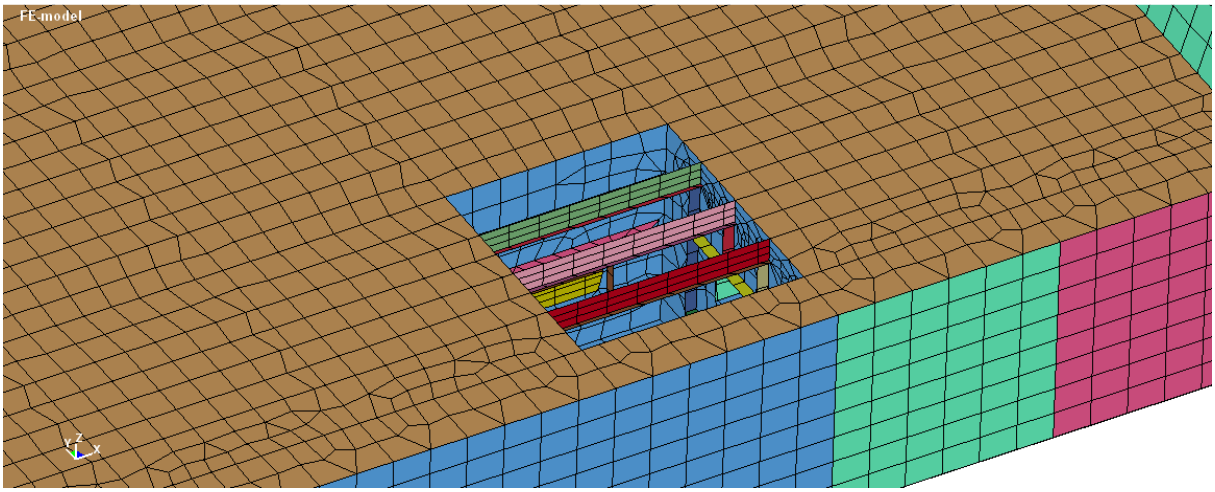

Figure 34 Mesh generated on the inner bottom

Results (8x2)

After running the calculations for the first mesh density the collapse was found. The picture of the hull girder collapse on the outer bottom is shown in the picture below.

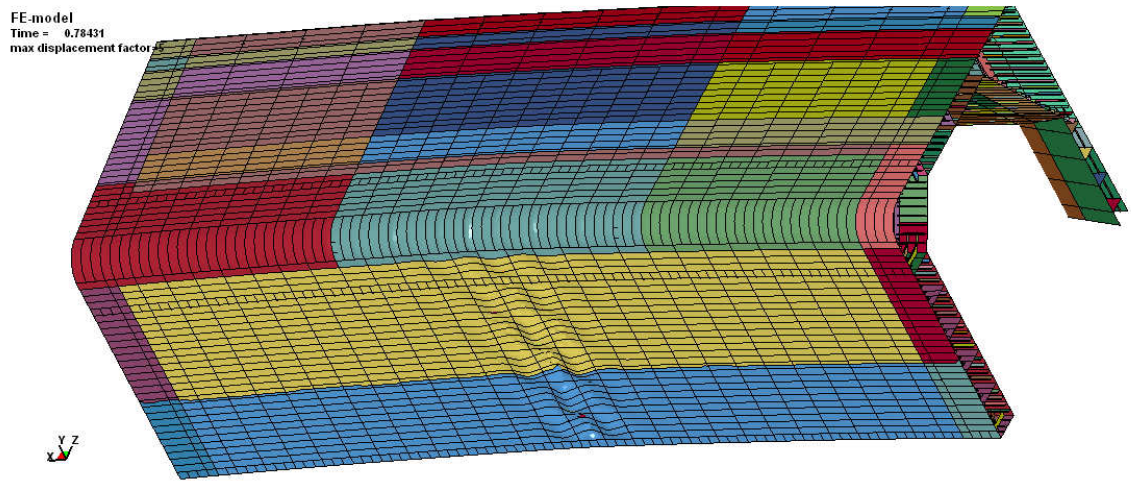

Figure 35 Structure deformation results

Buckling of the inner bottom region.

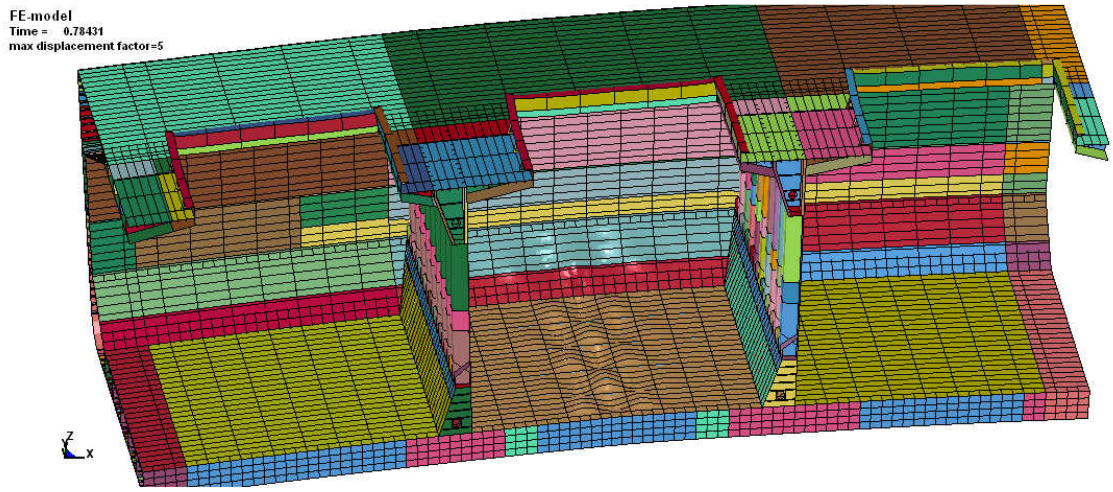

Figure 36 Deformation in the inner bottom

Buckling of the bottom side girders.

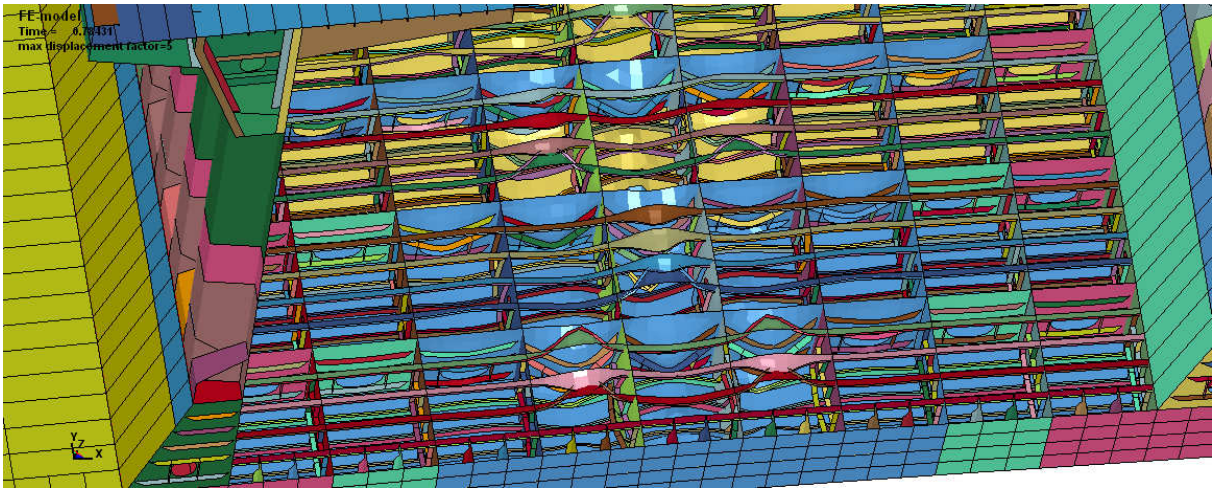

Figure 37 Deformation of the girders in the double bottom

The progressive collapse curve for the first mesh density is shown below. In the first part of the curve the linear relation is observed. With increase of the rotation the plastic deformations started to take place. Finally the ultimate moment capacity is found before the maximum value of rotation is applied.

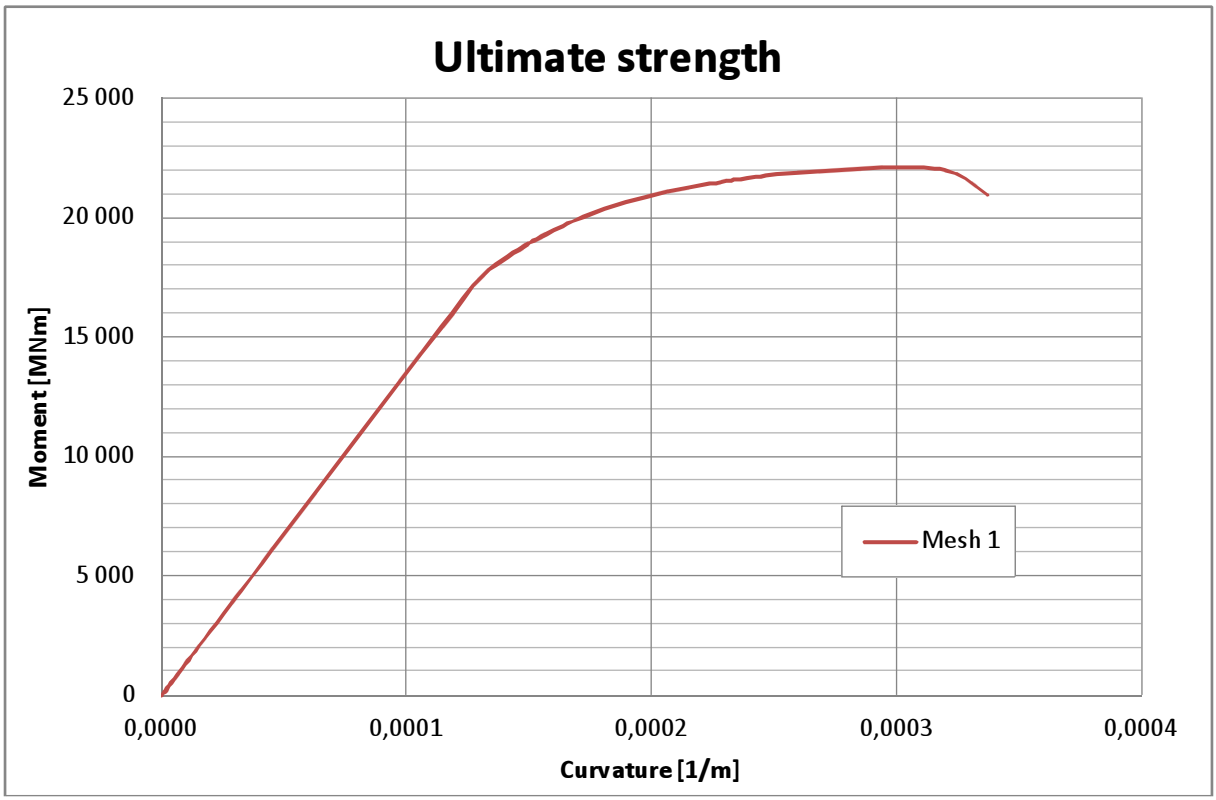

Figure 38 Progressive collapse curve for Model nr 1

The obtained ultimate moment is Mu = 22100 MNm.

3.4.2 Mesh 2 (9x3)

Picture below shows the refined mesh model in the inner bottom region. The quality of the mesh on the longitudinal stiffeners can be observed.

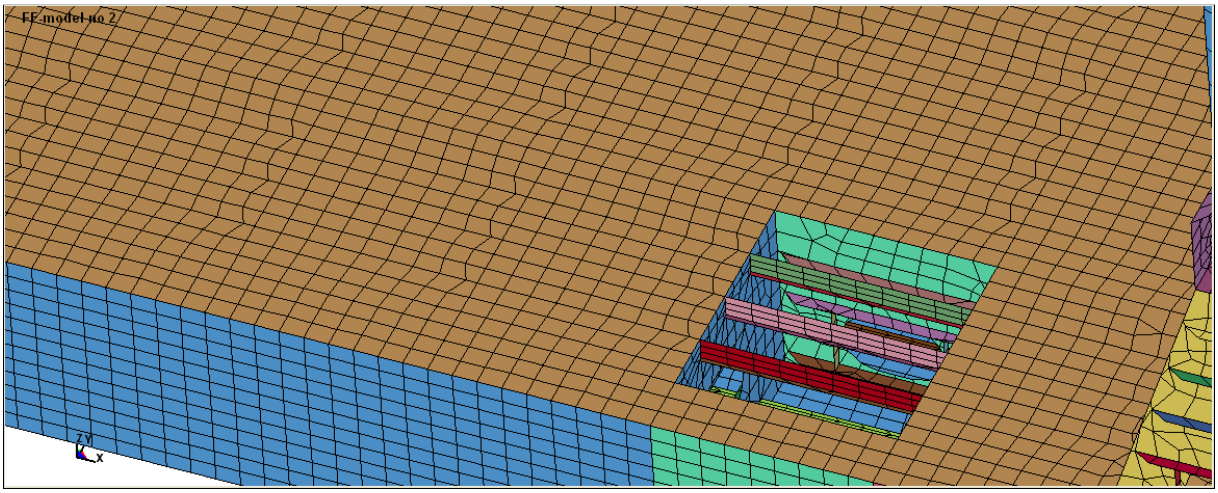

Figure 39 Mesh generated on the inner bottom

Results (9x3)

The buckling on the inner bottom is shown in the picture below.

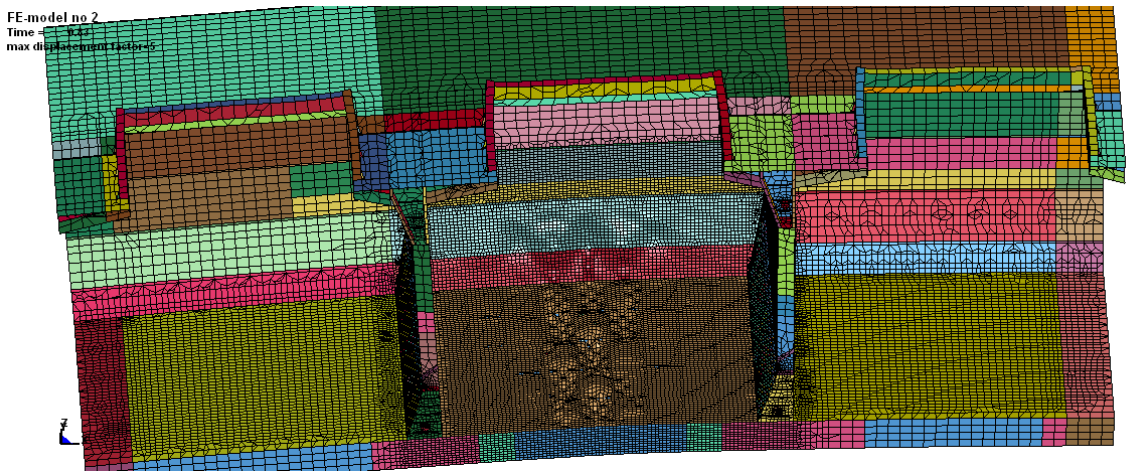

Figure 40 Deformation in the inner bottom

Buckling of the bottom side girders and longitudinal stiffeners.

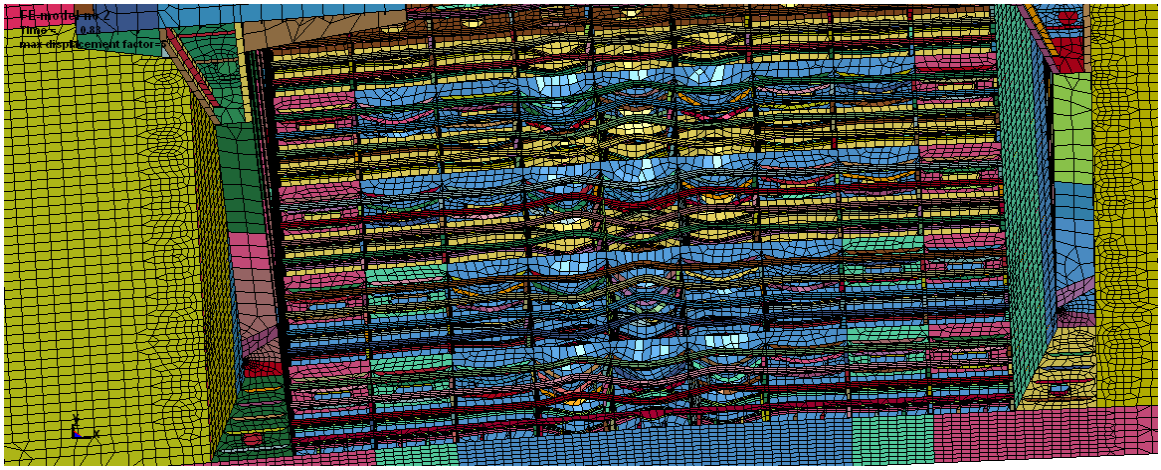

Figure 41 Deformation of the girders in the double bottom

Buckling on the outer shell.

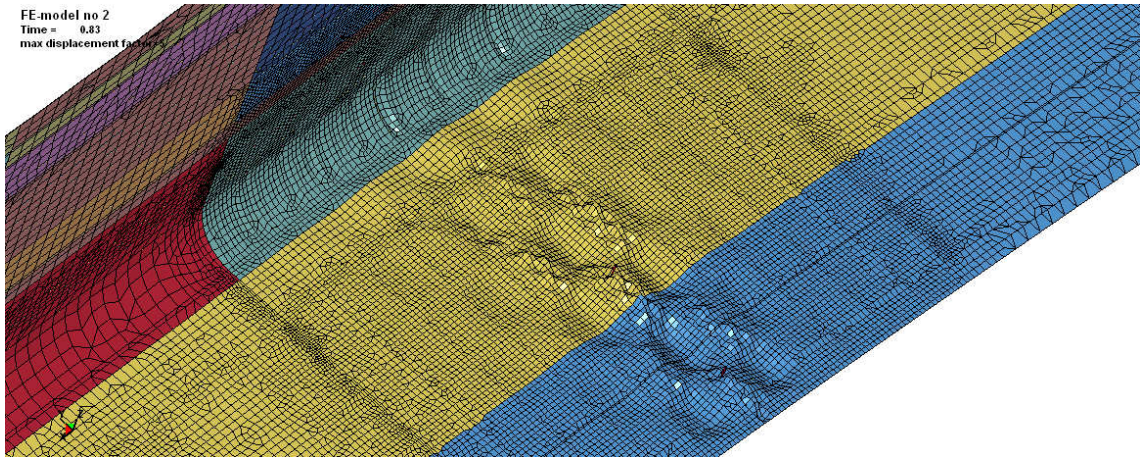

Figure 42 Deformation of the outer bottom plating

The progressive collapse curve for the mesh model nr 2 is shown below. Since the difference in the size of the elements is not big comparing with the first mesh, the shape of the curve and the value obtained are similar with the first mesh model.

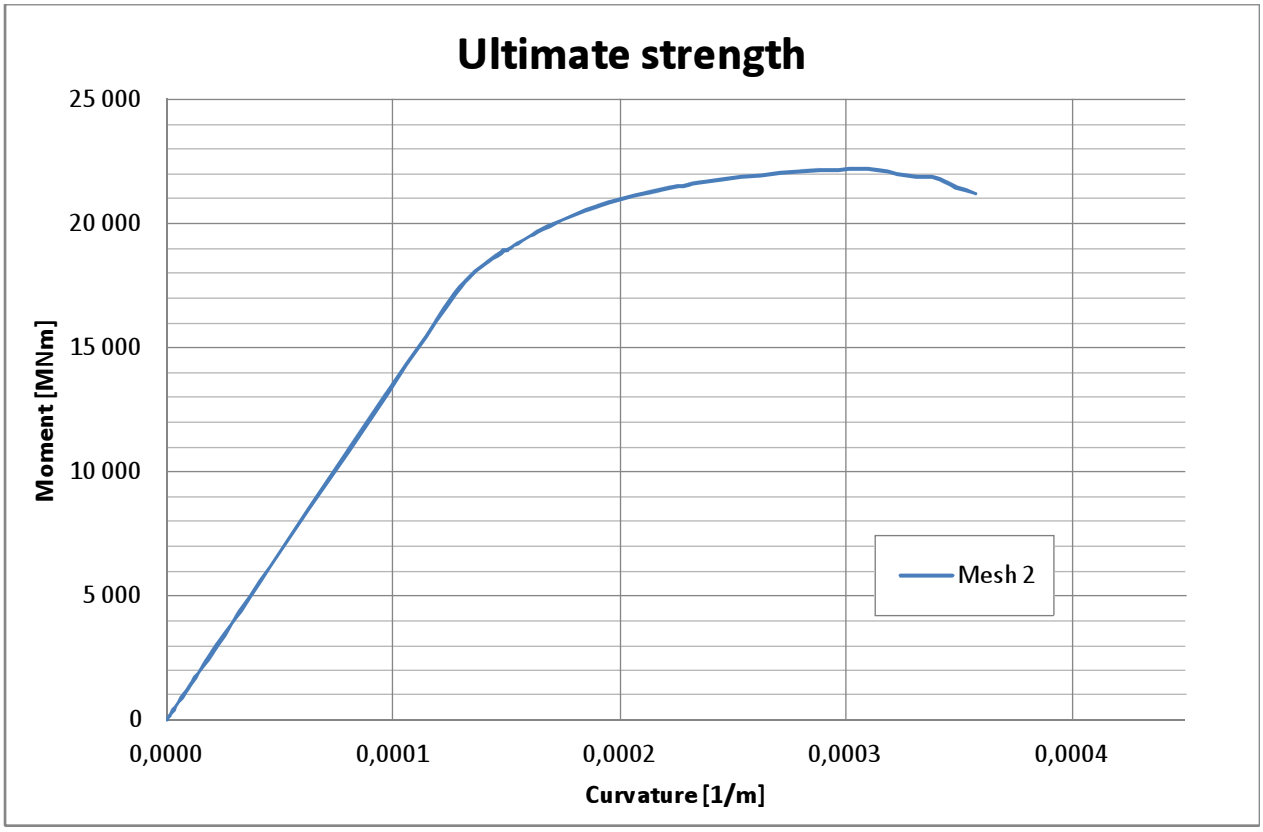

Figure 43 Progressive collapse curve for Model nr 2

The obtained ultimate moment is Mu = 22200 MNm.

3.4.3 Mesh 3 (18x5)

To better represent the buckling form between the longitudinal stiffeners the higher density was required. Therefore the third mesh model includes five elements between longitudinal stiffeners in the fine mesh region. Below is shown the picture of the mesh on the structure in the double bottom region in proximity of the bulkhead.

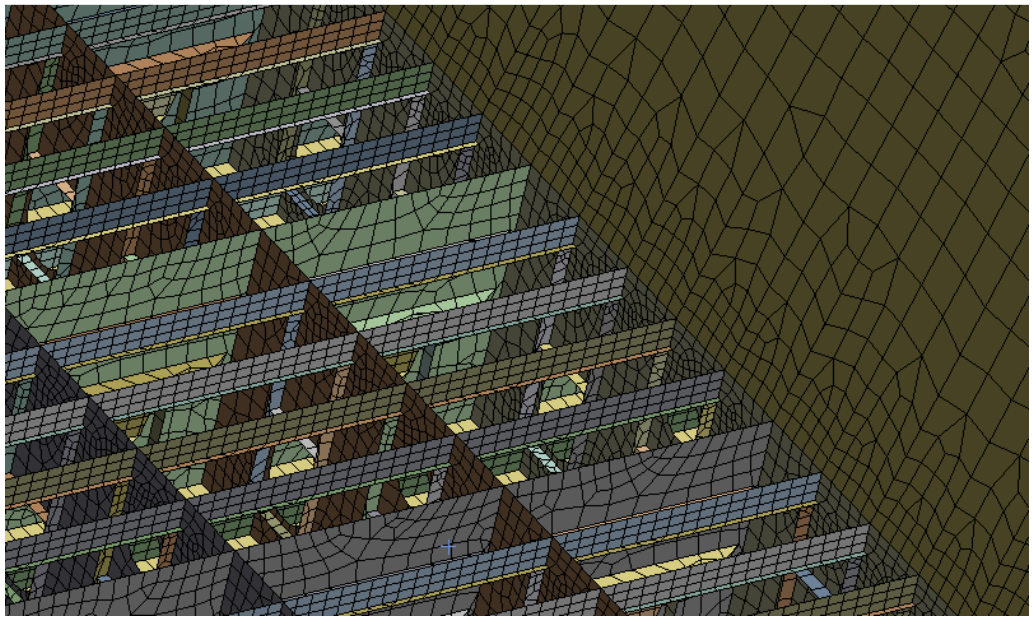

Figure 44Mesh generated on the inner bottom longitudinal stiffeners

The picture of the mesh generated on the inner bottom plating.

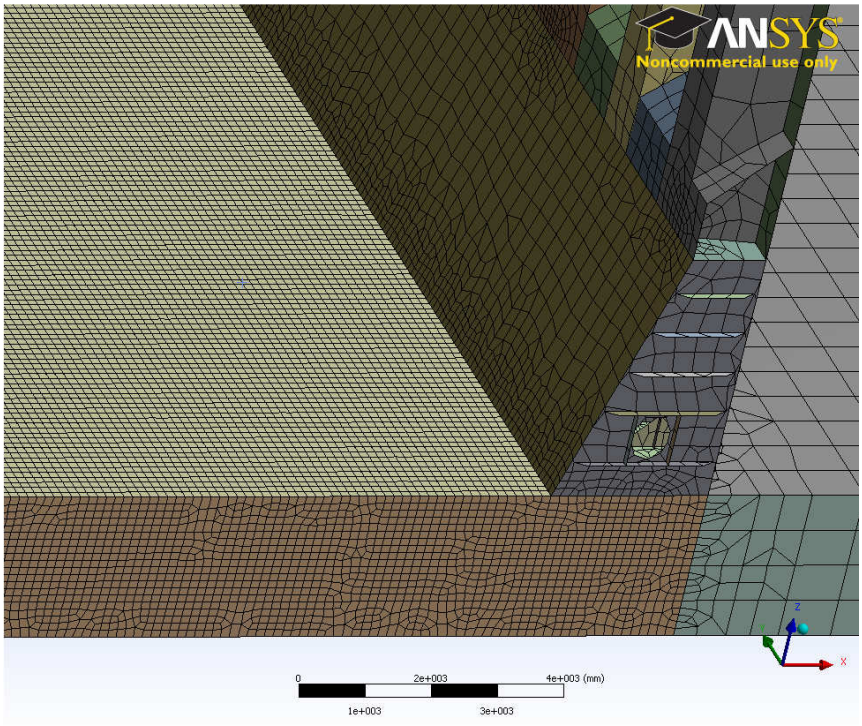

Figure 45 Mesh generated on the inner bottom plating

Results (18x5)

The buckling form on the outer shell is shown in the picture below.

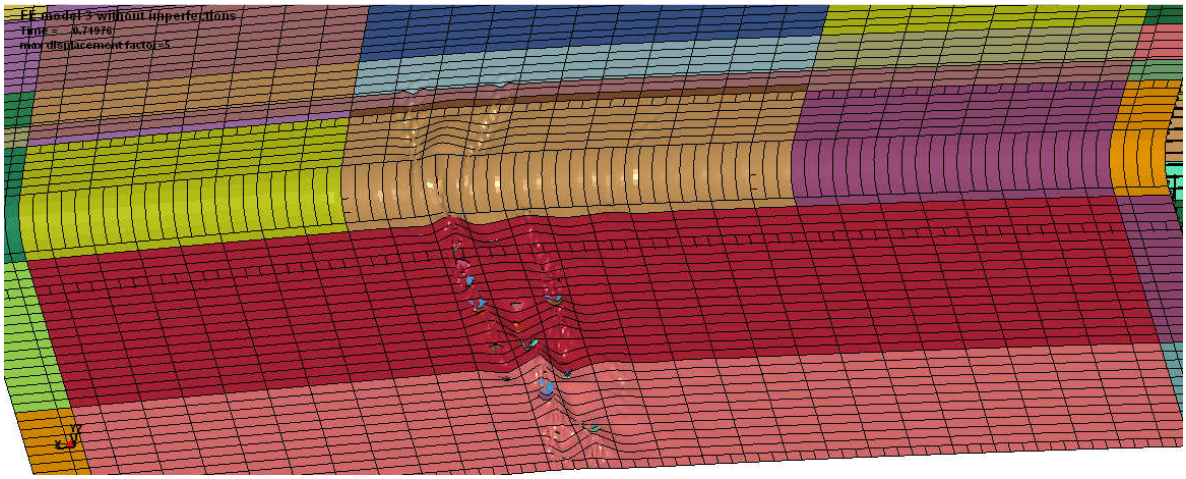

Figure 46 Deformation of the outer shell

Buckling on the inner bottom.

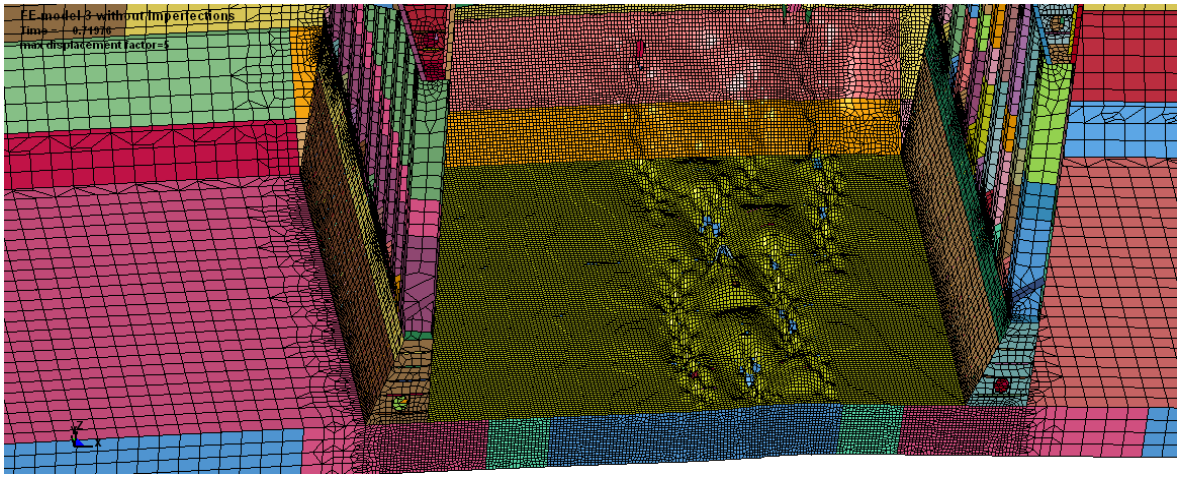

Figure 47 Deformation of the inner bottom plating

Collapse of the bottom side girders and longitudinal stiffeners.

Figure 48 Deformation of the bottom girders

The progressive collapse curve is shown below.

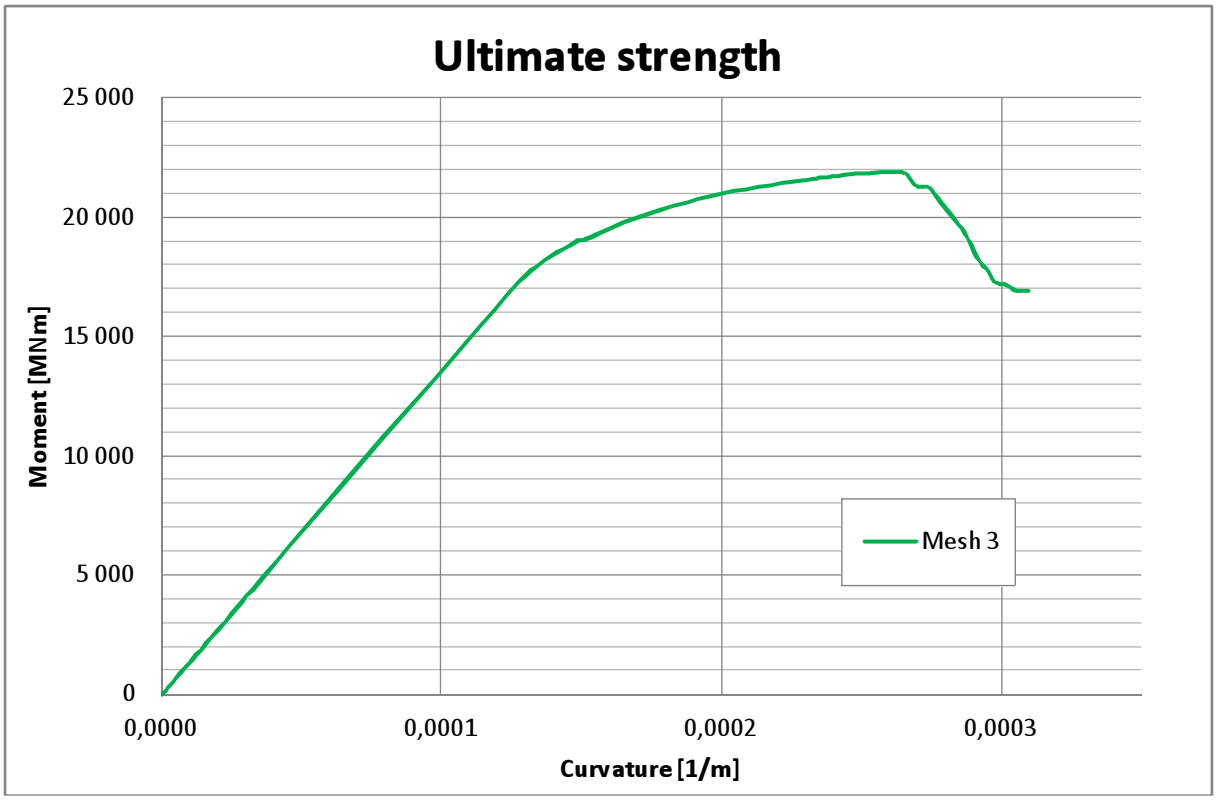

Figure 49 Progressive collapse curve for Mesh nr 3

The obtained ultimate moment is Mu = 21890 MNm.

3.4.4 Results of the mesh convergence

The progressive collapse curves were found for three considered mesh densities. The comparison is shown on the Fig.51.

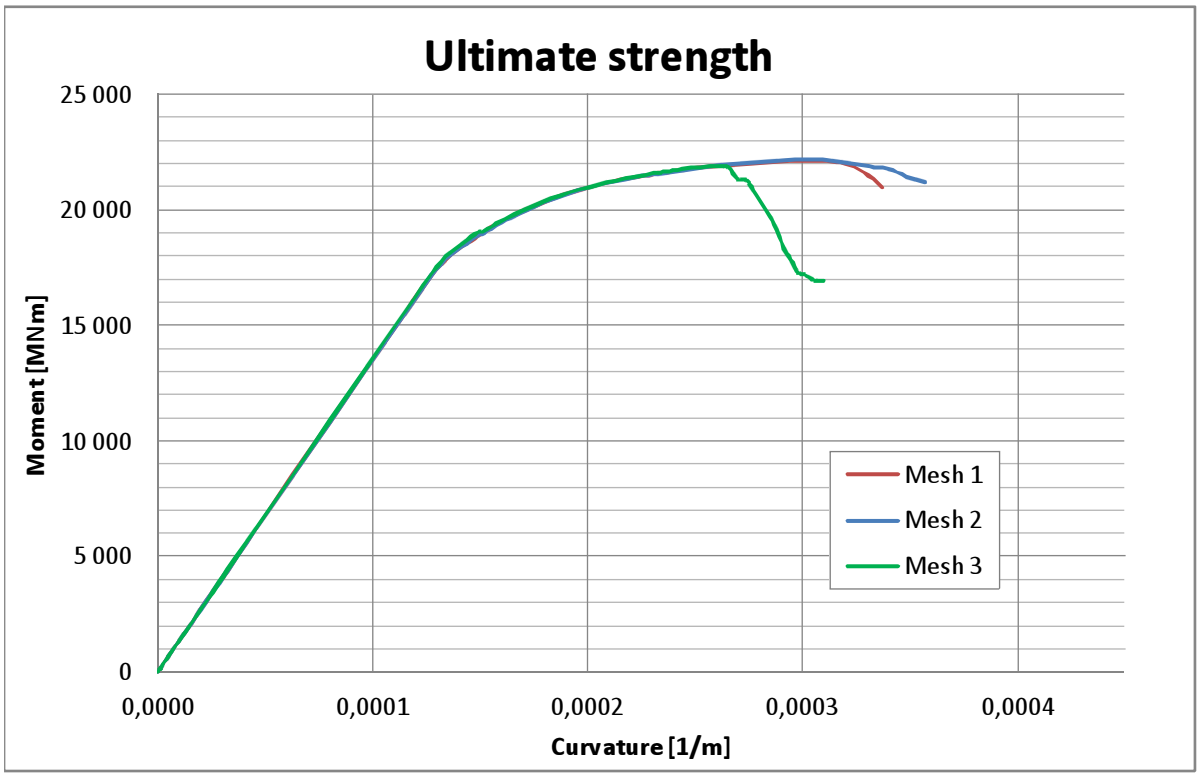

Figure 50 Comparison of the progressive collapse curve for different mesh densities

As it is shown the increase of the mesh density result is lower values for the ultimate moment obtained from the calculations. The maximum values of the moment are given below.

Table 5 Comparison of the ultimate moment for different mesh densities

	Maximum moment [MNm]	Difference [%] (to Model 1)
Mesh model 1	22100	-
Mesh model 2	22200	0,45
Mesh model 3	21890	-0,95

Mesh density nr 1 and 2 are very similar therefore difference in the results may be a result of local imperfections of the mesh or in the probabilistic incertentities in the solver. The difference between mesh nr 1 and mesh nr 3 is less than 1 percent with double the number of elements between main frames and between longitudinal stiffeners. Mesh nr 3 is considered as being sufficient to perform the further analysis therefore with all next steps it will be taken for calculations.

3.5 Imperfection

This chapter as well as imperfection modeling requirements were written according to the guidelines and rules used by the classification society.

General

The first step of a nonlinear analysis is normally to define the shape of an initial imperfection. This is included to take into account possible residual stresses and initial deformations from the fabrication of the vessel. Additionally geometrical imperfection will, in most cases be needed to trigger the nonlinear response in a stiffened panel and is normally required to be able to assess the buckling strength of the panel using nonlinear finite element method.
When an imperfection is applied the structure may continue to deform in the prescribed shape as the loads increase. It may also snap over to a more preferred shape i.e. a shape requiring less energy (associated with less internal strain energy). Such mode snapping leads to unstable response and may give numerical instability and problems with convergence. In general it is therefore desirable to prescribe an imperfection shape similar to the preferred (critical) collapse mode of the panel. However it may be difficult to predict which mode requires the least amount of energy and for slender geometries this may also change throughout the deformation history.
When an imperfection is applied with a large magnitude more energy is required to change buckling mode. Thus if the magnitude is large the structure may be forced into a non-preferred conservative prediction of the capacity.
It is therefore important that the imperfection is carefully chosen both in terms of shape and amplitude. For buckling and ultimate strength analysis using nonlinear finite element method a small magnitude should be applied with a shape equal- or similar to the preferred collapse mode of the structure.

3.5.1 Imperfection tolerances

The magnitude of the imperfections should be determined using the imperfection parameters

defined below. For the plate field between longitudinals the value of the imperfections should be as follows:

$$\delta_{P0} = \frac{s}{200} \tag{3-13}$$

3.5.2 Imperfections in production

The amplitude of imperfections was chosen also regarding the production standard for ship structures. Acceptable limits for production imperfections in German shipyards are shown in the picture below.

BULGES

(Deviations from the straight lines)

Bulges in the plate panel

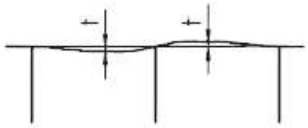

Seam sag

GROUP	AREA	BULGE DEPTH t [mm]		SEAM SAG t [mm]	
		(1)*	(2)*	(1)*	(2)*
Shell Plating	above waterline	4	7	5	9
	below waterline	4	7	5	11
Strength Deck and Superstructure Decks	free areas	4	6	5	10
	covered areas	7	9	7	10
Tween Decks		6	9	6	10
Superstucture and House Walls	exposed walls	4	6	4	6
	interior walls, visible within accomodation	4	6	4	6
	interior walls, outside accomodation	6	8	6	8
Deck House Tops	free areas	4	6	4	6
	covered areas	7	9	7	9
Double Bottom Walls		6	8	6	12
		6	8	6	10

(1)* in 95% of all cases
(2)* in 5% of all cases

Figure 51 Level of deformations in production in German shipyards

It was chosen that the amplitude of imperfections will not exceed 4,0 mm.

3.5.3 Imperfections modelled in LS-Dyna

Imperfections in the constructions were modelled in LS-Dyna software using inbuilt function. It was possible to implement local disruptions in the nodes coordinates to follow the wave pattern with given amplitude and wave length.

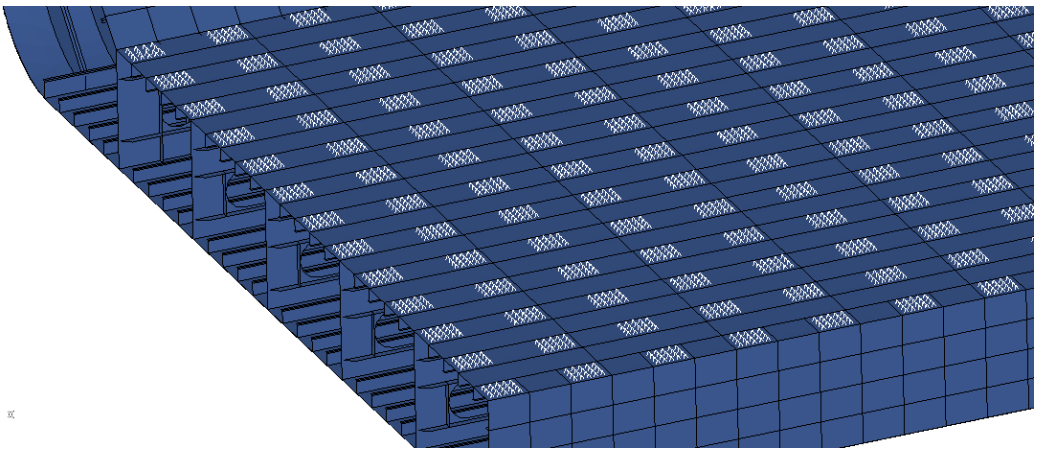

Figure 52 Set of nodes for the imperfection modelling

The wave shape was carefully chosen to preserve the continuity of deflection in the adjacent structures. The imperfections were modelled on the following structures with given value of amplitude:

- Double bottom plating – 2,8 mm (outer bottom plating thickness 22,0 mm)
- Side shell plating – 2,8 mm (plate thickness 17,5 mm)
- Side girders in double bottom – 2,5 mm (girders thickness 18,0 mm)
- Hopper tank plating – 2,8 mm (plate thickness 22,0 mm)

Imperfections modelled in the inner bottom plating is shown below.

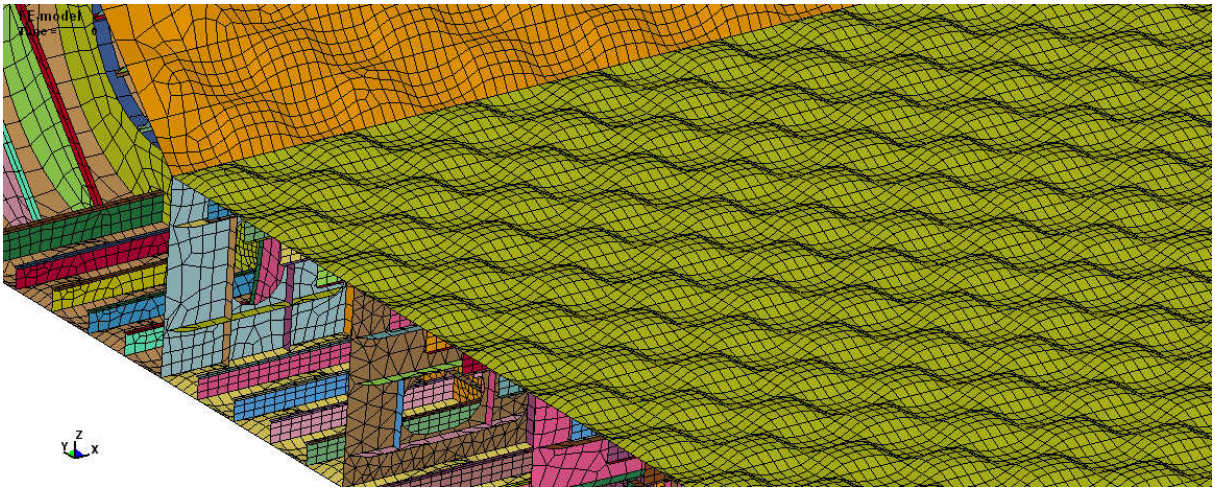

Figure 53 Imperfections on the inner bottom plating

Imperfections modelled in the outer shell plating in the bottom and side area.

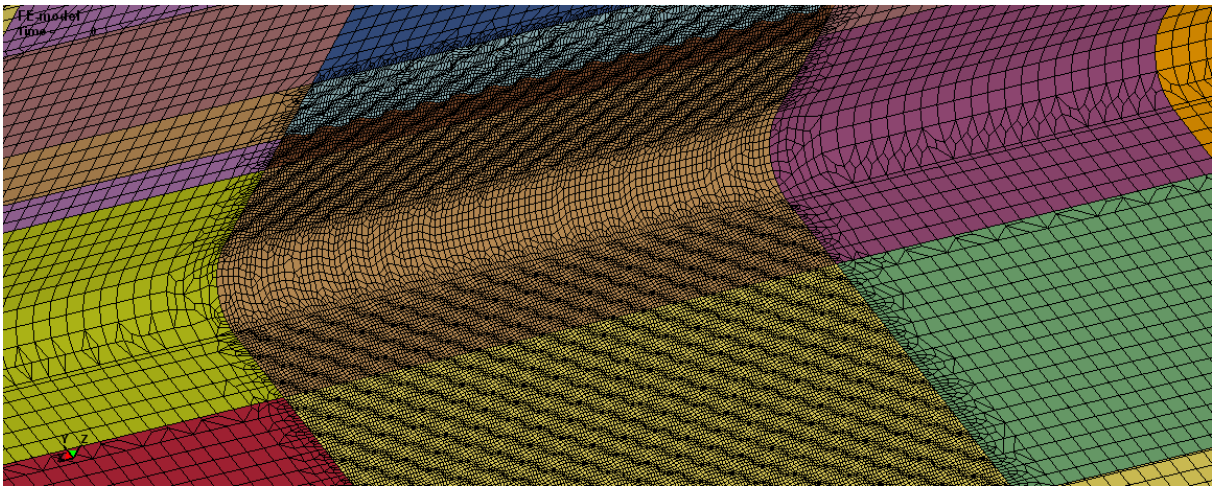

Figure 54 Imperfections on the outer shell

Imperfections modelled in the side girders in double bottom are shown below.

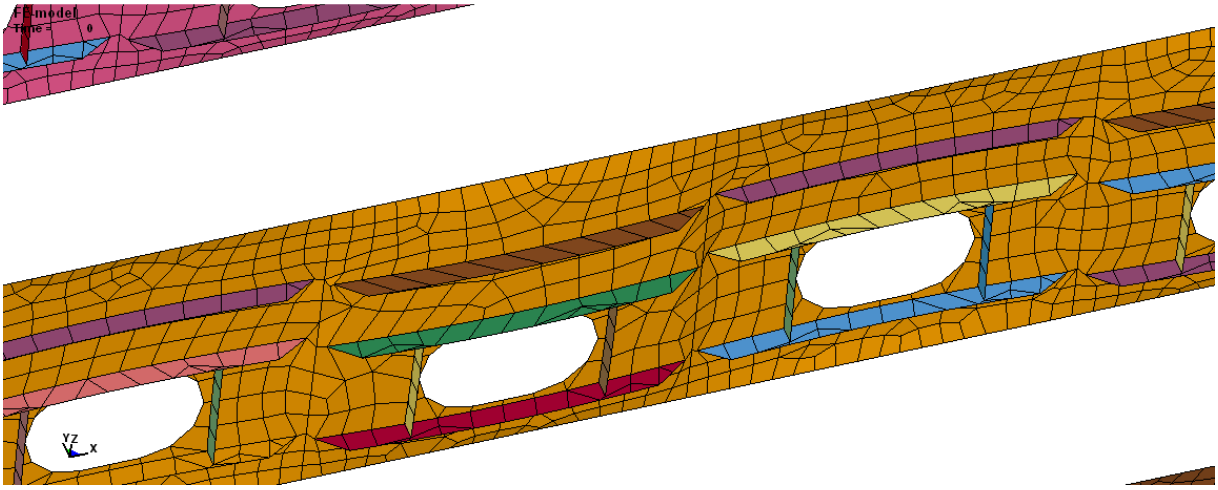

Figure 55 Imperfections on the side girders in double bottom

3.5.4 Results with imperfections

After imperfections were modelled the progressive collapse calculations were run. In the Fig.57 we can see the collapse form with existence of imperfections.

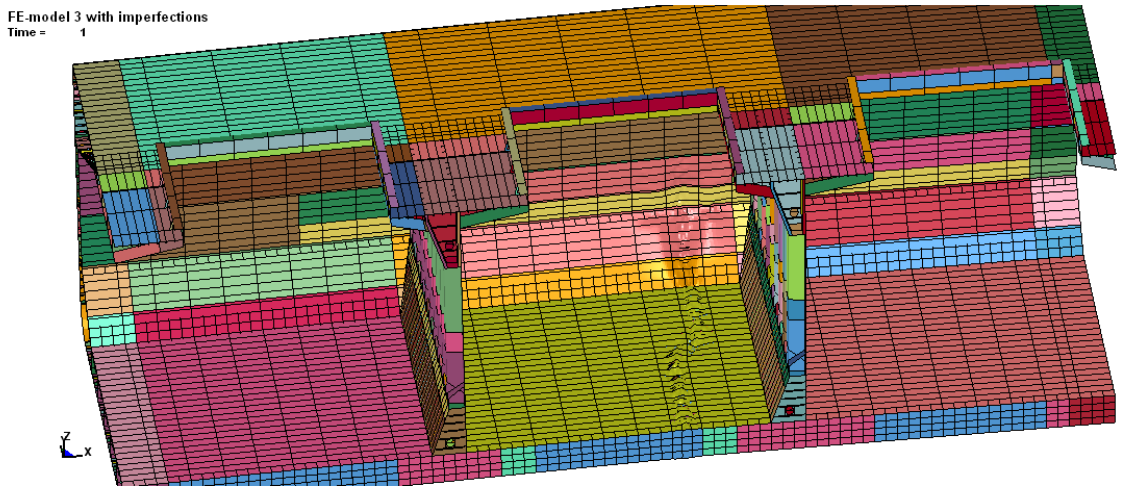

Figure 56 Collapse shape on the inner bottom

It can be seen that the place where collapse occurred and the shape of the buckling is slightly different than previously. The collapse shape on the outer bottom is shown below.

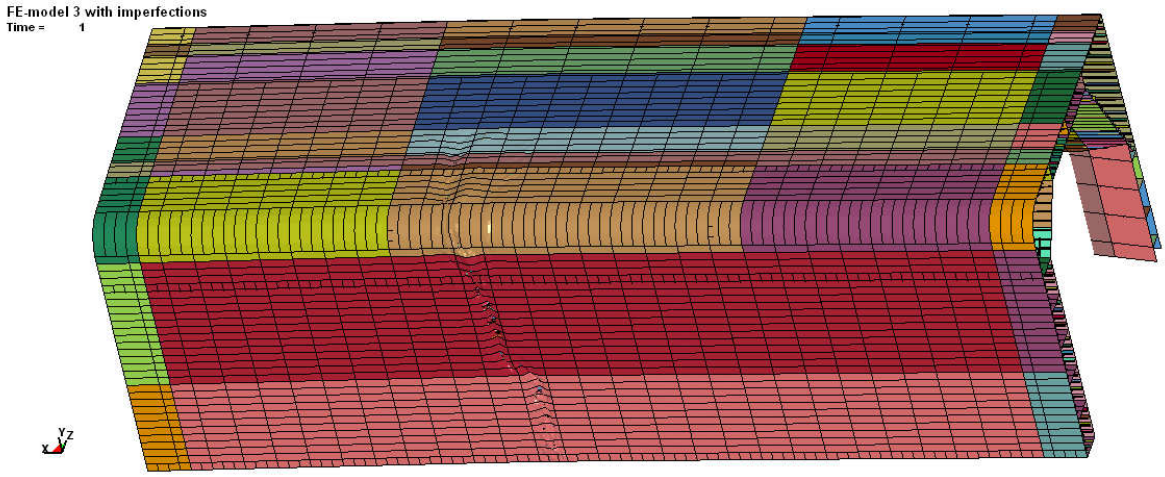

Figure 57 Collapse shape on the outer shell

Buckling of the side girders and longitudinal stiffeners in the double bottom is shown below.

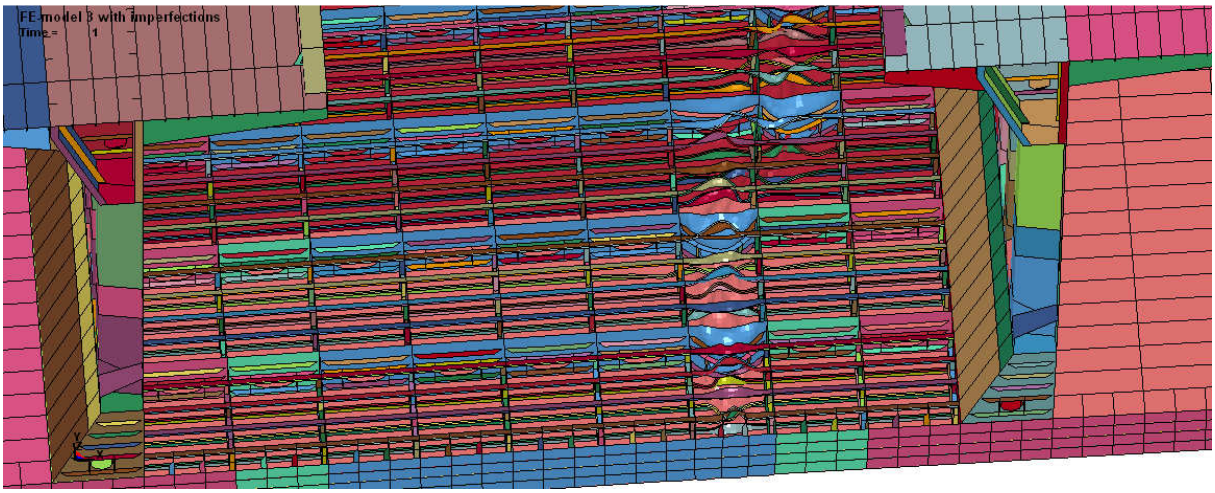

Figure 58 Deformation in the side girders in the double bottom

Progressive collapse curve for the model with imperfections is shown below.

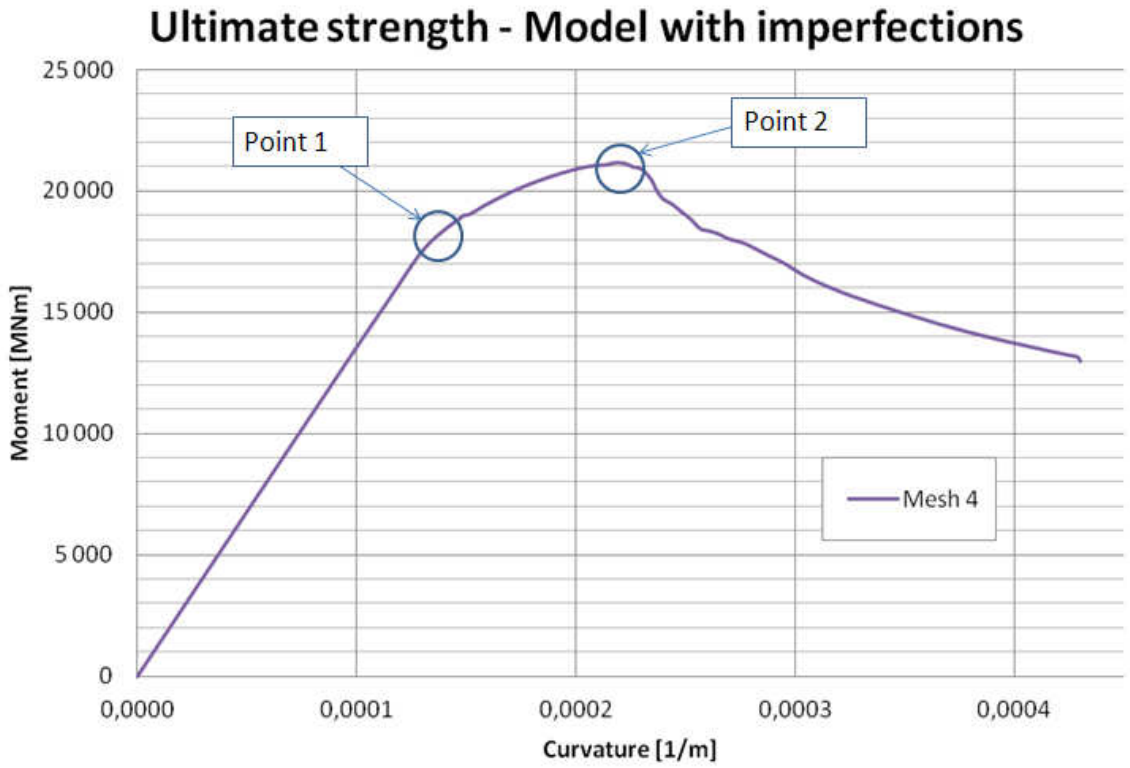

Figure 59 Progressive collapse curve for the mesh model with imperfections

The obtained ultimate moment is Mu = 21180 MNm.

The ultimate bending moment is a summation of the still water bending moment and a wave bending moment acting on the ship. The still water bending moment Msw is known and for the homogenous cargo distribution is equal 4300 MNm. It is assumed that the rest is the wave bending moment Mwv.

Mu = Msw + Mwv = 4300 MNm + 16880 MNm = 21180 MNm

The first yield was noticed for the hatch corners in the main deck, however the first plastic deformations in the analyzed area are registered for the side girders in double bottom for the Point 1 on the moment-curvature curve presented above. The picture of plastic strain is shown in the Fig.60.

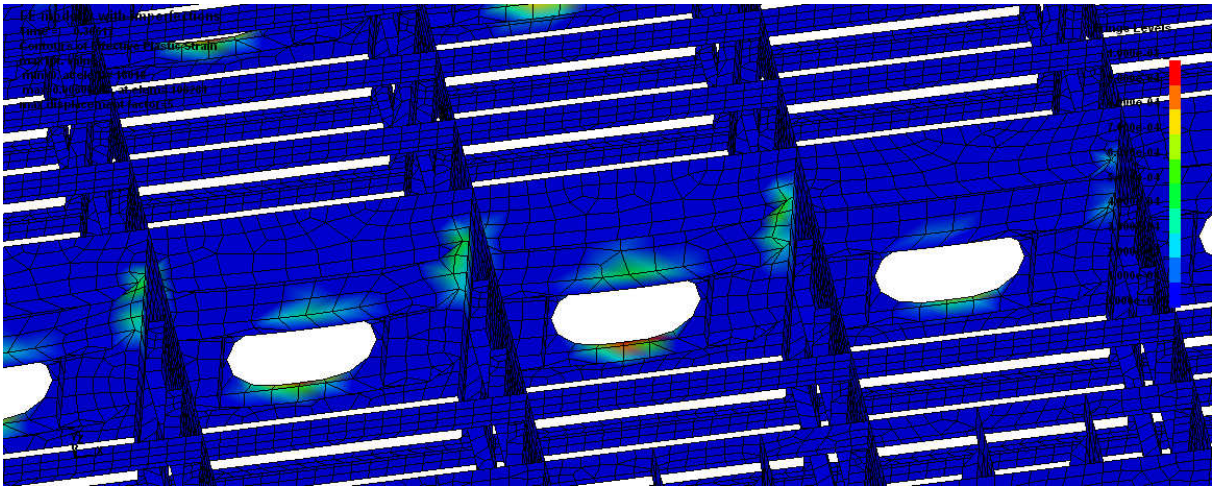

Figure 60 Plastic strain in the side girders in double bottom in Point 1

Next buckling occurred in the outer shell plating following the imperfections pattern. After buckling happened in the outer bottom longitudinal. The picture showing the plastic strain in the outer bottom plating in shown below.

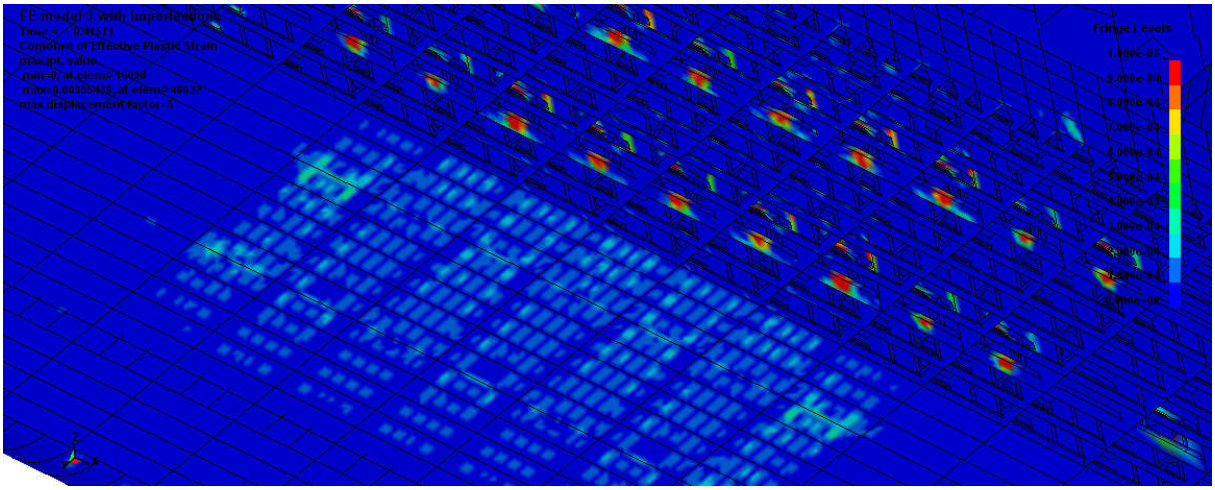

Figure 61 Plastic strain in the outer bottom plating for the curvature 0,00017 [1/m]

It can be seen that the level of plastic strain in the outer bottom longitudinals is lower than in the outer bottom plating.

Below we can see the plastic strain in the outer bottom plating for the Point 2 on the moment-curvature curve.

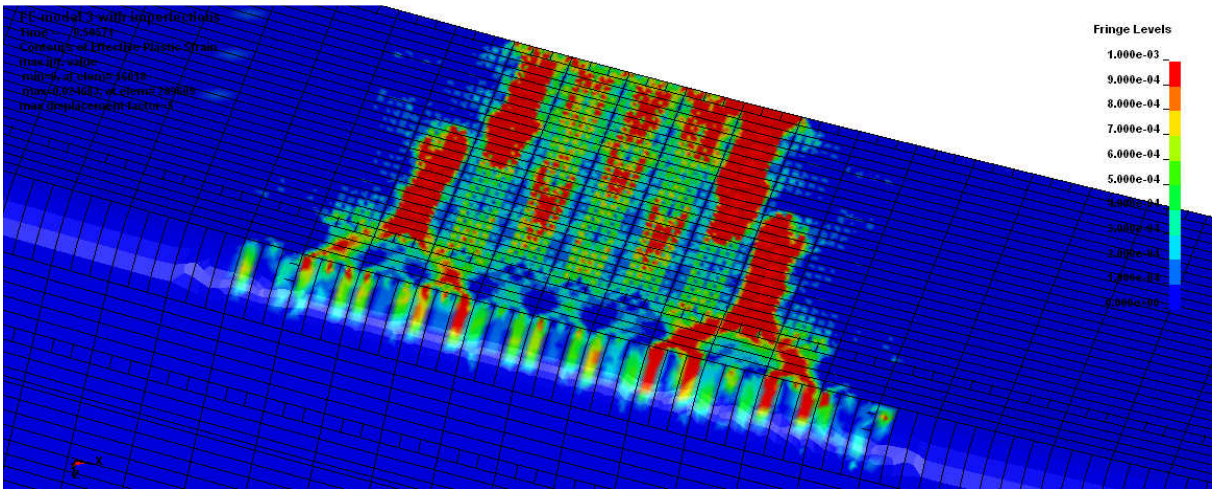

Figure 62 Plastic strain in the outer bottom plating for the Point 2

Plastic strain for the inner bottom plating in Point 2 is shown below.

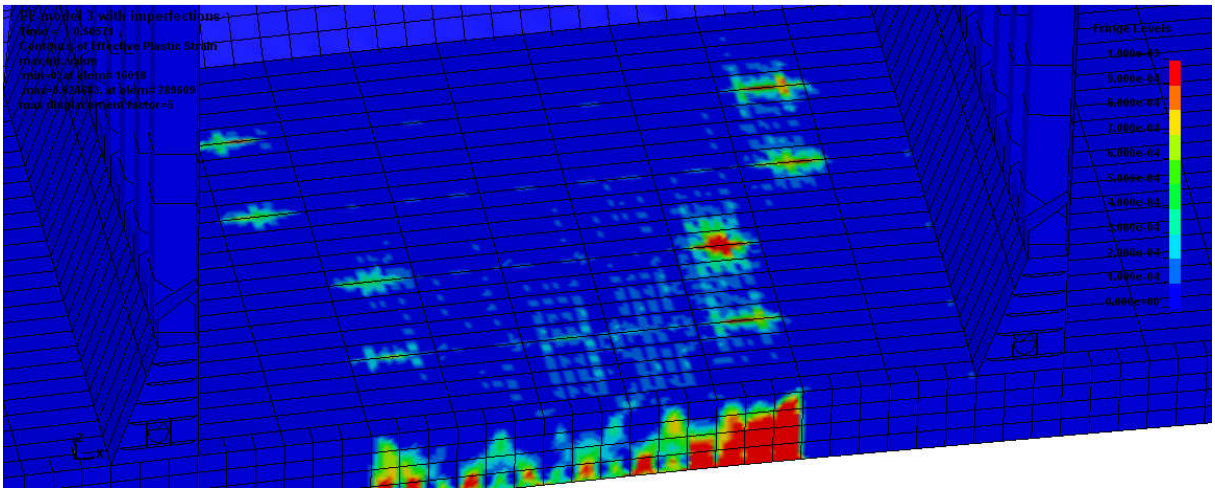

Figure 63 Plastic strain in the inner bottom plating in Point 2

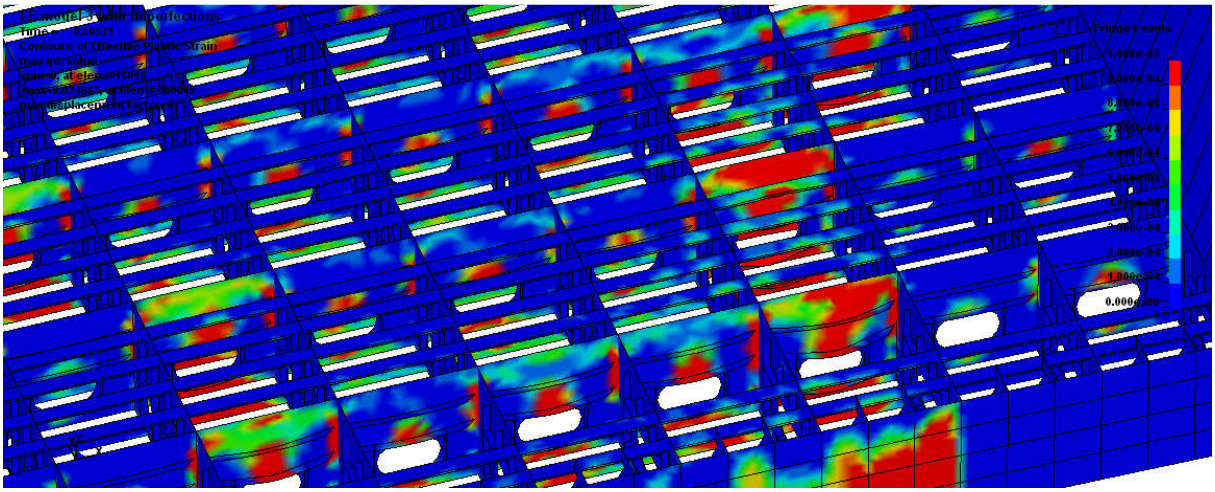

Figure 64 Plastic strain in the side girders in double bottom in Point 2

3.5.5 Comparison of the results with and without imperfections

The comparison of the results for different mesh qualities together with model with imperfections is shown below.

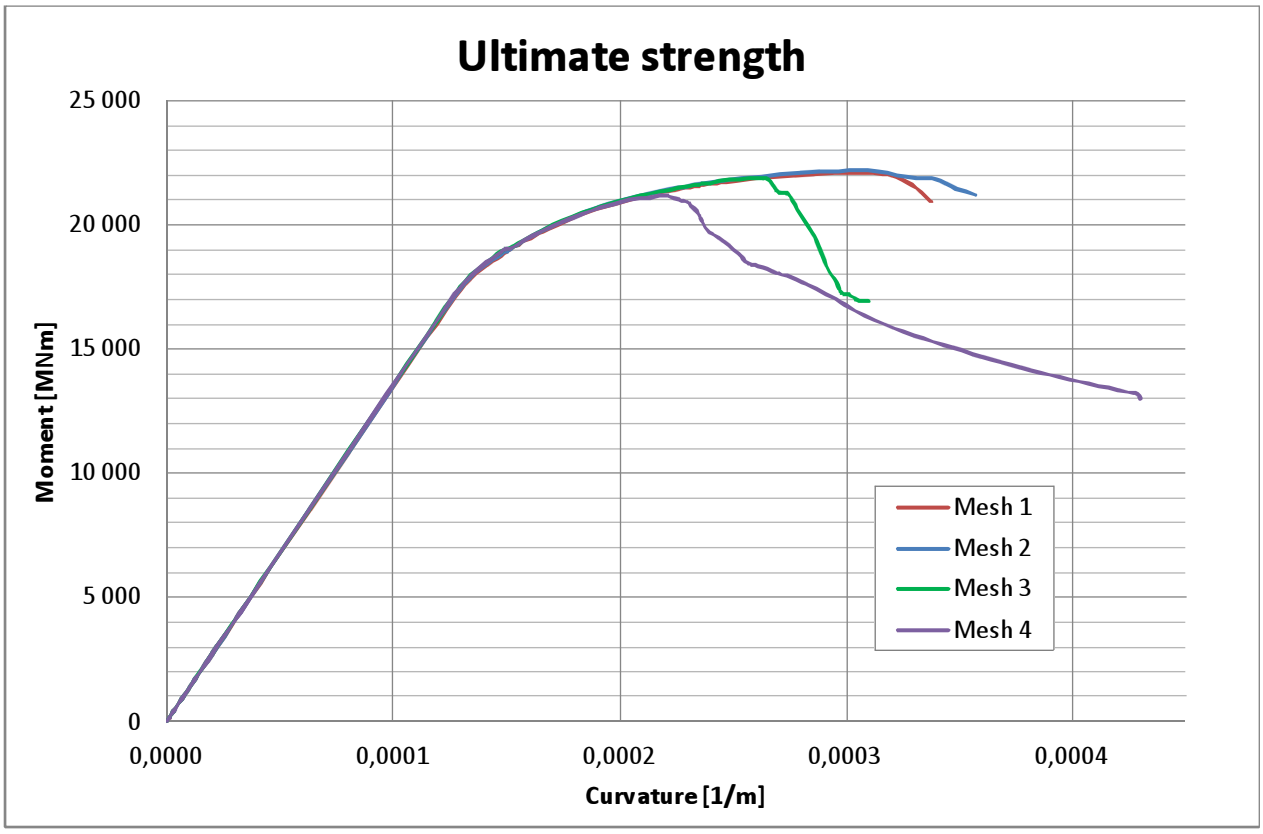

Figure 65 Comparison of the progressive collapse curves for different mesh models and with imperfections included

From the graph we can see that imperfections resulted in decrease of the ultimate bending moment capacity of the ship. The difference in the calculated moment is shown below.

Table 6 Comparison of the ultimate moment for mesh nr 3 and model with imperfections

	Maximum moment [MNm]	Difference [%]
Mesh model 3	21890	-
Mesh 4 (imperfections)	21180	-3,24

We can see noticeable difference in the obtained value of the ultimate bending moment. However the results are dependent on the modelled shape of the imperfections and assumed value of amplitude of the imperfections. For the further calculations model with imperfections is taken.

3.6 Load cases

To perform FE analysis of the structure under global and local loads the loading condition needs to be generated. The procedure of generating loads from the cargo as well as the static and dynamic sea loads is presented following the paper by Schellin et al. “Load Generation For Finite Element Analysis” of the book “Ship structural analysis and design” of Paik et al. 2010.

Classification society rules require the ship to withstand given global loads that subject the hull girder to given (rule-based) shear forces, bending moments and torsional loads. Accordingly, major classification societies publish guidelines that are specially suited for a structural analysis of ships. Generally, these guidelines are based on the equivalent regular wave approach to obtain load combinations relevant for dimensioning ship structure.

The interactive software package GL ShipLoad was developed as an aid to assess the global structural integrity of containerships. Using the equivalent regular wave approach, it constitutes the standard tool to generate rule-based loads for a global FE analysis. The global FE model of the ship’s structure serves as input, and nodal forces that can be applied to that same FE model are its output. Performing a structural analysis on this basis comprises several tasks, schematically presented in the Fig. 67.

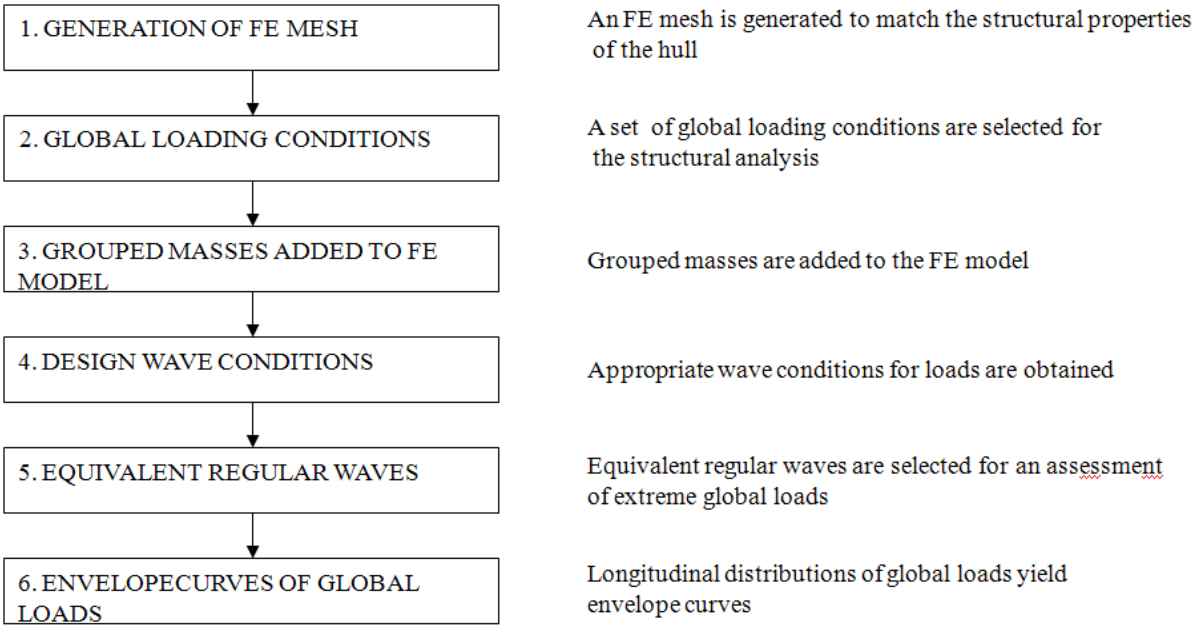

Figure 66 Generation of Loads in GL-ShipLoad

Step 1: An FE mesh is generated to idealize all major structural components, such as decks, transverse and longitudinal bulkheads, walls, floors, web frames, and shell plating.

Step 2: Global loading conditions are selected from load cases specified in the ship's stability booklet. One selected load case subjects the ship to the maximum allowable vertical still-water bending moment in hogging. Another load case subjects the ship to the maximum allowable vertical still-water bending moment in sagging or to the minimum allowable still-water bending moment in hogging. The distribution of containers for these two load cases causes the ship to float at its maximum displacement.

Step 3: To facilitate convenient access and reuse for different loading conditions, components of the ship's basic masses are typically grouped into assembled mass items made up of reusable mass components. These grouped masses are added to FE model.

Step 4: A large number of sea states, characterized by different wave heights, wave lengths, and wave headings are investigated systematically for a realistic representation of wave-induced loads. Containerships, having a high deck opening ratio, may need special consideration because load conditions in oblique seas often are decisive from a structural strength point of view. In such cases, it is not enough to separately analyze vertical, horizontal, and torsional hull girder loads; such effects have to be combined in a phase correct manner to achieve realistic design loads. A strip theory-based code solves the linear problem of a ship advancing at constant speed in waves, considering a sufficiently wide range of wave frequencies and wave headings. Viscous roll damping is added and hydrodynamic pressures in finite amplitude waves are corrected according to Hachmann (1986). The resulting pressures for rule-based equivalent regular (design) waves are generally specified for a lower probability level of about 10^{-6}, which is less than the probability level of 10^{-8} for extreme loads. These resulting pressures are integrated to obtain nonlinear pseudo transfer functions of wave-induced global loads. Generally, these computations, one or more dominant load parameters (DLPs) are usually specified by the classification society to represent design wave loading conditions.

Step 5: From a large number of sea states, a smaller number of regular equivalent design waves are selected which subject the hull girder to the required design loads. For head and stern wave cases, the selected wave heights subject the hull girder to rule-based bending moments. For other wave headings, wave length, wave phase, and roll angle are systematically varied, such that the resulting equivalent regular design waves subject the hull girder to the other global design loads, such as shear forces torsional moments. For each wave, some 50 different equidistant wave phases are considered to assess critical loads for maximum values.

Step 6: The longitudinal distributions of global loads result in envelope curves.

The resulting pressures and inertial forces corresponding to the design load cases are transferred as nodal forces to the FE model, ready as input for the structural analysis of hull components.

Load groups

In GL Shipload all loads for each load case comprise a linear combination of load groups. This loads to an efficient storage of loads for many different wave conditions. Loads on the hull structure result from acceleration of masses (inertia loads) and from external (hydrostatic and hydrodynamic) pressures of the surrounding water. Loads applied to the FE model for each load case are sorted into the following load groups:

1. Hydrostatic buoyancy loads
2. Static weight loads
3. Static tank loads
4. Six inertial unit load groups, resulting from three translational and tree rotational rigid body accelerations of all masses except tanks
5. Six inertial unit load groups, resulting from three translational and tree rotational rigid body accelerations of tanks(Tanks are grouped separately because the fluid distribution inside the tanks depends on the ship’s floating position.)
6. One hydrostatic load group for each selected wave pressure distribution

Any load case applied to the FE model is a combination of these load groups. Combining the first three load groups yields balanced hydrostatic load cases. To obtain balanced hydrodynamic load cases, factors for unit load groups are computed, based on the condition that no residual forces and moments remain when combining hydrostatic and hydrodynamic load groups. These factors represent rigid body accelerations. For any chosen load case, longitudinal distributions of sectional forces and moments are immediately displayed.

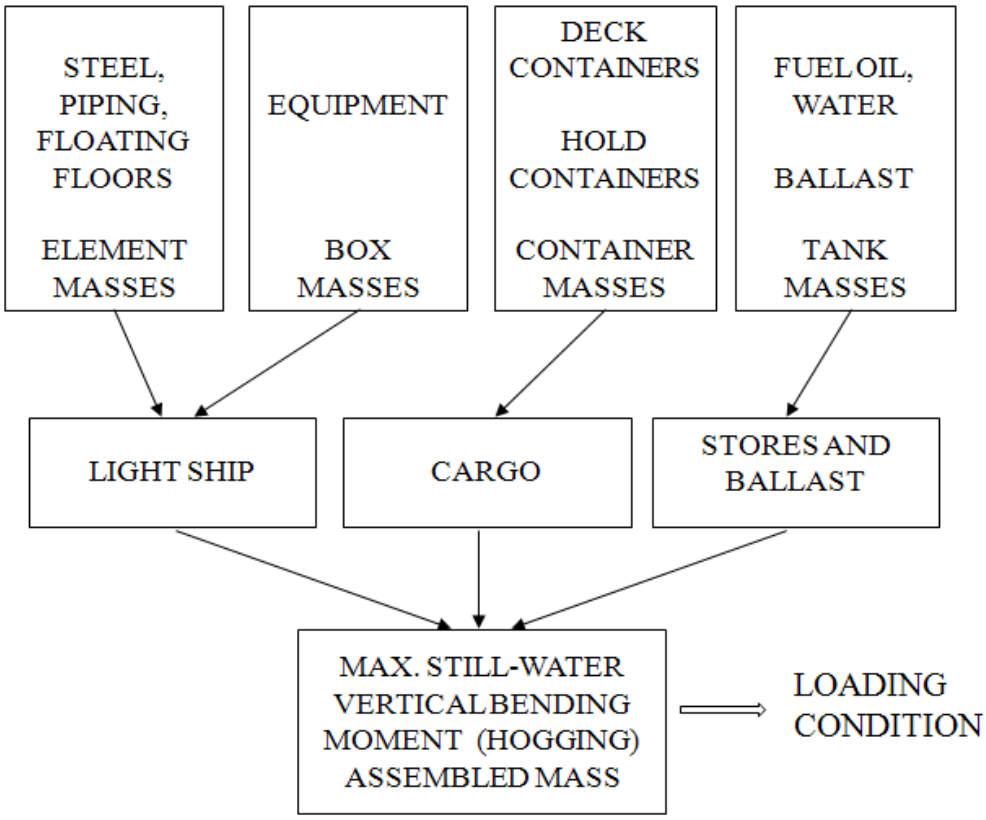

Figure 67 Definition of masses in GL-ShipLoad

Load Cases

The determination of load cases used for the finite element analysis is based on loading conditions, critical load parameters, and wave conditions. Both static and dynamic loads are included. The former are modeled quasi-statically as the product of the mass involved and the local acceleration. Using these loads, the finite element analysis determines the resulting stresses in the hull structure. In assessing dynamic loads, it is necessary to consider a range of sea conditions and headings that produce a critical response of the structure. Typical critical wave load cases for a strength analysis are: wave hogging, wave sagging, oblique wave and rolling.

In this work only wave hogging is considered as critical hence only hogging condition for the vertical bending moment will be included in the calculations.

The ultimate strength is checked for the following set of wave heights:

Load case 1: Wave height 13 meters,

Load case 2: Wave height 15 meters,

Load case 3: Wave height 20 meters,

In all mentioned conditions alternate cargo loading is considered.

3.6.1 Local loads plus vertical bending moment methodology

To perform the progressive collapse analysis with influence of local loads the following procedure in solver will be realized. First static loads from water pressure and cargo distribution will be applied. The values will grow incrementally to reach the maximum values. Next step is to add water wave loads. The final bending moment acting on the structure has to be according to the bending moment distribution given for the specific loading condition from the GL-Shipload.

Pressures acting on the ship for the given loading condition are mapped on the structure. To represent the bending moment on the structure two pilot nodes are used on both ends of the model. The specific value of rotation is applied to obtain the bending moment distribution.

3.6.2 Results reading planes – load cases

The results of the calculations for the vertical bending moment with influence of local loads are written for five sections along the model. Since water pressure and cargo loading is changing for different points and cargo holds the expected results should vary for different measurement planes. The interesting results are those given by the section plane in the middle cargo hold.

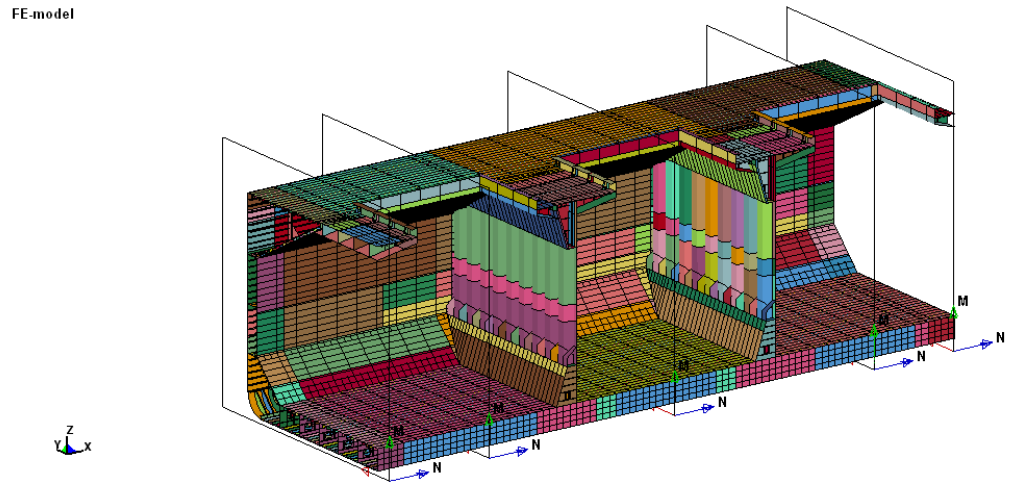

Figure 68 Results reading planes

The reading planes are localized at the following positions:

- Frame 109 + 600 mm (89,60 m from APP)
- Frame 124 + 600 mm (102,50 m from APP)
- Frame 152 + 600 mm (126,60 m from APP)

- Frame 182 + 600 mm (152,40 m from APP)
- Frame 194 + 600 mm (162,80 m from APP)

3.6.3 Still water bending moment

The still water bending moment distribution along the hull is given from the GL-Shipload. The graph for the alternate loading condition is shown below. The change of the shear forces and bending moments in different sections due to cargo loading can be noticed.

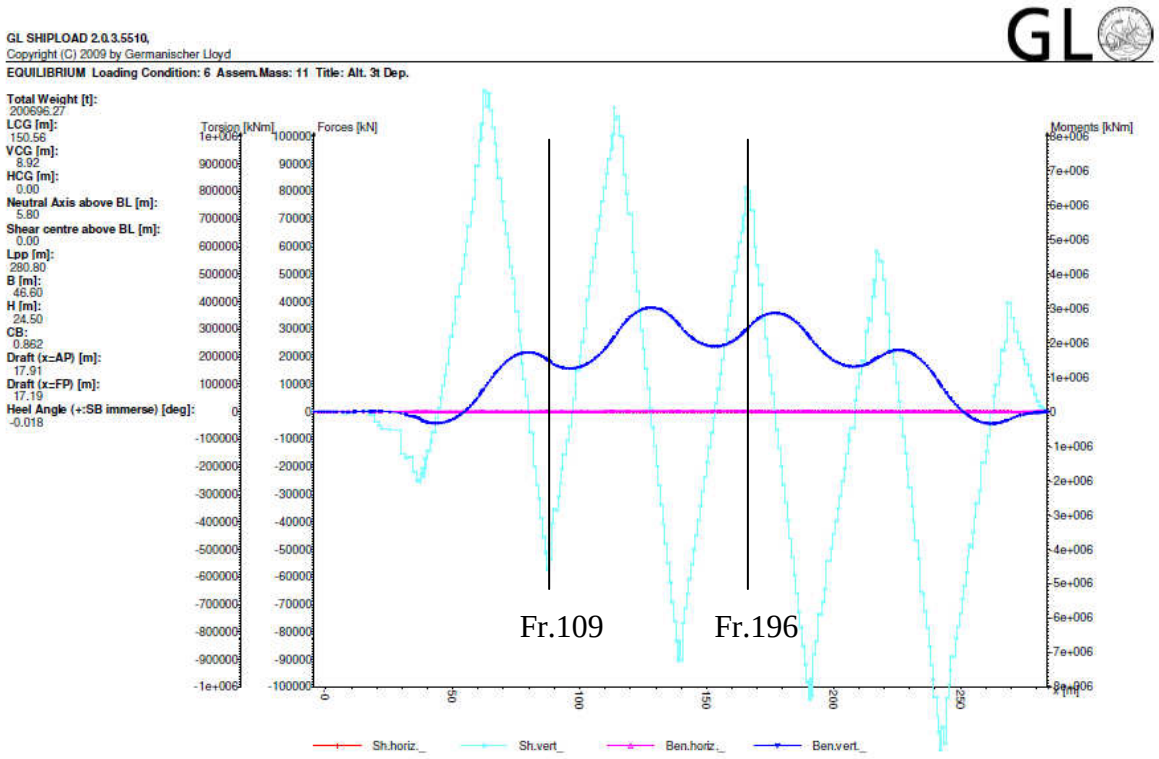

Figure 69 Shear forces and bending moment distribution in the still water for the alternate cargo loading

Maximal still water bending moment acting on the hull is Ms = 3100 MNm.

3.6.4 13 m wave

The graph from GL Shipload showing distribution of the bending moment and of the shear forces along the hull. The values here are given for the wave amplitude of 13 meters including alternate loading condition. The vertical lines shows the extent of the model.

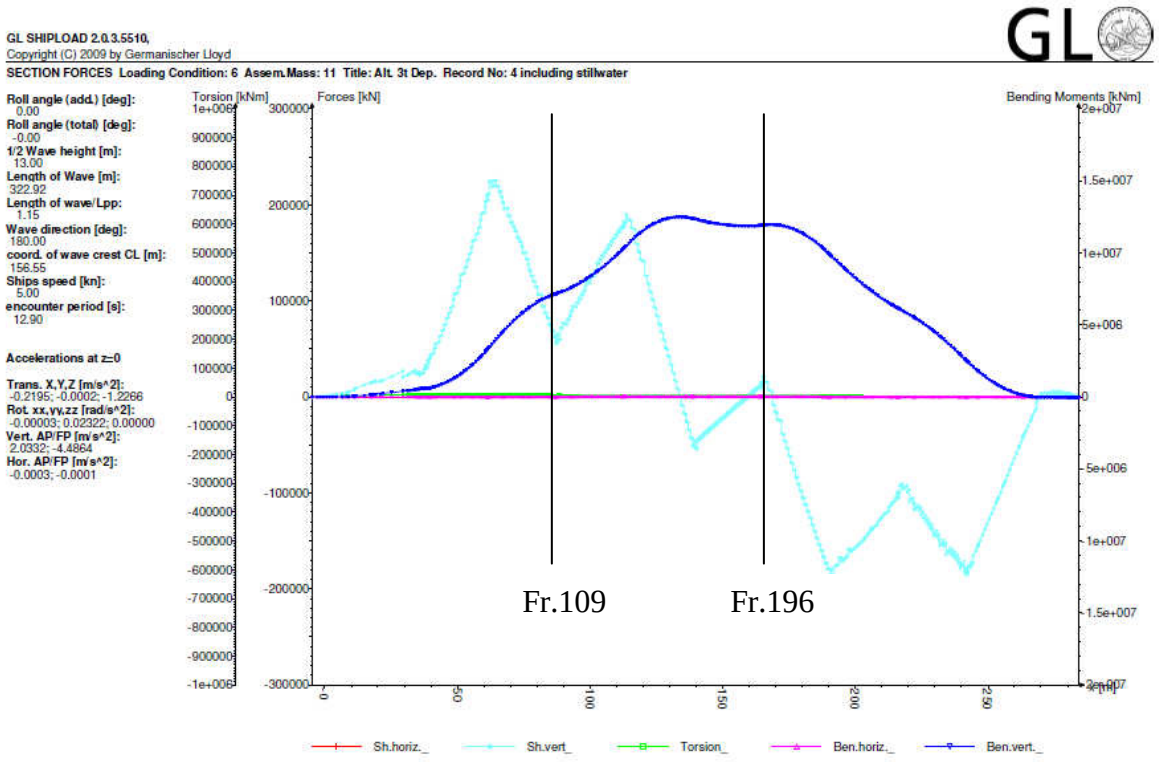

Figure 70 Bending moment and shear forces distribution for the 13 meter wave

After running the calculations the following graph was obtained. It is clearly seen the different phases of applying loads on the construction. Even though the maximum values of loads for this loading condition were applied the collapse was not reached.

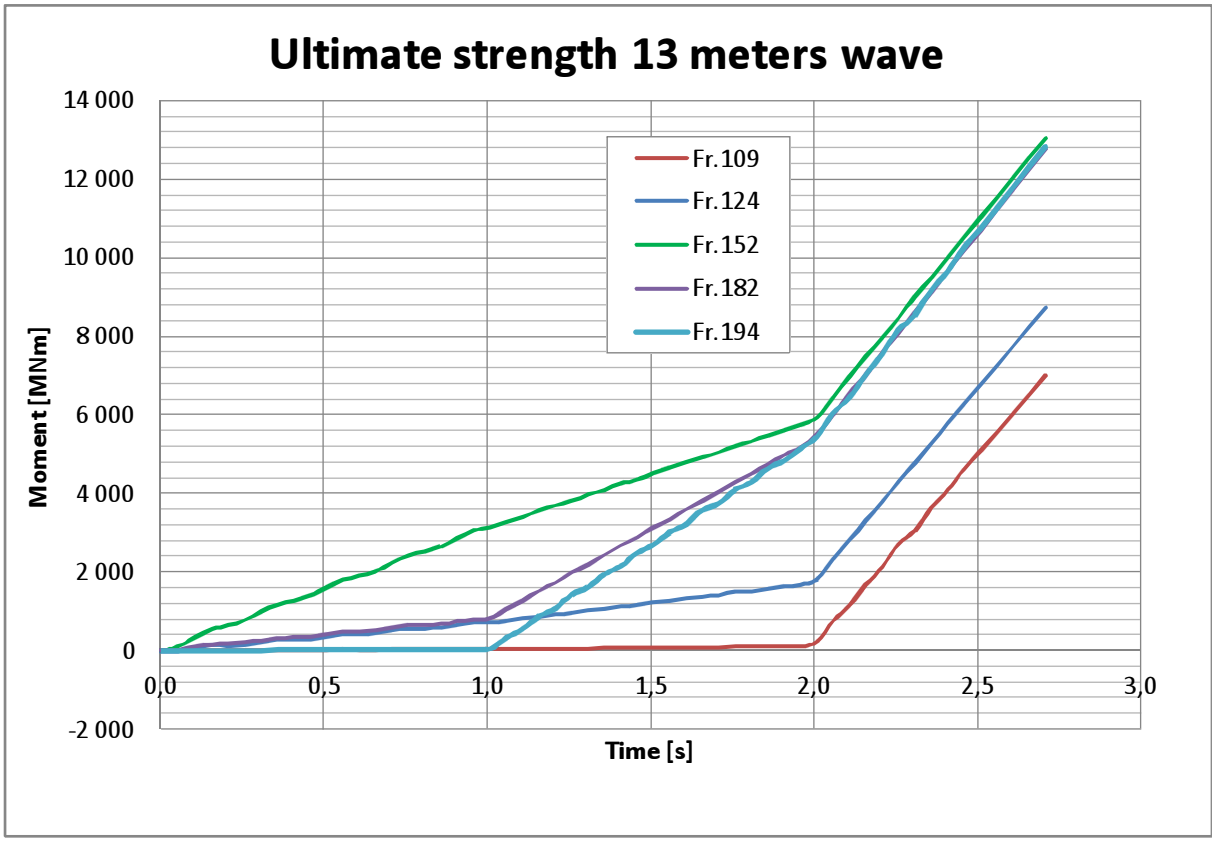

Figure 71 Moment acting on construction with increase of generated loads

The global and local hull deflection is shown in the picture below.

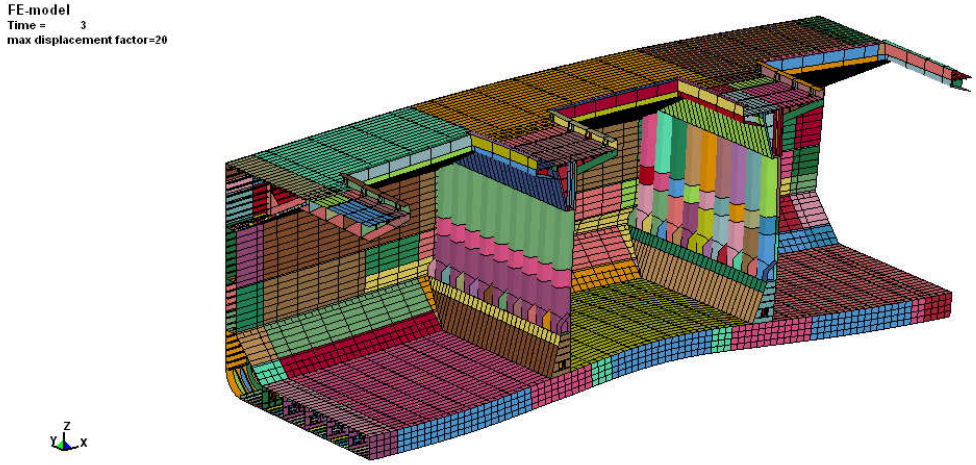

Figure 72 Deformations in construction, scale factor 5

The Von Misses stresses distribution in the outer shell bottom plating. The level of the stresses in the middle cargo hold in some places reaches yield strength.

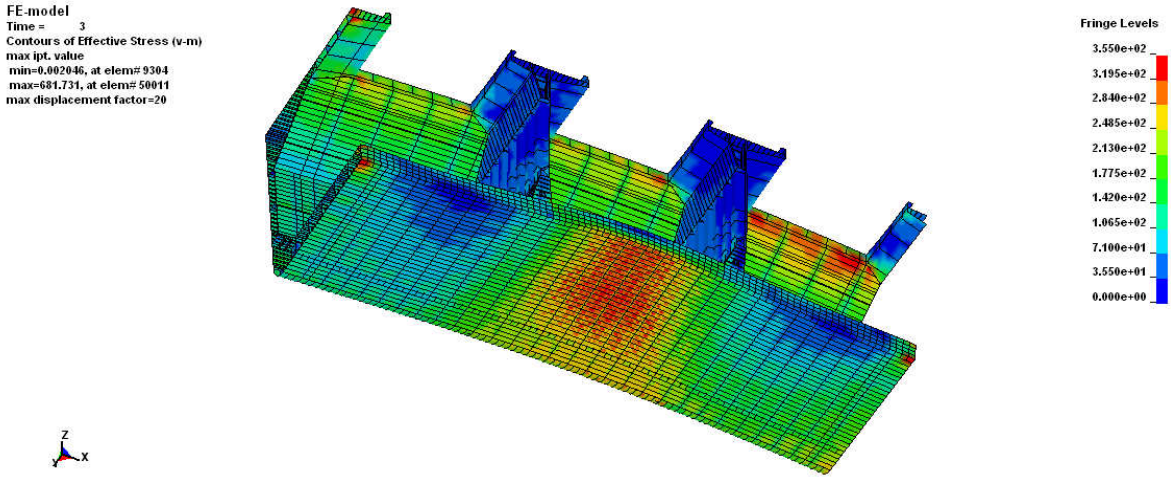

Figure 73 Distribution of Von Misses stresses in the outer bottom plating

Level of stresses in the inner bottom plating is relatively low.

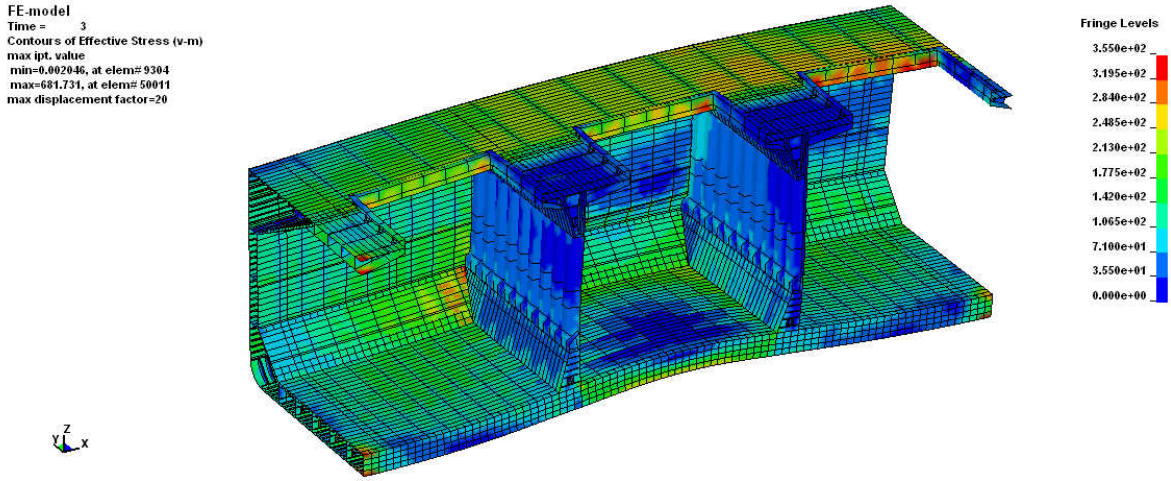

Figure 74 Distribution of Von Misses stresses in the inner bottom plating

3.6.5 15 m wave

The second loading condition analyzed for the ultimate strength of the hull is the wave of 15 meters height in the hogging condition with the alternate loading in the cargo holds. The distribution of the bending moments and shear forces is shown in the Fig.75.

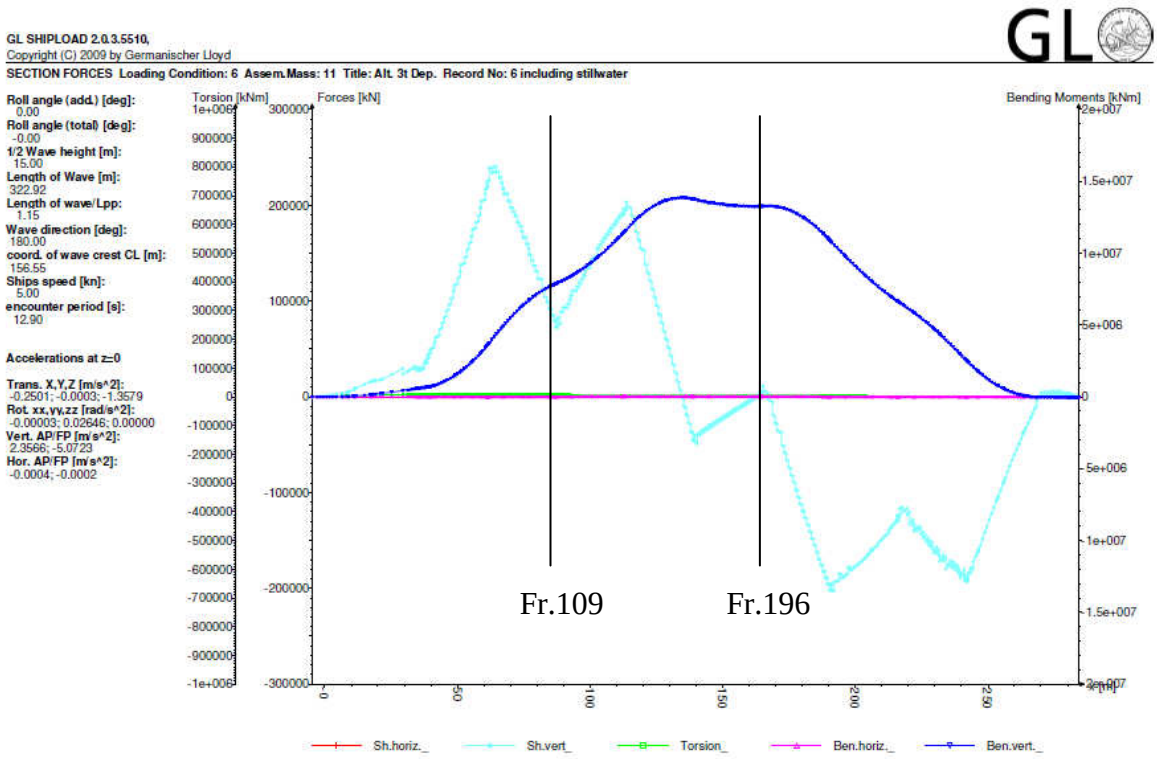

Figure 75 Bending moment and shear forces distribution for the 15 meter wave

After running the calculations we can see the increase of the resultant moment acting in different locations along the model. Even though the value of the moment in step three was increased, the collapse of the structure was not reached.

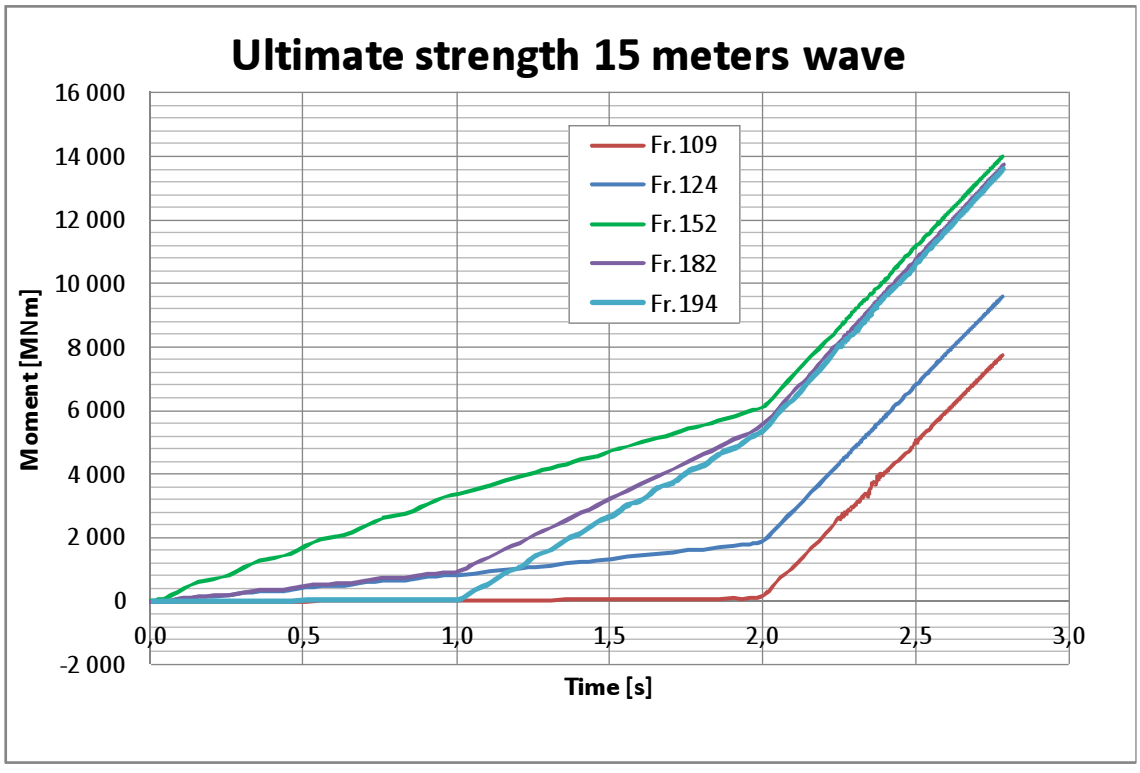

Figure 76 Moment acting on construction with increase of generated loads

3.6.6 20 m wave

Third loading condition taken into consideration includes alternate loading in cargo holds with wave of amplitude equal 20 meters. The graph showing bending moments and shear forces is shown below.

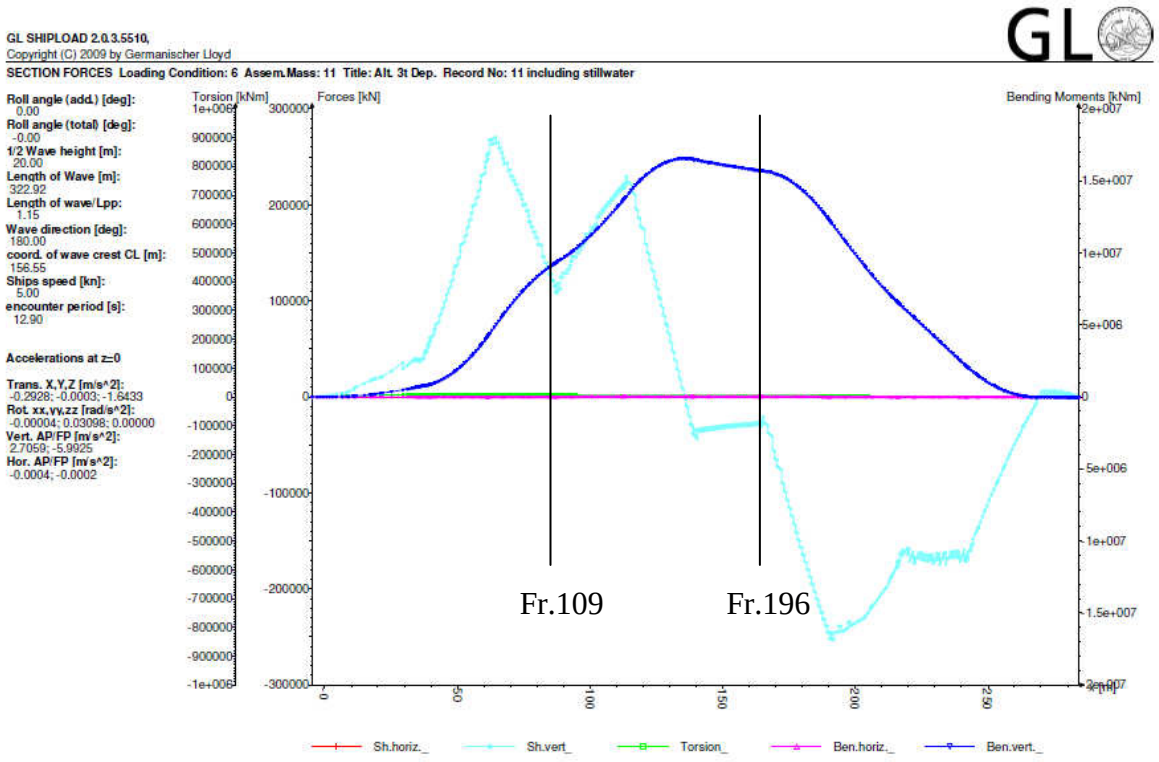

Figure 77 Bending moment and shear forces distribution for the 20 meter wave

The applied rotation was further increase to reach the collapse. The highest acting moment was obtained in the middle cargo hold.

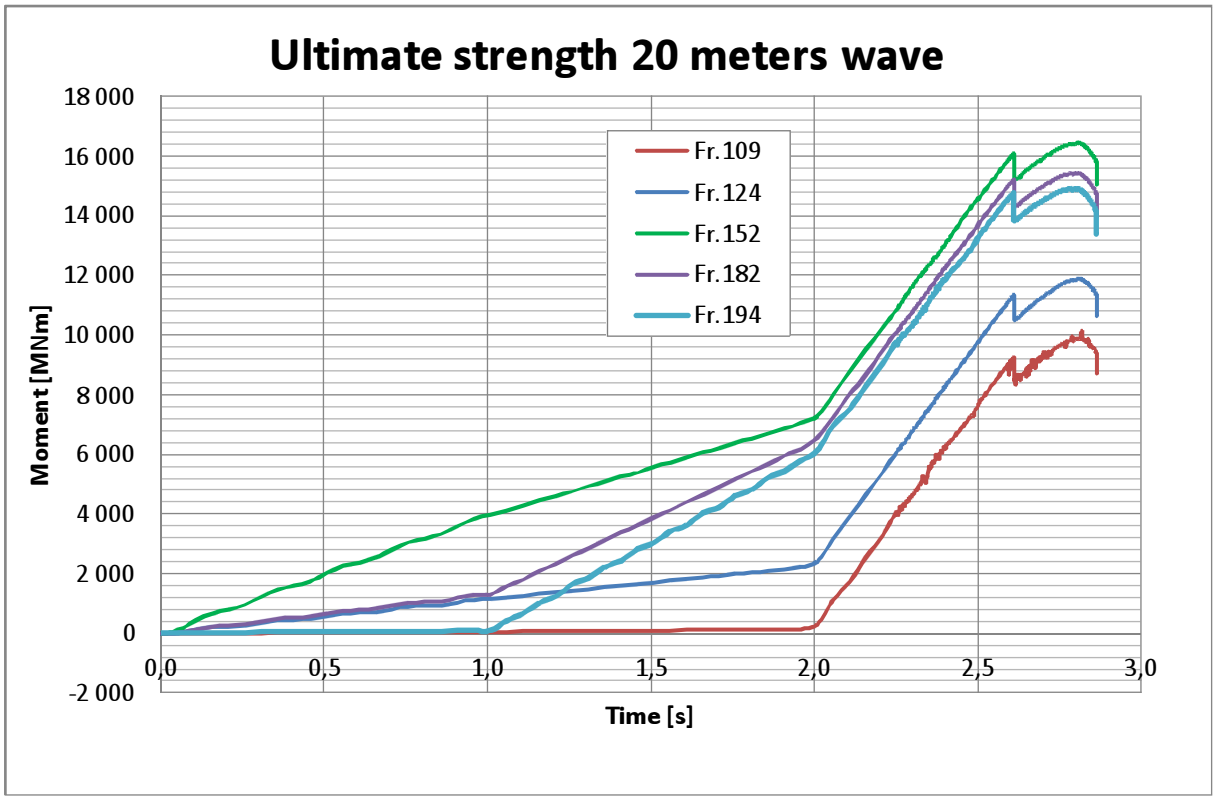

Figure 78 Progressive collapse curve for the 20 meter wave

The maximum obtained value of the moment is Mu = 16460 MNm.

From the still water bending moment distribution for the alternate loading condition the value of the Ms is 3100 MNm. Therefore ultimate moment can be written as shown below:

Mu = Ms +Mwv = 3100 MNm + 13360 MNm = 16460 MNm

For the pure bending moment acting on the hull for the homogenous cargo distributionwas obtained:

Mu = Ms + Mwv = 4300 MNm + 16880 MNm = 21180 MNm

Therefore the significant reduction in the hull girder capacity is observed due to the bottom bending effect.

The Von Misses stress distribution in the modelled part of the hull is shown in the Fig.80. It can be seen that significant part of the deck reached yielding. Value of stresses in the inner bottom outside the middle cargo hold is still at the lower level.

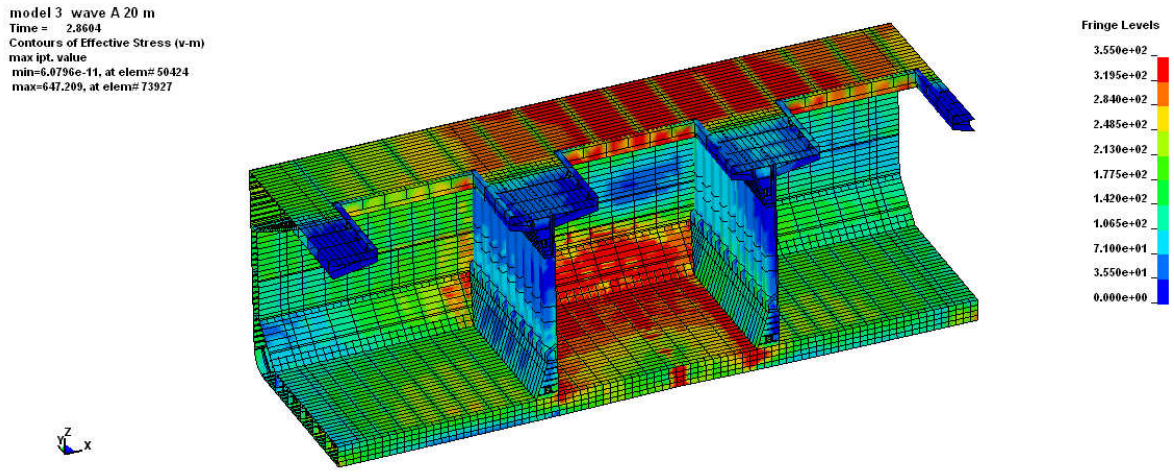

Figure 79 Distribution of Von Misses stresses in the inner bottom plating

The distribution of Von Misses stresses on the outer bottom plating shows high concentration of stresses in the region there collapse occurred. We can also see that stresses in the area of the holds with cargo are at the lower level.

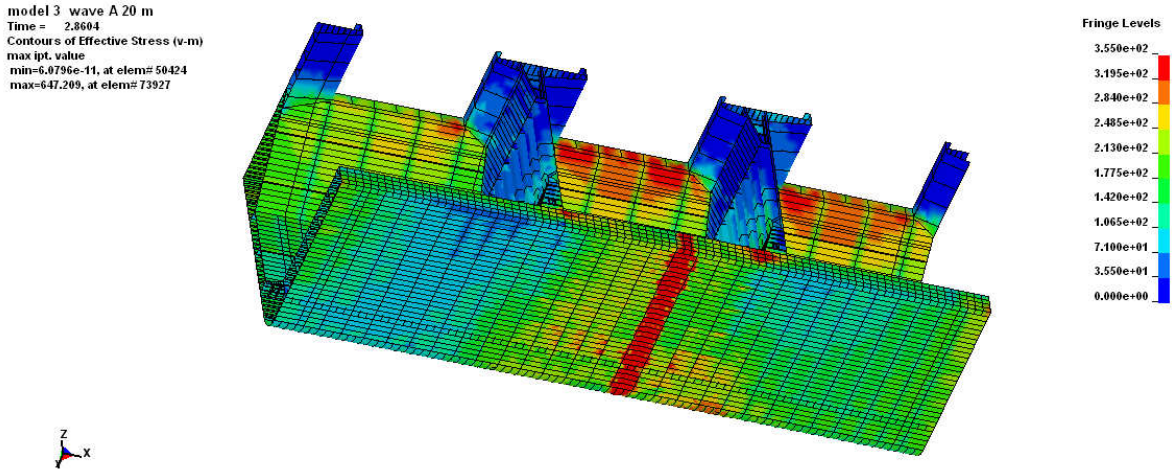

Figure 80 Distribution of Von Misses stresses in the outer bottom plating

Distribution of stresses in the bottom side girders is shown below.

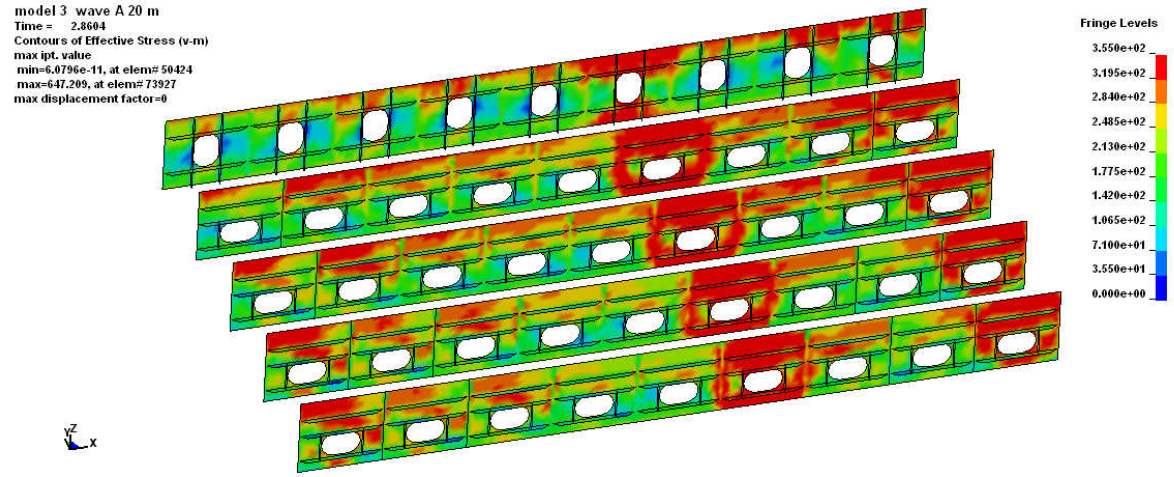

Figure 81 Distribution of Von Misses stresses in the side girders in the double bottom

The picture of the outer bottom deflections shows the picture where the collapse happened as well as that the outer bottom plating starts to buckle following the imperfections pattern in adjacent region.

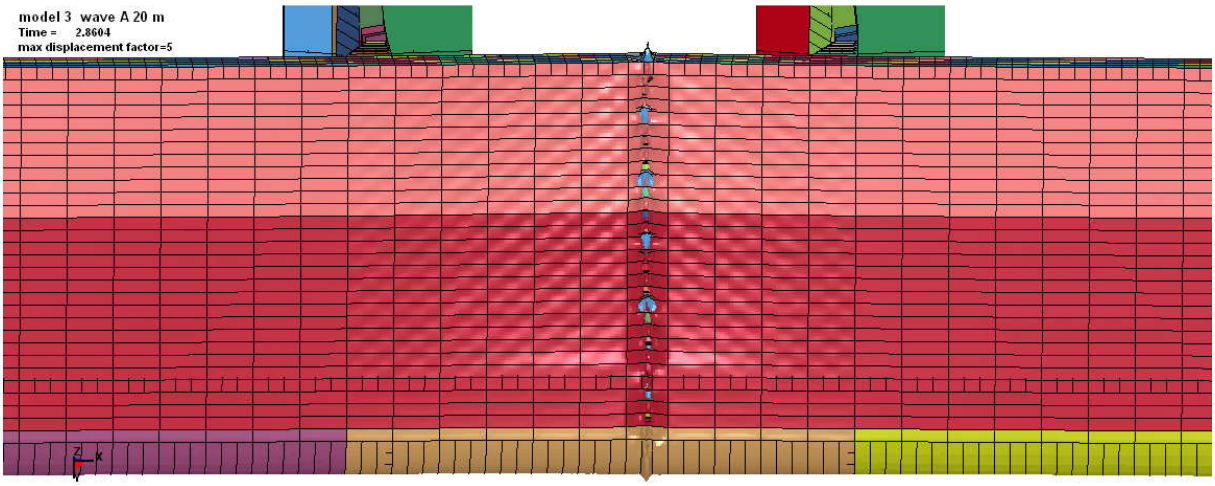

Figure 82 Deformation of the outer bottom structure

4. CONTAINER SHIP – FINITE ELEMENT MODEL

Performing analysis of the container ship followed similar approach as with the bulk carrier. Some parts common for both models like chosen coordinate system or shell element modelling are presented in the chapter concerning bulk carrier.

4.1 Structure modelling

Similar as in case of analyzed bulk carrier, container ship model was done in Ansys Workbench 14, Design Modeller module. All the elements were modelled as shell elements with constant thickness in all directions. The details considering the scantlings of the main structural members were kept. The container ship model in Ansys is shown in the Fig.84.

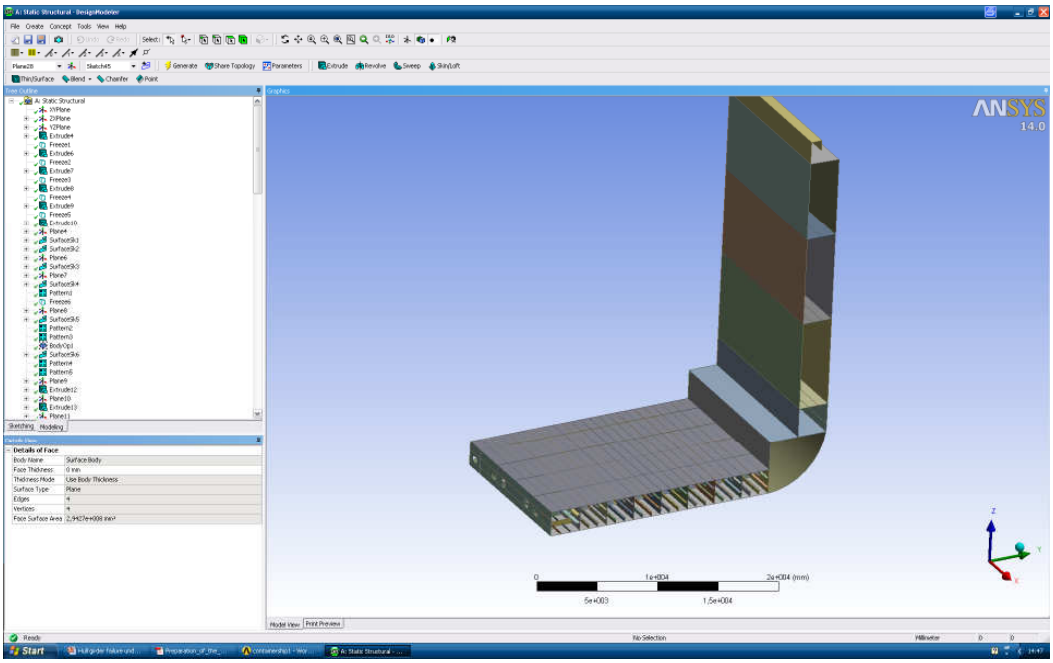

Figure 83 Generation of the container ship model in Ansys Workbench, Design Modeller

Details of the construction in the bilge and double bottom area are shown in the picture below.

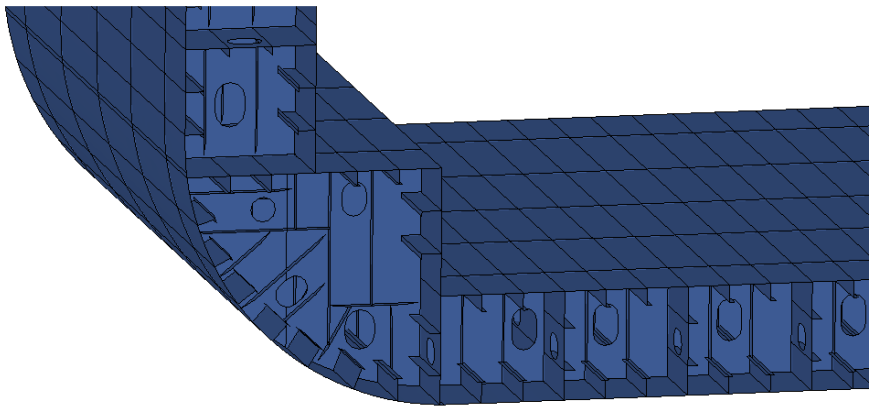

Figure 84 Structural details of container ship model

4.1.1 Initial container ship model

Initially it was planned to perform global and local analysis of the container ship on the relatively big model consisting of five cargo holds and six bulkheads. The goal was to represent the loads from the water pressure and cargo distribution on the bigger extent to minimize the influence of the boundary conditions at the ends and to obtain very realistic results. Therefore the model of the container ship was made in the Ansys Workbench, Design Modeller module. Structural members were modeled with respect to the construction drawings, keeping the detail level including plate stiffening flat bars and brackets in crucial locations. The initial model of the container ship is shown below.

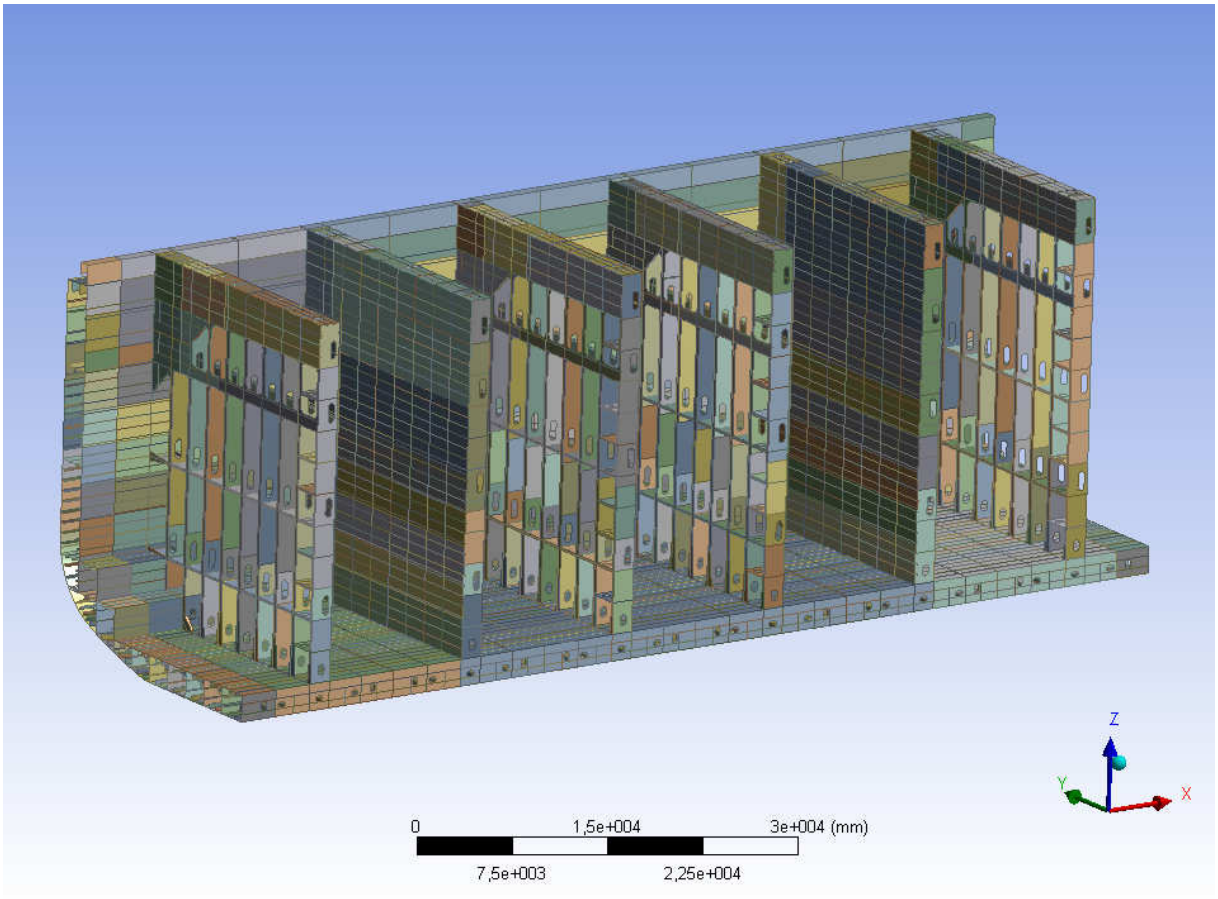

Figure 85 Initial container ship model

The built model after divisions to apply different material properties consisted around five thousands of structural elements. Such big model was not easy to handle by Ansys software which was a new experience. Even thought modeling is relatively intuitive and changes to the model can be easily applied, with models of such sizes time needed to perform single operation is significantly increased.

Next step was to generate a mesh on the built model. Initial mesh was generated with respect to requirements for the mesh density. Limitations of the computer capacity required manual definition of mesh parameters in different model regions to reduce the model size. The initial mesh on the container ship model is shown in the picture below.

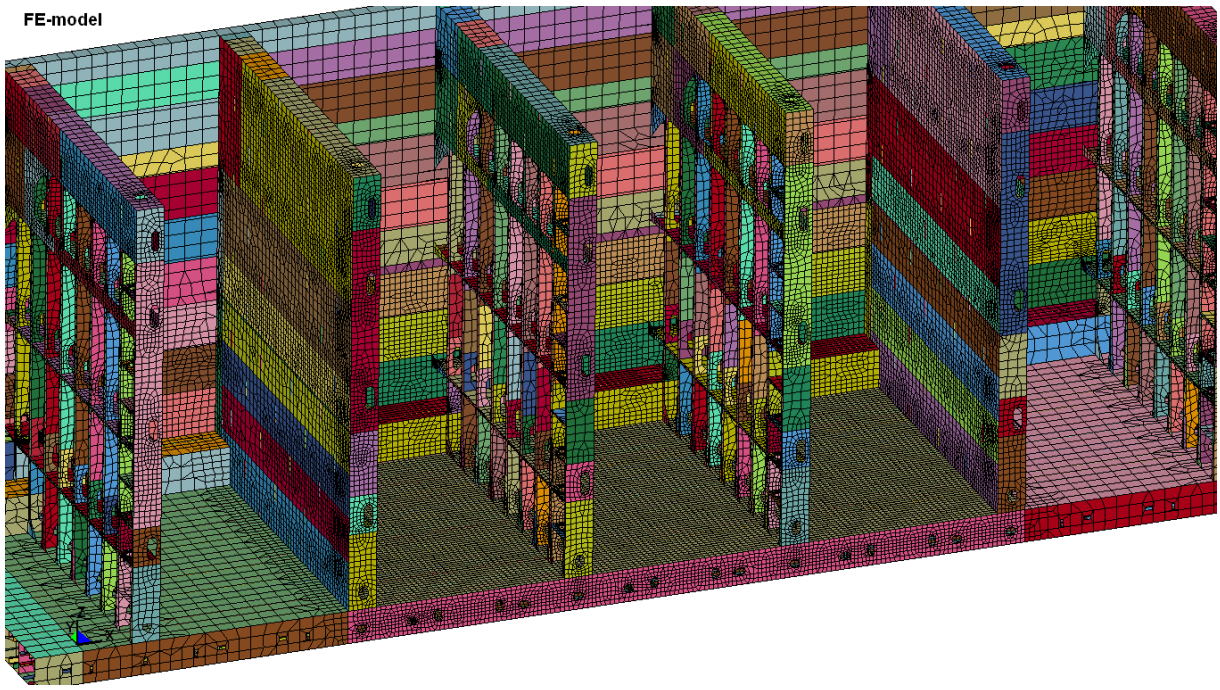

Figure 86 Initial mesh on the container ship model

Due to size of the model and complexity of construction which could affect the mesh quality especially in the bilge region it was very difficult to have stable calculations. Finally after several attempts to obtain reasonable results it was decided to reduce the model to one hold and to analyze only the pure vertical bending moment. Therefore for the analyze of the ultimate strength of the container ship the one hold model shown before is chosen and analyzed further in the report.

4.2 Methodology

4.2.1 Model extent

In case of container ship only the vertical bending moment is analyzed hence the extent of the model is smaller comparing to the bulk carrier. One cargo hold in the midship are is modelled with additional main frame spacing extensions on both ends to reduce the influence of the boundary conditions. Therefore the model is 1+4+1 main frame spacings. In transverse direction symmetry condition in the centre line was applied as well.

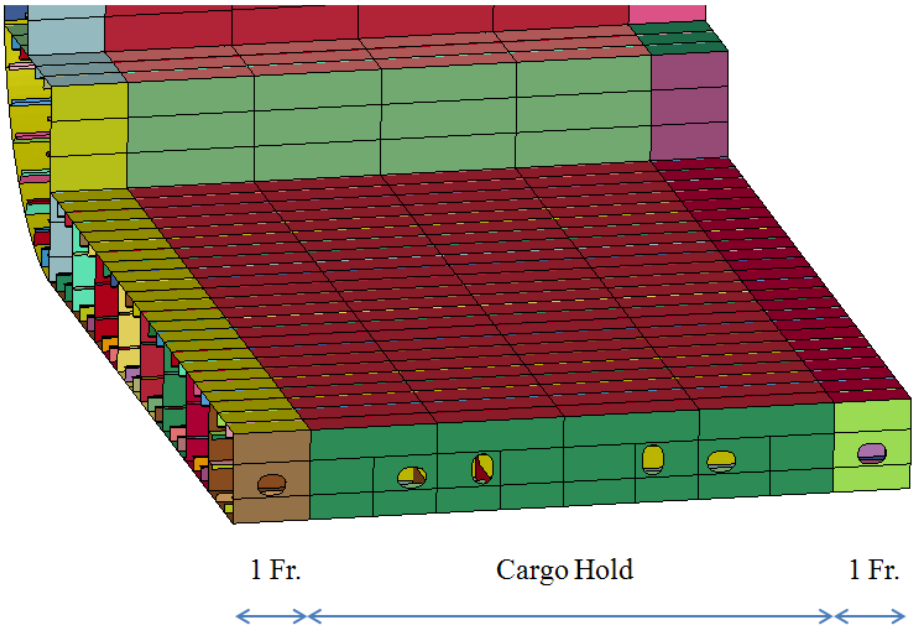

Figure 87 Container ship model extent

4.2.2 Material

For the model of container ship high tensile steels materials with different yield strengths were used. Significant part of the model is with high tensile steel 315 MPa. Steel 355 MPa and 390 MPa is used for the upper part of the side and the main deck area. Stringer in the double side at the level of neutral axis is characterised by steel 235 MPa. In the table 7 are shown the steel types used in the structures:

Table 7 Steel properties

		Steel 235	Steel 315	Steel 355	Steel 390
Young's modulus	E [N/mm2]	206 000	206 000	206 000	206 000
Poisson ratio	ν	0.3	0.3	0.3	0.3
Yield stress	Re [MPa]	235	315	355	390
Strain hardening parameter	ET [N/mm2]	1000	1000	1000	1000

At the aft and fore and of the model pure elastic material is used.

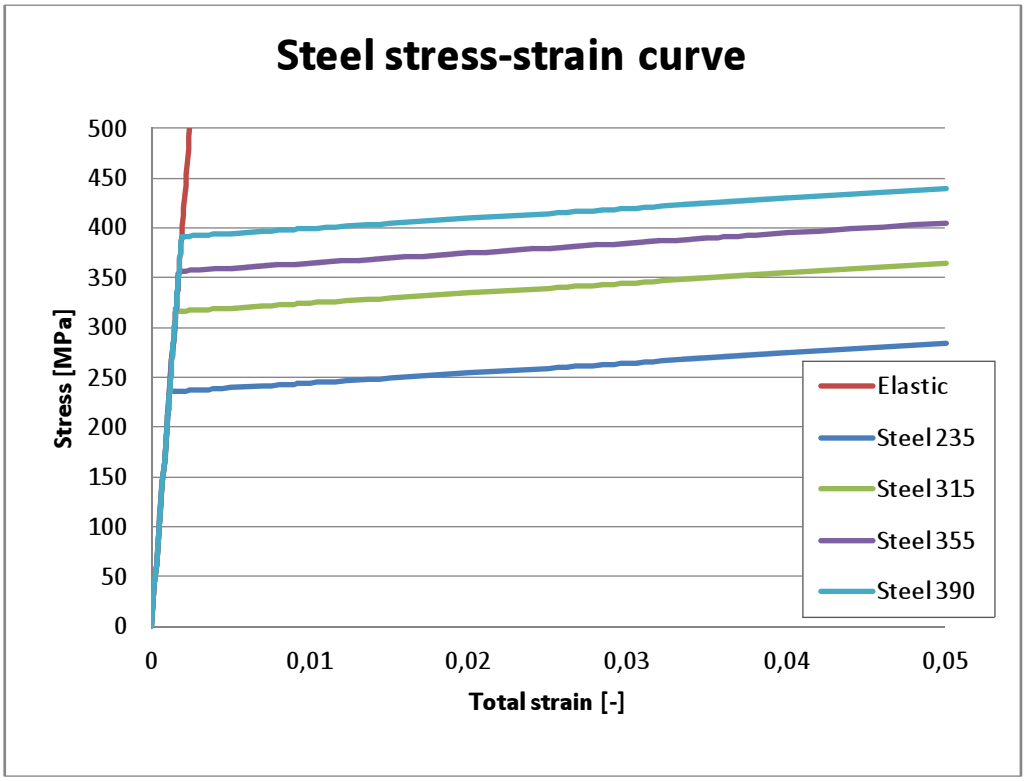

Figure 88 Steel properties

4.2.3 Boundary conditions

The boundary conditions of the container ship were applied in the similar way as it was in the case of the bulk carrier. The fore end of the model was fixed in all six degrees of freedom i.e. three translations and three rotations. It was done by constrain all the nodes on the fore end section of the model. The picture is shown in the Fig.90.

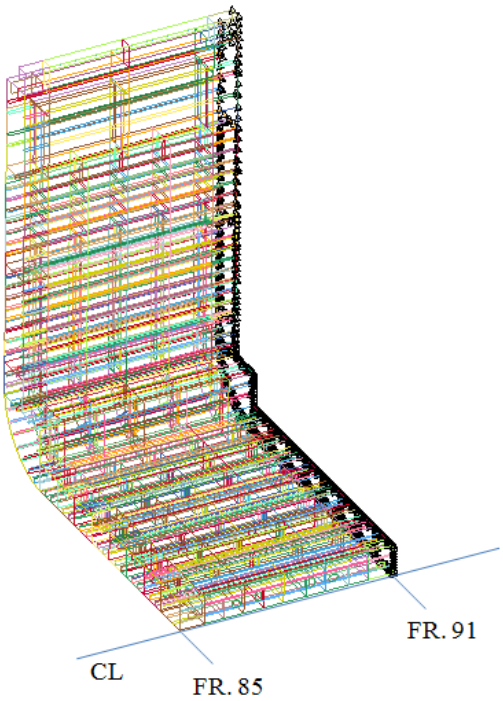

Figure 89 Boundary condition on container ship model - fixed end

In the centre line the symmetry condition was applied with following set of parameters.

Table 8 Symmetry condition in the center line parameters

x	y	z	ox	oy	oz
free	fixed	free	fixed	free	fixed

The picture is shown below.

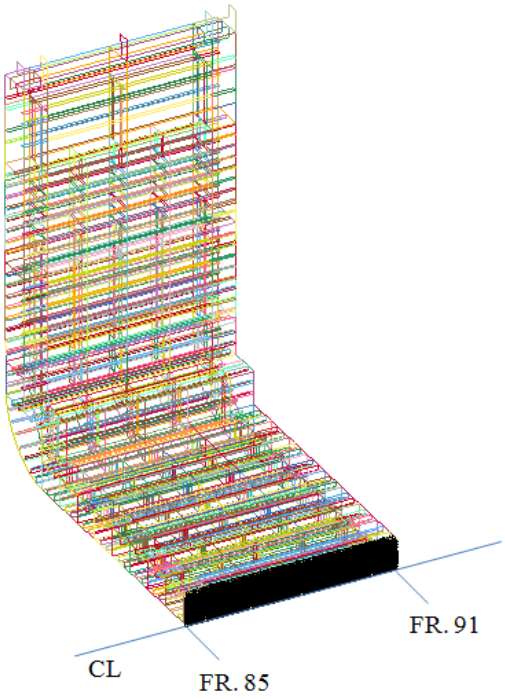

Figure 90 Boundary condition – symmetry condition in ship's center line

To realize the rotation at the aft end of the model the coupling between the section and the rotation point was applied. By this all the nodes at the first section follow the rotation given at the rotation node. The picture of the coupling at the aft end is shown below.

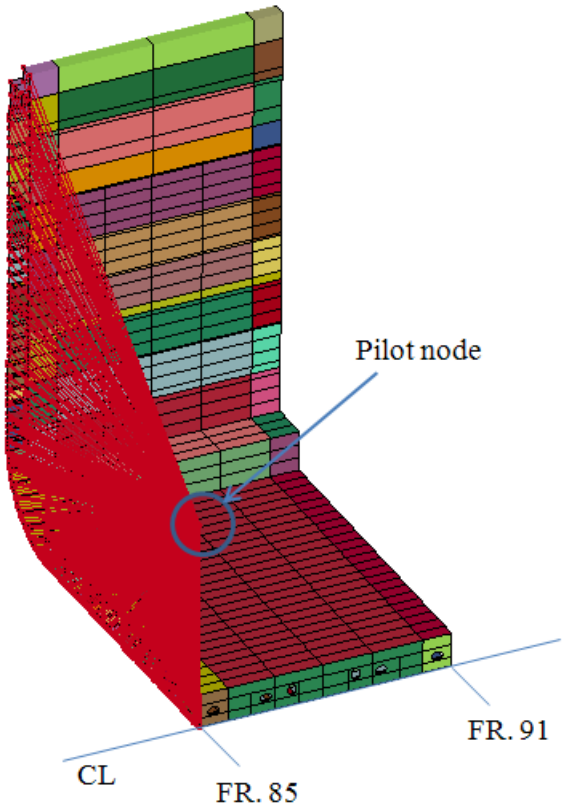

Figure 91 Boundary condition on container ship model – coupling on the aft end section

4.2.4 Defined sections for results reading

The results of the ultimate moment are written for three different locations. Since the value of the moment is constant the results should be the same in all three points.

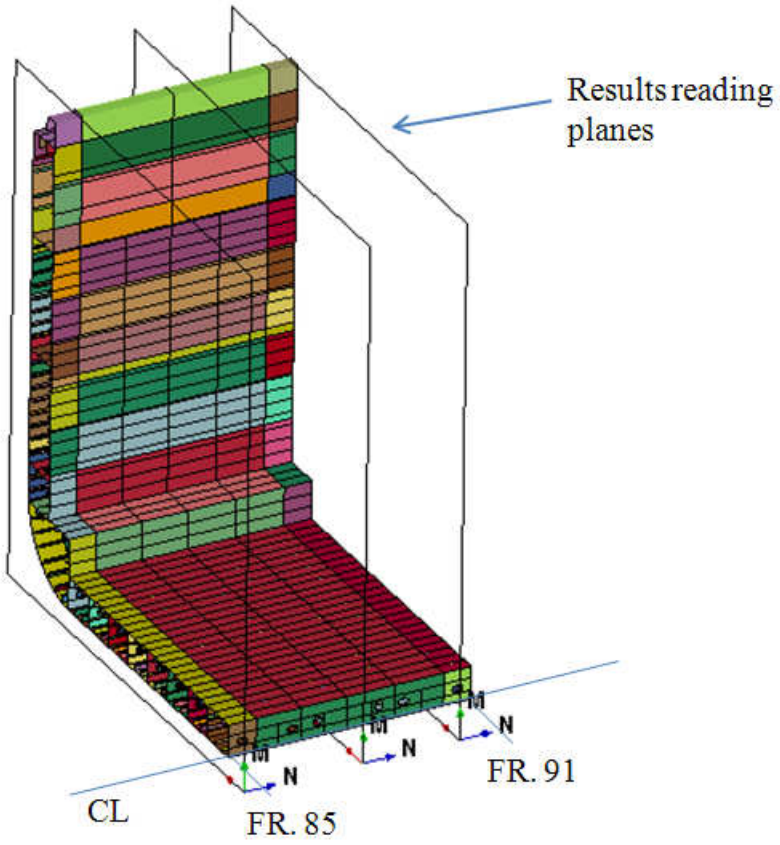

Figure 92 Results reading planes

4.3 Mesh

Mesh for the container ship was generated in the Ansys Workbench Mechanical. The main part of the mesh was done using quadrilateral shell elements.

4.3.1 Mesh requirements

Mesh generated for container ship model follows the same approach as the mesh for analyzed bulk carrier. The general idea was to achieve fine mesh in the middle part of the model and below the cross section neutral axis. The coarse mesh was generated above the cross section neutral axis and at the extremities of the model. The set of requirements is similar as with the bulk carrier.

4.4 Study on the mesh convergence

To ensure that the quality of the mesh has no higher influence on the obtained results the mesh convergence study was performed. Three following mesh densities were checked with increasing number of elements between frames and longitudinal stiffeners. All analyzed mesh densities meet the requirements for the mesh quality.

The following mesh models were studied:

- Mesh 1 – 6 elements between main frames, 2 elements between longitudinal stiffeners, the size of the element 500 mm,
- Mesh 2 – 9 elements between main frames, 3 elements between longitudinal stiffeners, the size of the element 350 mm,
- Mesh 3 – 18 elements between main frames, 5 elements between longitudinal stiffeners, the size of the element 170 mm,

4.4.1 Mesh 1 (6x2)

Mesh generated on the container hull model is shown below.

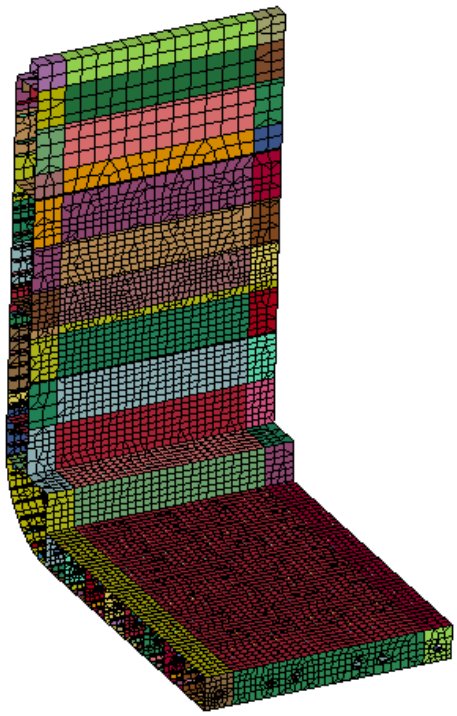

Figure 93 Mesh nr 1 generated on the container ship model

The details of the mesh on the longitudinal stiffeners and on the inner bottom plating are shown below.

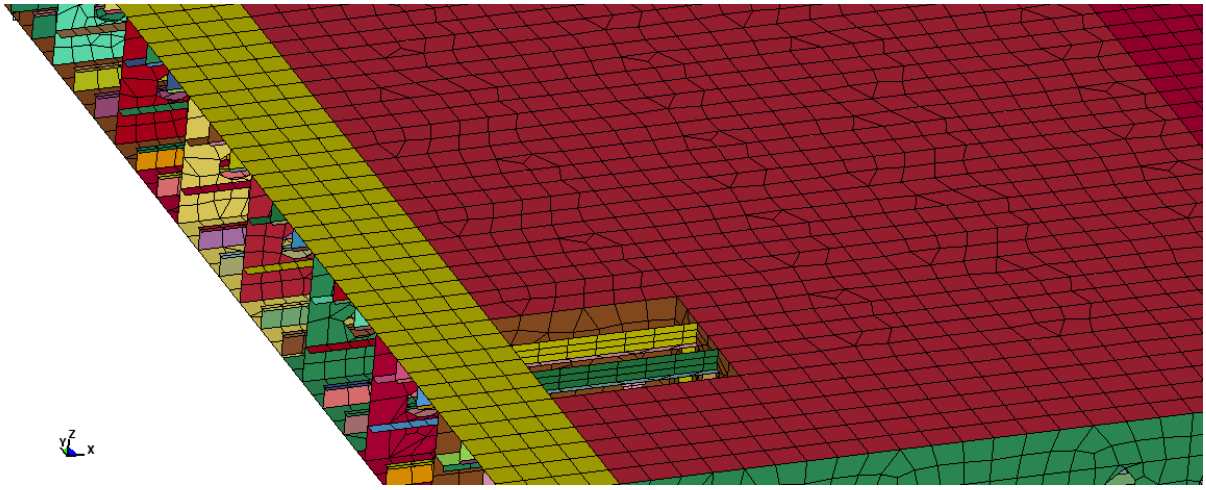

Figure 94 Mesh generated on the inner bottom

Results

Deformations in the inner bottom plating are shown in the picture below.

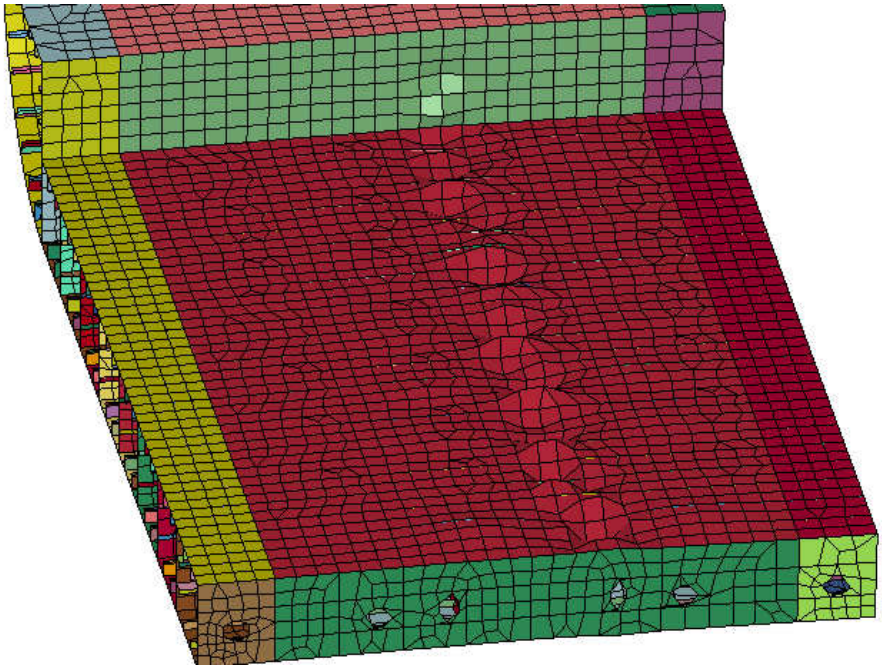

Figure 95 Deformation in the inner bottom

Plastic strain results for the construction are shown below.

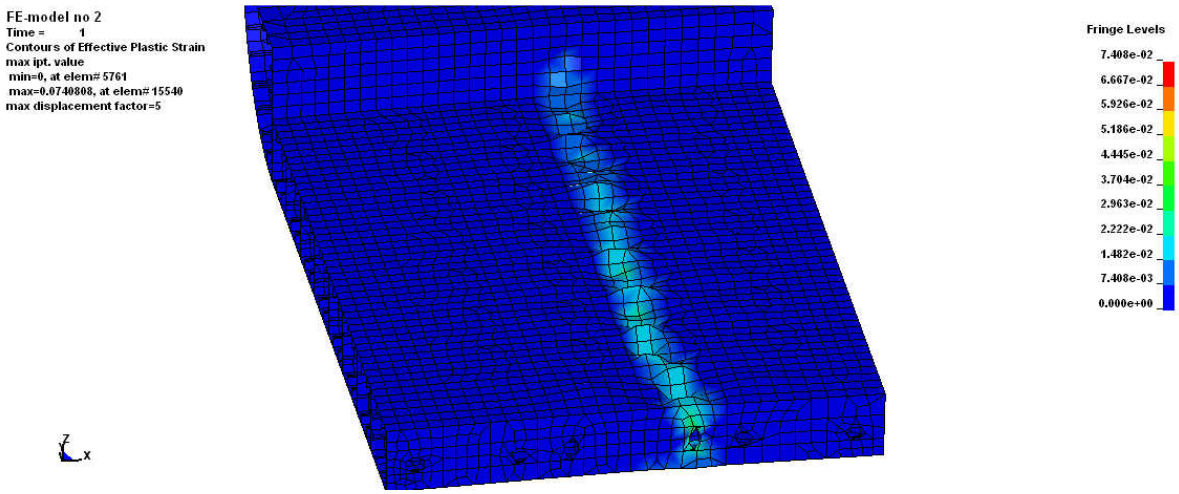

Figure 96 Plastic strain in the inner bottom

The progressive collapse curve for the mesh nr 1 is shown below.

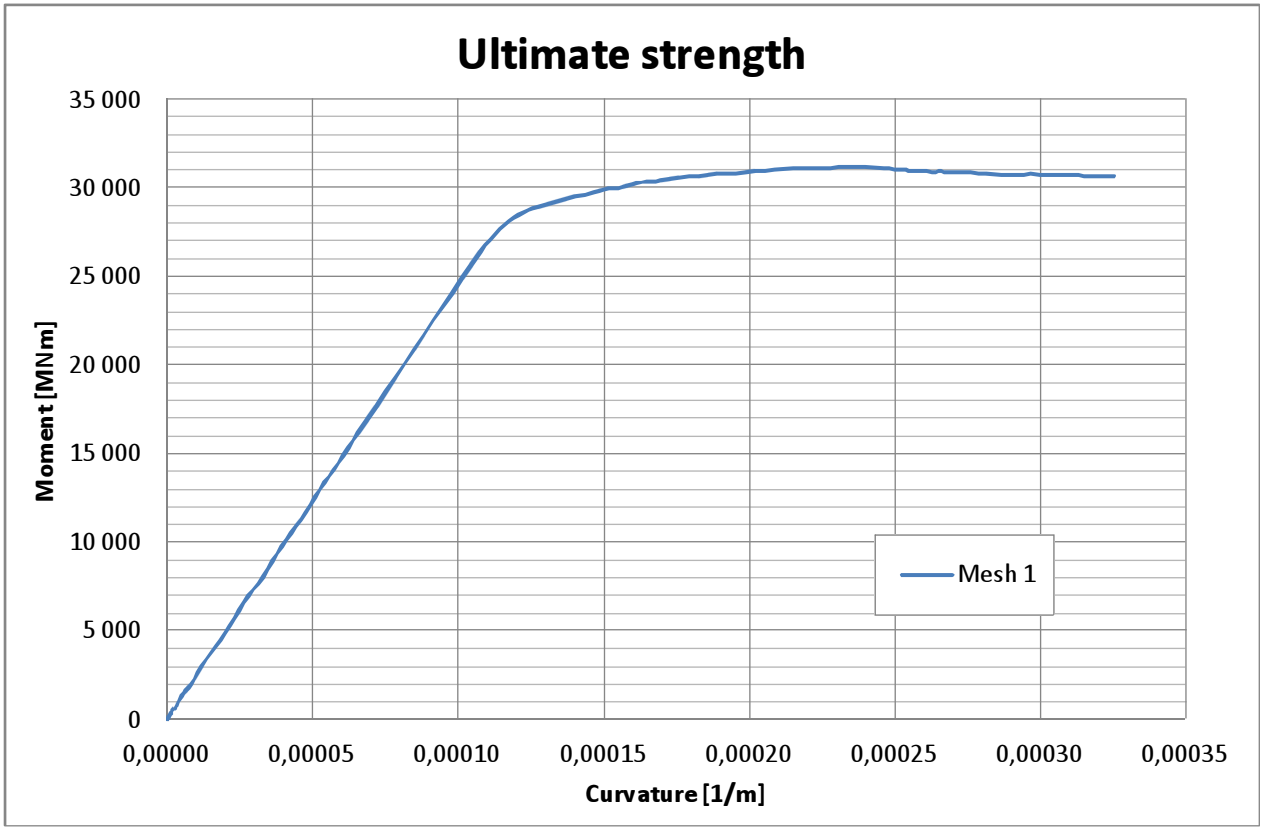

Figure 97 Progressive collapse curve for the mesh nr 1

It can be seen that the collapse of the structure was reached. The ultimate moment measured is Mu = 31200 MNm.

4.4.2 Mesh 2 (9x3)

Mesh nr 2 on the container ship model is shown below.

Figure 98 Mesh nr 2 generated on the container ship model

Details of the mesh on the longitudinal stiffeners and on the inner bottom are shown below. Since smaller elements are used the mesh is more regular.

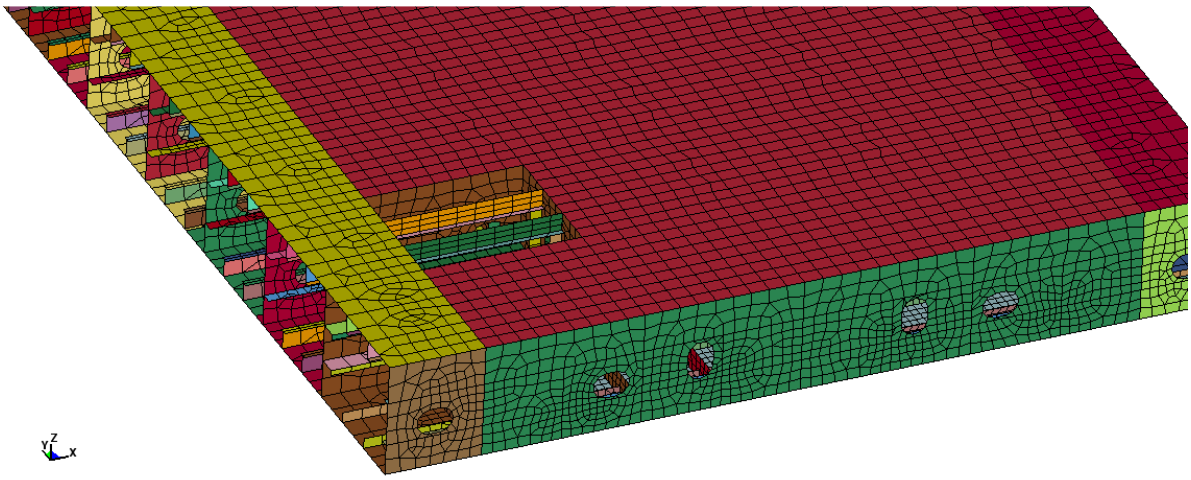

Figure 99 Mesh generated on the inner bottom

Results

Buckling in the bottom area for the collapse is shown below.

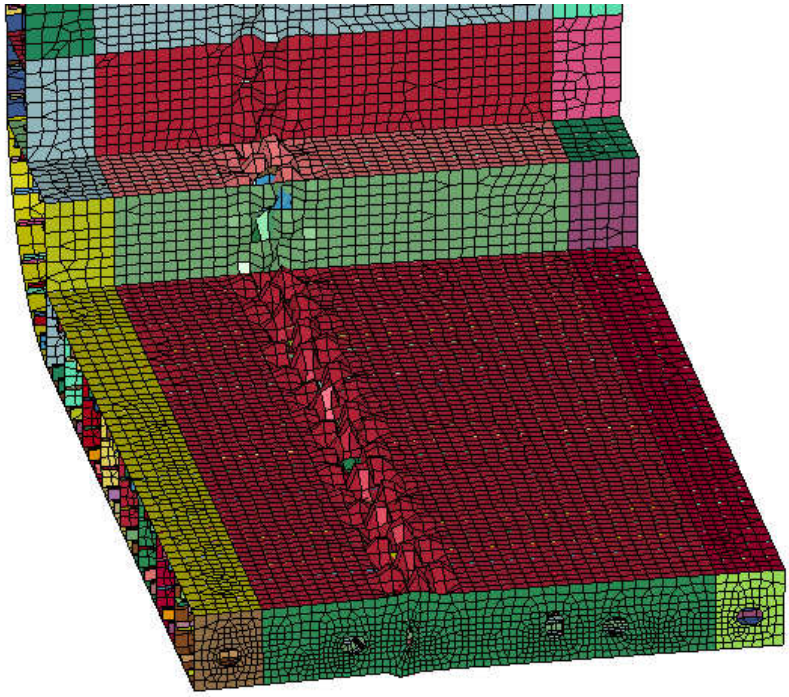

Figure 100 Deformation in the inner bottom

The results of the plastic strain in the bottom region for the mesh nr 2 is shown below.

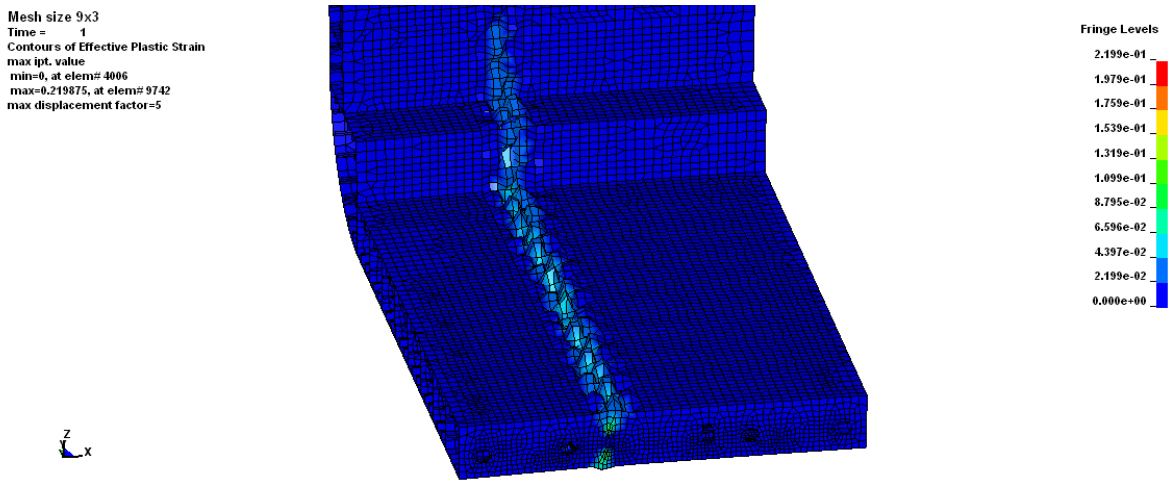

Figure 101 Plastic strain in the inner bottom

The graph showing progressive collapse of the structure is shown below.

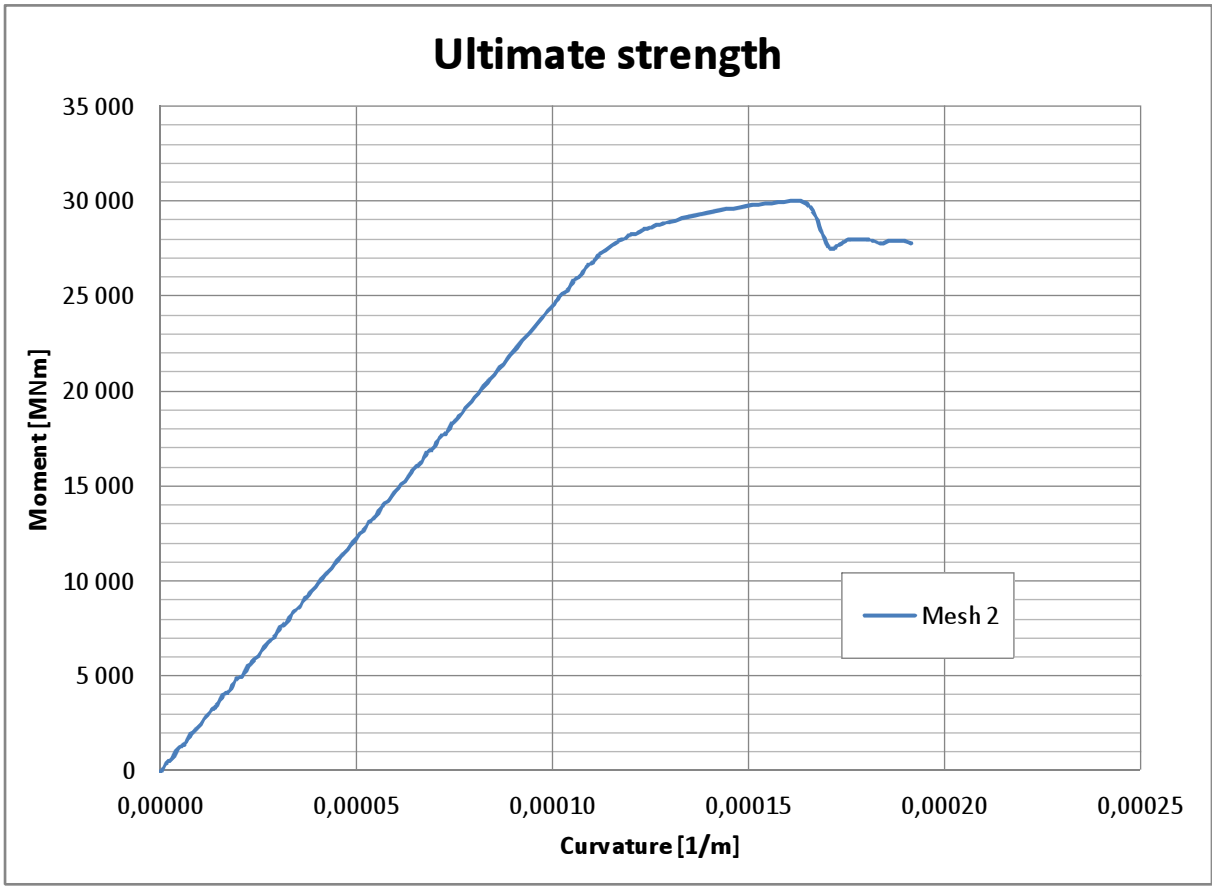

Figure 102 Progressive collapse curve for the mesh nr 2

It can be seen that the collapse was reached. The ultimate moment of the analyzed structure is Mu = 30040 MNm.

4.4.3 Mesh 3 (18x5)

The mesh with the highest considered density on the container ship is shown in the Fig.103. The coarse mesh in the deck area can be shown as well as fine mesh on construction below the neutral axis.

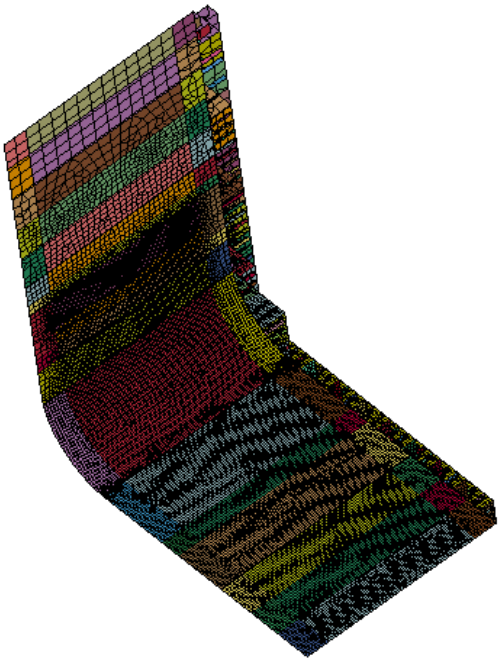

Figure 103 Mesh nr 3 generated on the container ship model

The details of the fine mesh on the shell are shown below.

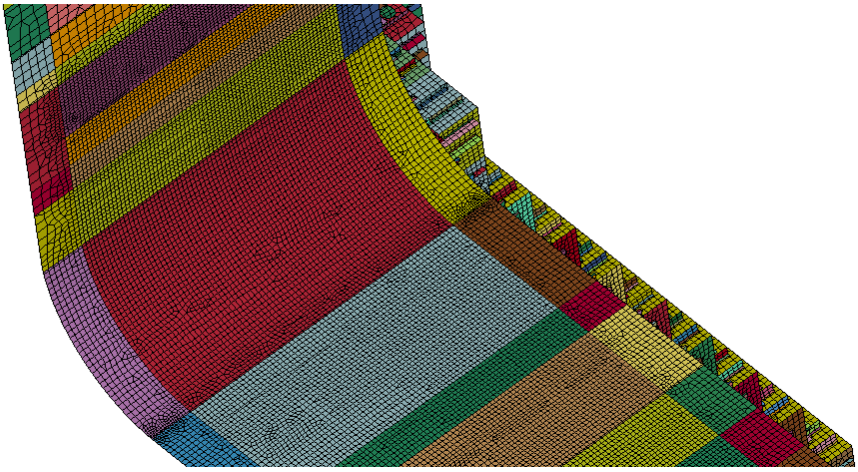

Figure 104 Mesh generated on the outer shell of the container ship model

The details of the mesh in the double bottom region are shown below.

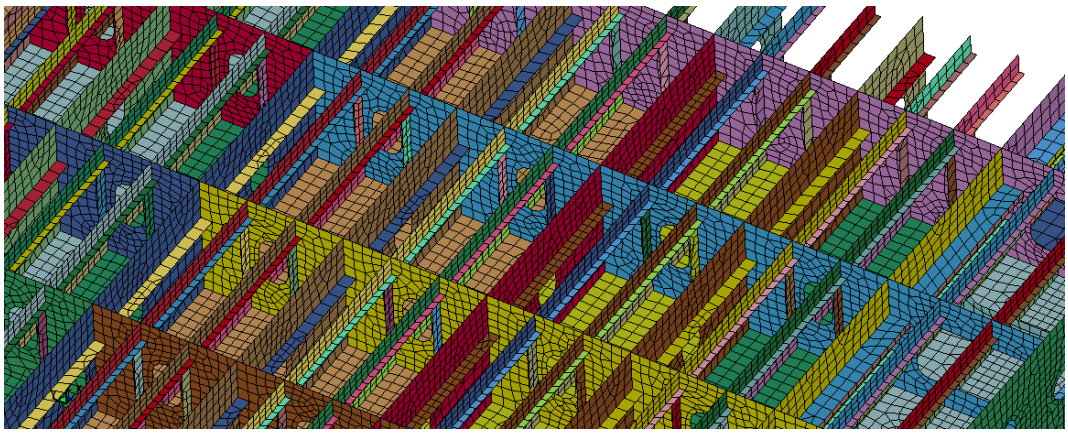

Figure 105 Mesh generated on the inner bottom longitudinals

The details of the mesh around the neutral axis position are shown below.

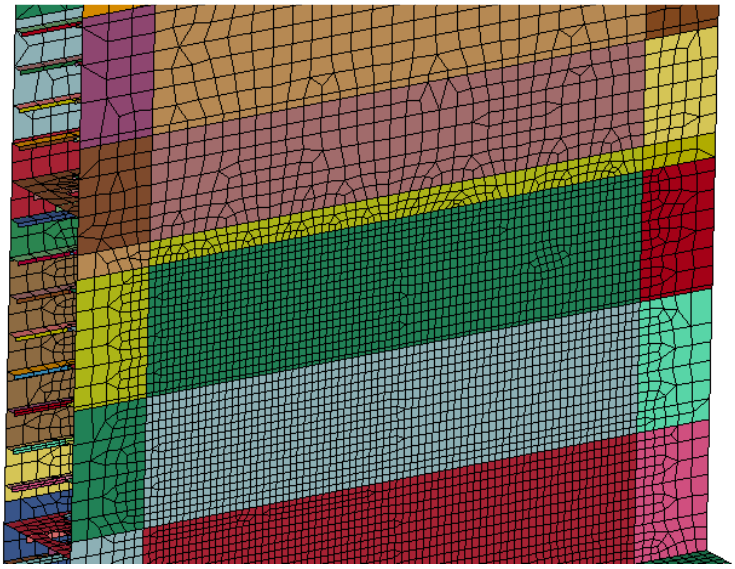

Figure 106 Mesh generated in the neutral axis region

Results

The shape of deflection in inner bottom plating for the collapse is shown below.

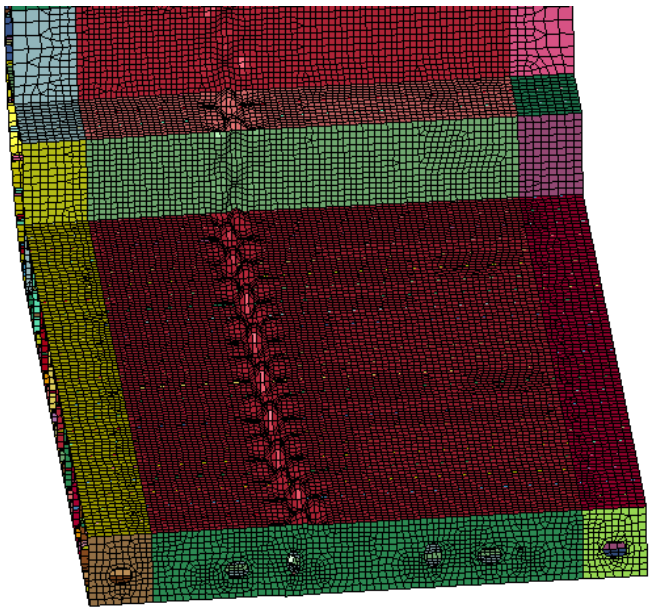

Figure 107 Deformation in the inner bottom

The buckling shape in the outer shell is shown below.

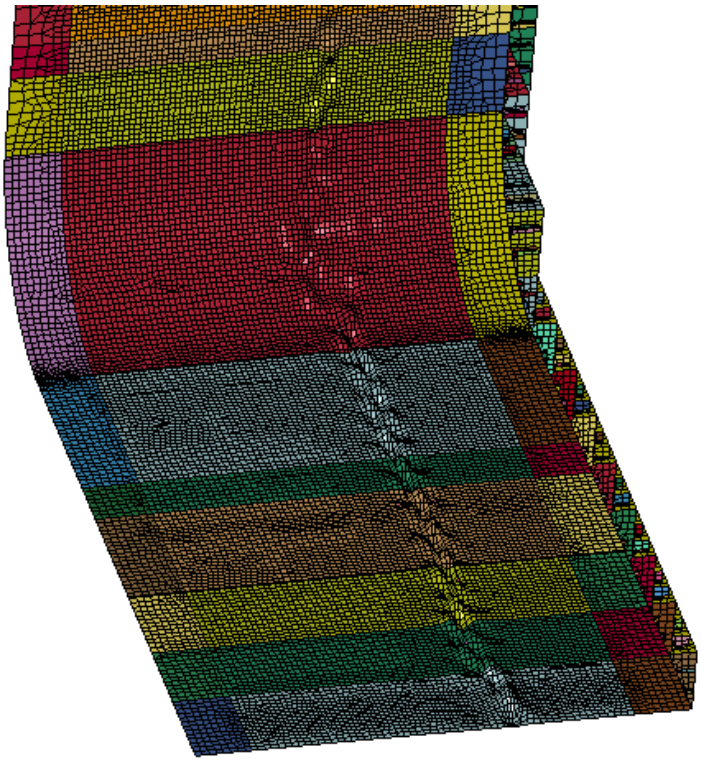

Figure 108 Deformation in the outer shell

The plastic strain level in the inner bottom plating is shown below.

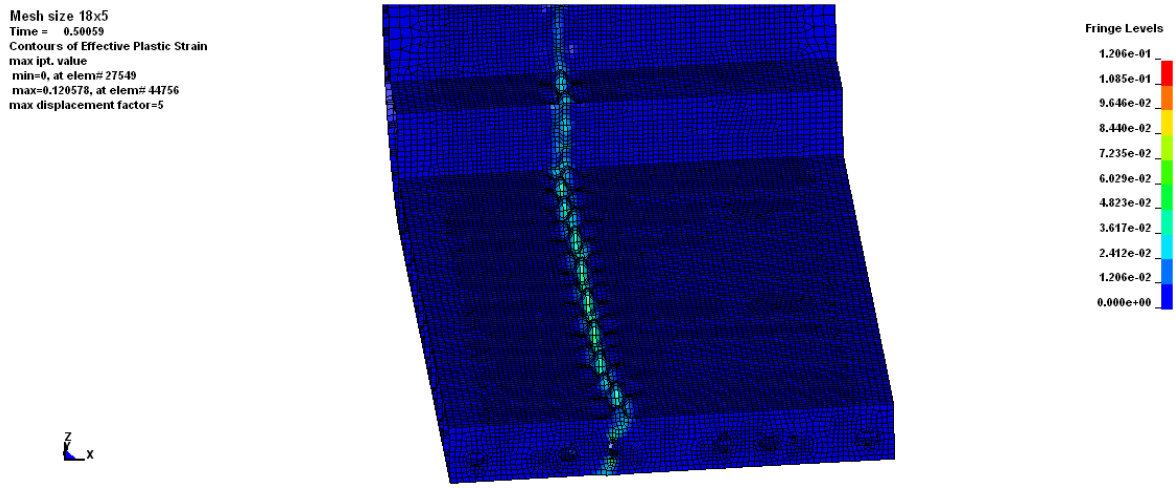

Figure 109 Plastic strain in the inner bottom

The progressive collapse curve for the mesh model nr 3 is shown below.

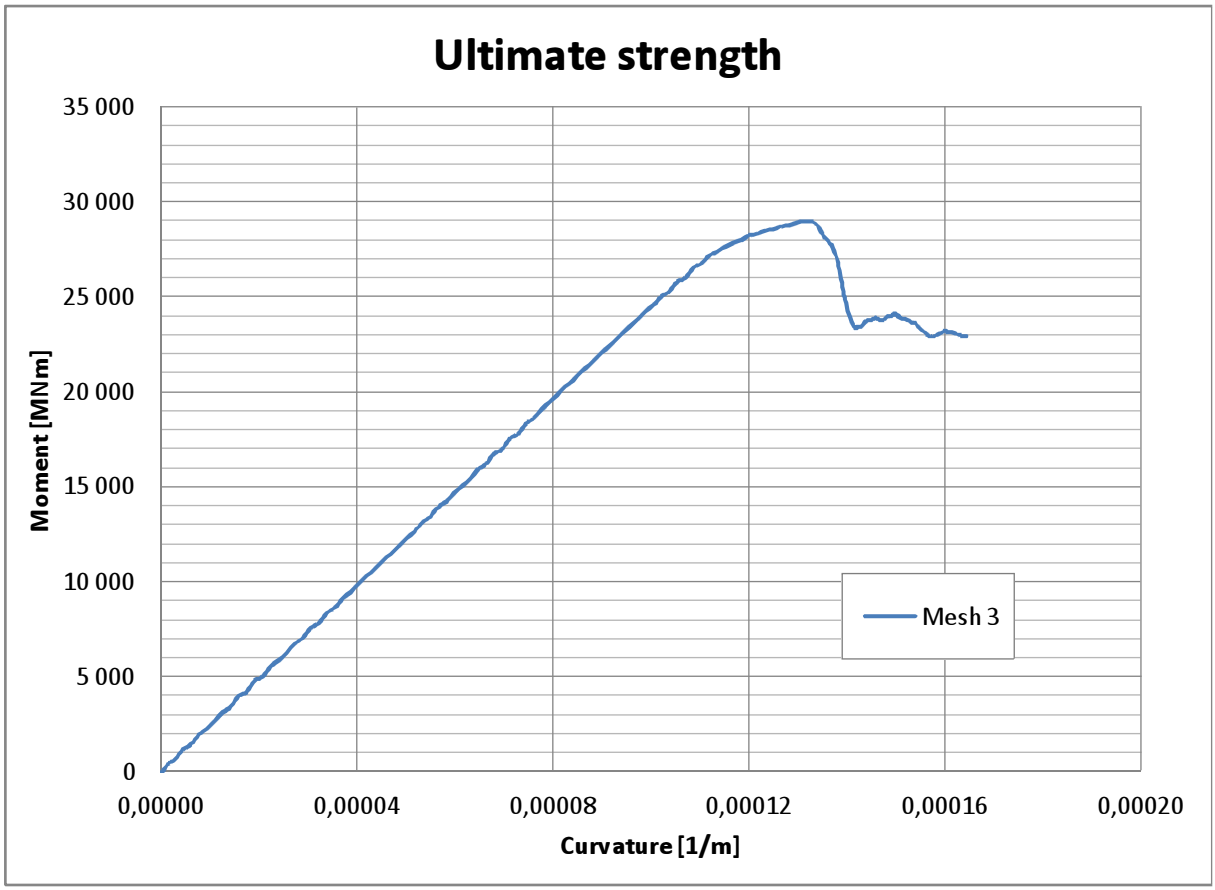

Figure 110 Progressive collapse curve for the mesh nr 3

The graph shows that the collapse of the structure was reached. The ultimate moment measured is Mu = 28990 MNm.

4.4.4 Comparison of results of the different mesh densities

The progressive collapse curves were found for three considered mesh densities. The comparison is shown on the graph below.

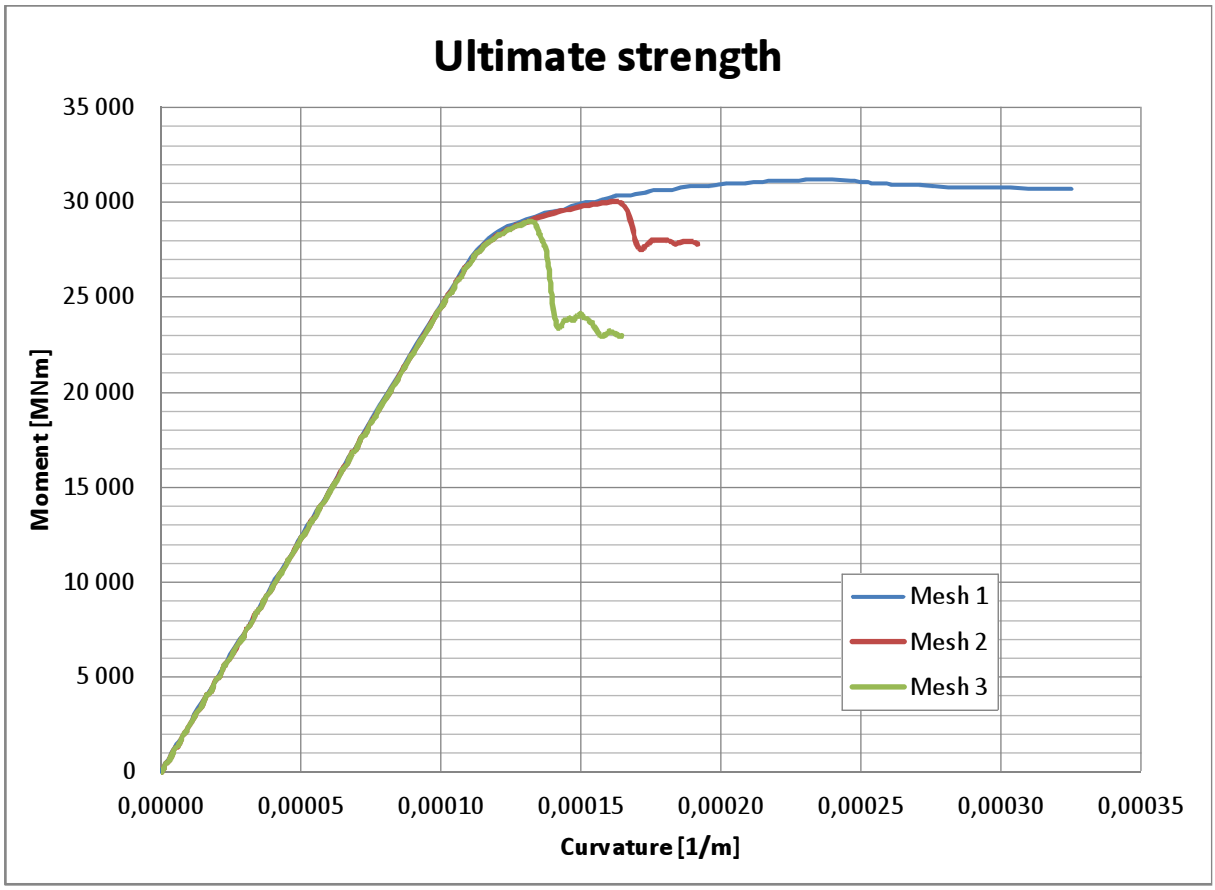

Figure 111 Comparison of the progressive collapse curves for different mesh densities

As it is shown the increase of the mesh density result is lower values for the ultimate moment obtained from the calculations. The maximum values of the moment are given below.

Table 9 Comparison of the ultimate moment for different mesh densities

	Maximum moment [MNm]	Difference [%] (to Model 1)
Mesh model 1	31200	-
Mesh model 2	30040	-3,72
Mesh model 3	28990	-7,08

All analyzed mesh densities fulfill the requirements. However it can be seen that the mesh quality significantly influence the obtained results. Mesh nr 3 is the most detailed therefore is considered as being sufficient to perform the further analysis. With all next steps mesh nr 3 will be taken for calculations.

4.5 Imperfections

General requirement for the modelled imperfections and chosen methodology is similar as with bulk carrier. Both requirements for the FE modelling as well as production standards paper were chosen into consideration.

4.5.1 Representing imperfections in LS-Dyna

Imperfections in the constructions were modelled in LS-Dyna software using similar inbuilt function as with the bulk carrier model. The imperfections were modelled on the following structures with given value of amplitude:

- Double bottom plating – 3,0 mm
- Side shell plating – 3,0 mm
- Side girders in double bottom – 4,0 mm

Picture showing modelled imperfections on the inner bottom plating is shown below.

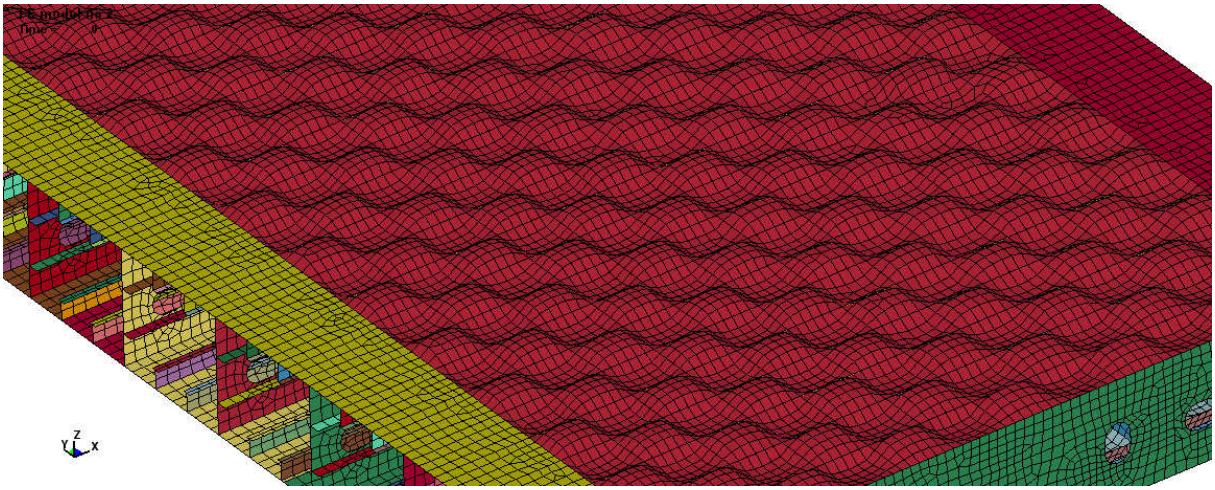

Figure 112 Imperfections on the inner bottom plating

Imperfections on the outer shell is the bottom and side plating are shown in the Fig.113.

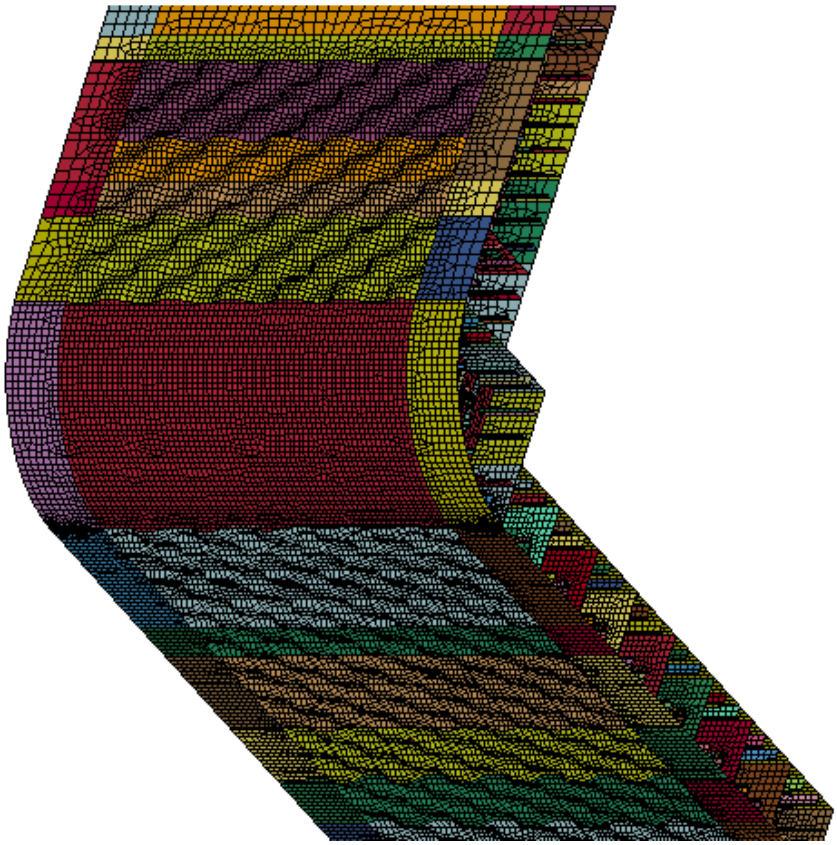

Figure 113 Imperfections on the outer shell

4.5.2 Results with imperfections

After imperfections were modelled the progressive collapse calculations were run. Below we can see the picture showing the collapse form with existence of imperfections.

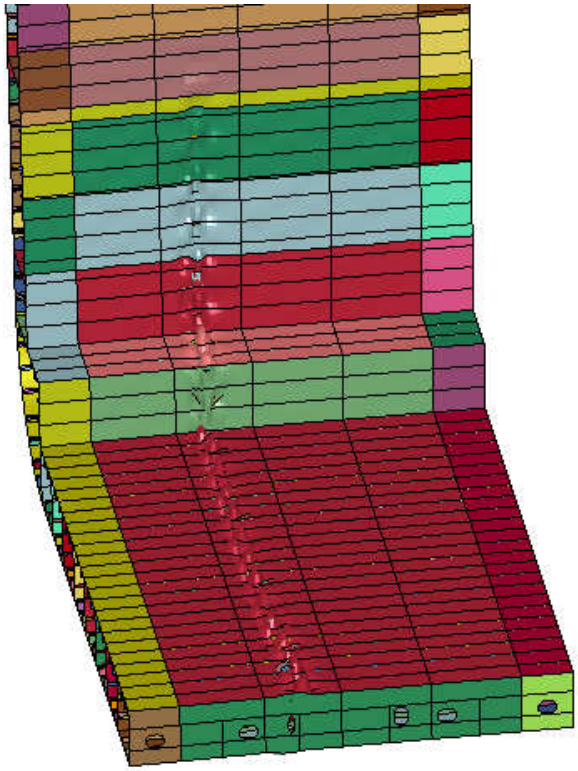

Figure 114 Deformation in the inner bottom

Progressive collapse curve for the mesh model with imperfections is shown below.

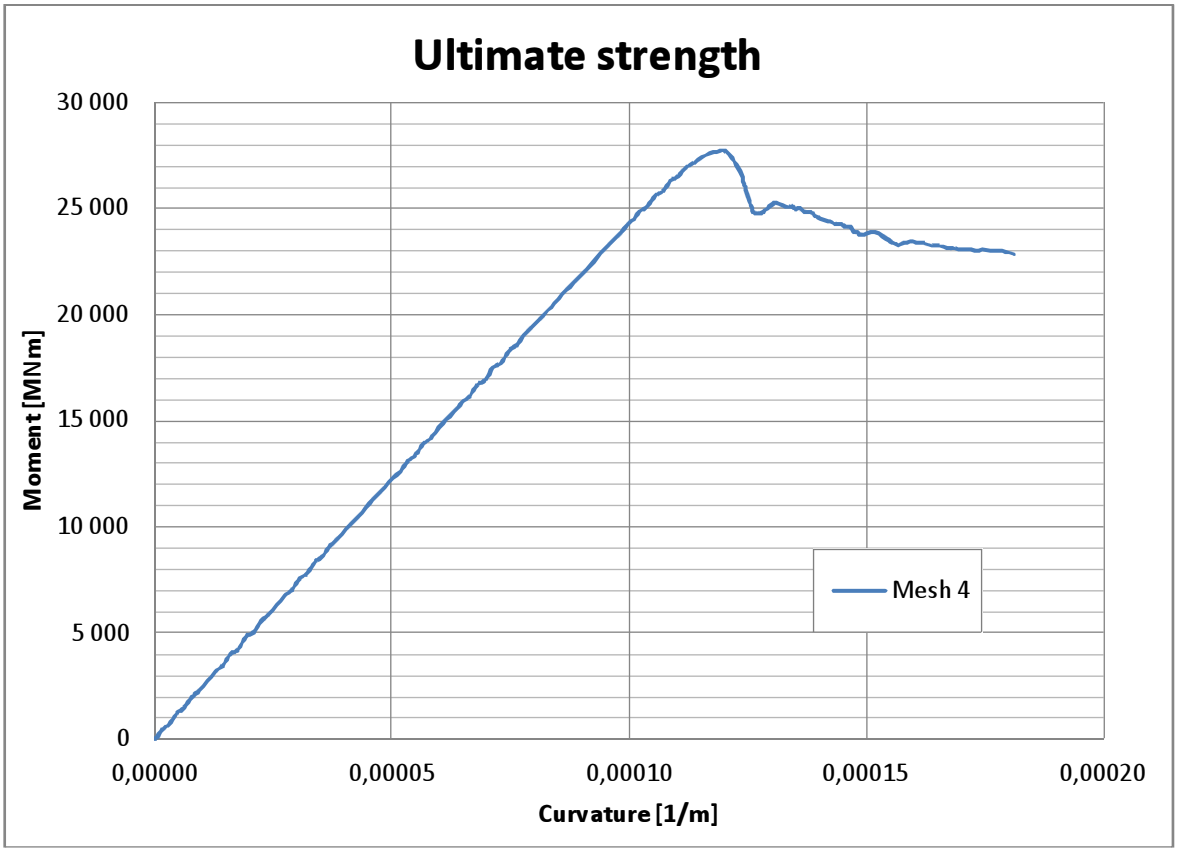

Figure 115 Progressive collapse curve for mesh model with imperfections

The maximum moment in construction is Mu = 27710 MNm.

4.5.3 Comparison of the results with and without imperfections

The comparison of the results for mesh model nr 3 with model with imperfections is shown below.

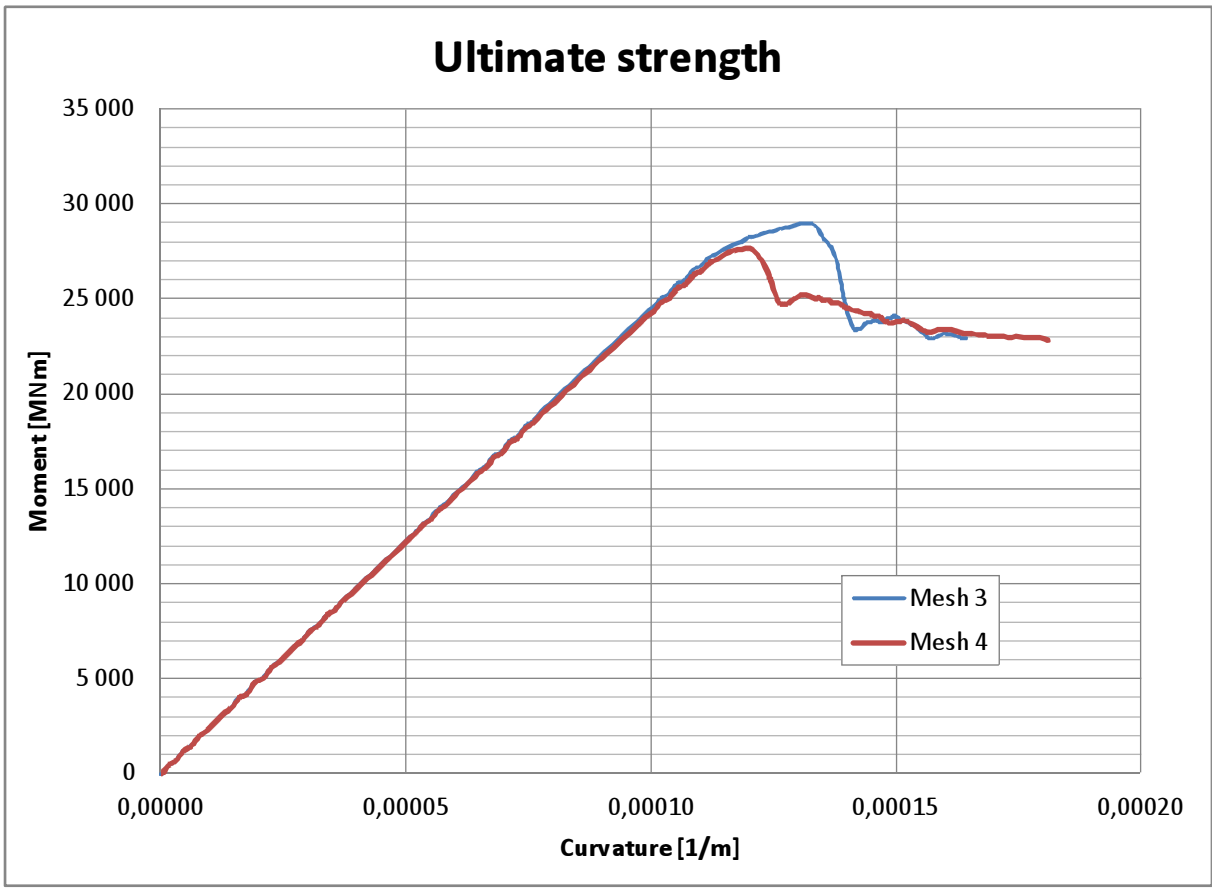

Figure 116 Comparison of the progressive collapse curves for Mesh 3 and model with imperfections

From the graph we can see that imperfections resulted in decrease of the ultimate bending moment capacity of the ship. The difference in the calculated moment is shown below.

Table 10 Comparison of the ultimate moment for mesh nr 3 and model with imperfections

	Maximum moment [MNm]	Difference [%]
Mesh model 3	28990	-
Model (imperfections)	27710	-4,42

We can see noticeable difference in the obtained value of the ultimate bending moment. However the results are dependent on the modelled shape of the imperfections and assumed value of amplitude of the imperfections. For the further analysis model with imperfections is taken.

5. BULK CARRIER – POSEIDON SOFTWARE

5.1 Bulk carrier Poseidon model

One of the output of the calculations is the comparison between the direct FE analysis and the results from the model in Poseidon. Therefore the model of the capsize bulk carrier was given with definition of all structural elements. To ensure that the models are equal all elements were carefully checked both by means of scantlings as well as applied material. The picture of cross section of the bulk carrier in Poseidon is given below.

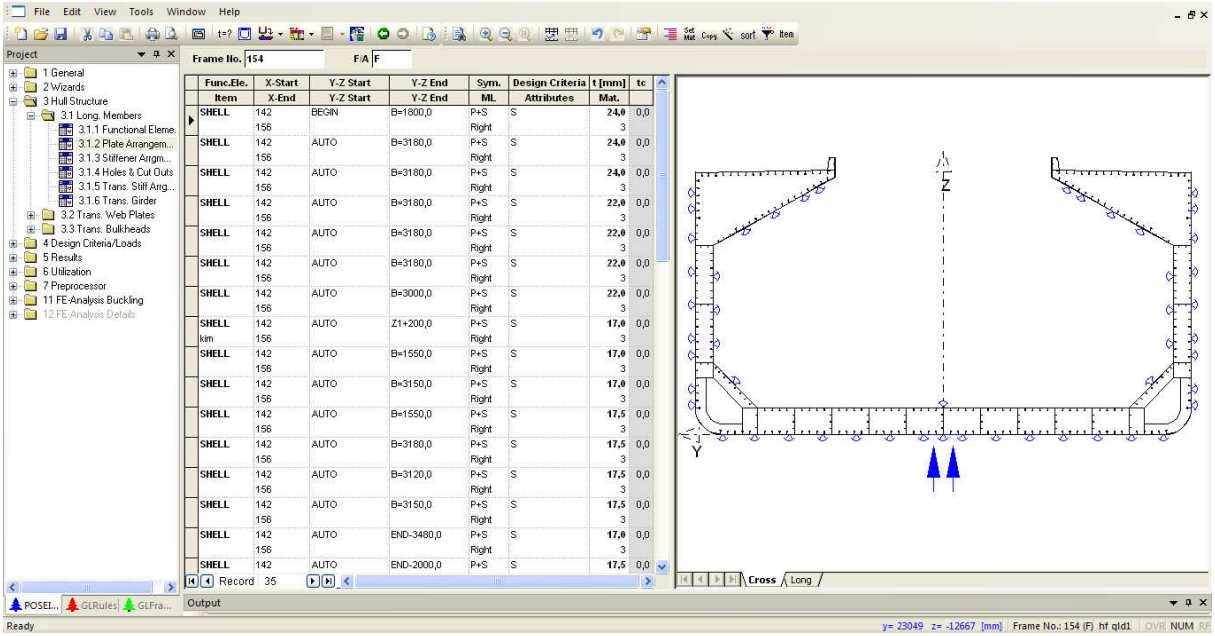

Figure 117 Bulk carrier section view in Poseidon software

5.2 Poseidon ultimate strength calculation results

One of the goals of the work is to compare the results obtained by FE direct analysis with results using Poseidon software with Smith's method implemented. Below we can see the cross section taken for the ultimate strength calculations together with plate-stiffener modules and hard corners.

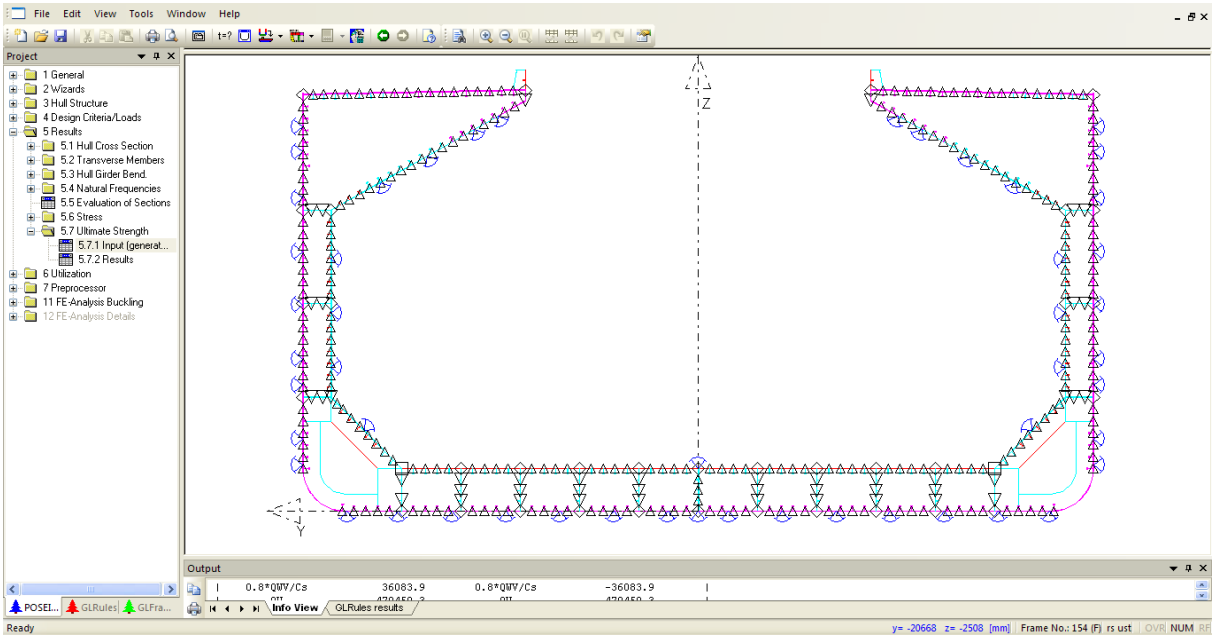

Figure 118 Bulk carrier sectional view for computation of results in Poseidon software

The obtained results are for both hogging and sagging condition, however in this case only the hogging condition is analyzed.

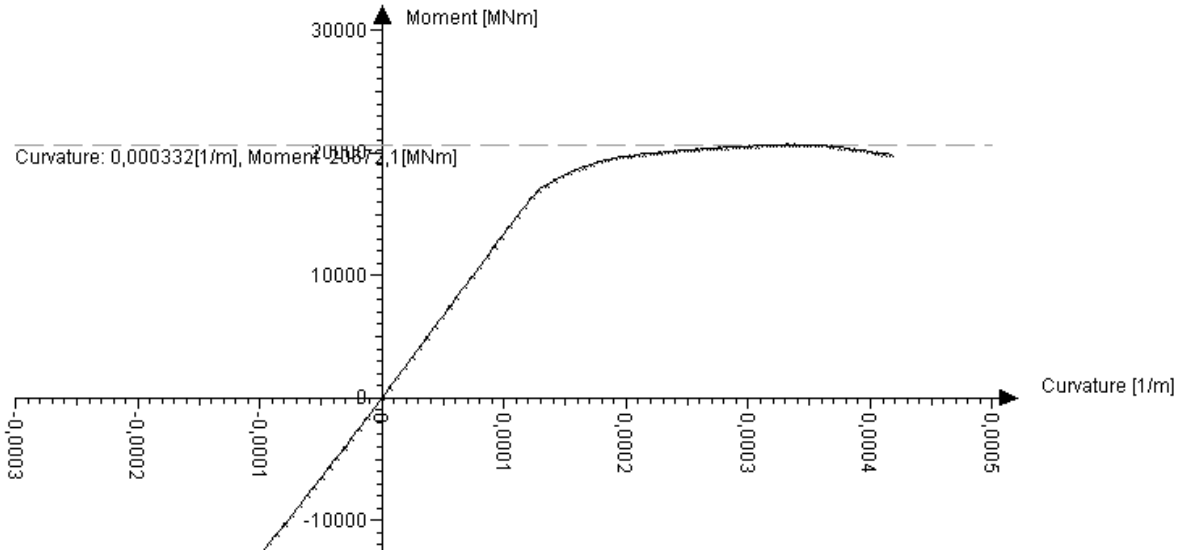

Figure 119 Progressive collapse curve in Poseidon software

The maximum value of the moment is 20670 MNm.

Movement of neutral axis

With increase of the global moment and stresses in construction a movement of the neutral axis can be observed. It is a result of the plastic deformations caused by yielding in the main deck area and buckling of the elements in the double bottom region. The shift of the neutral axis is shown in the graph below.

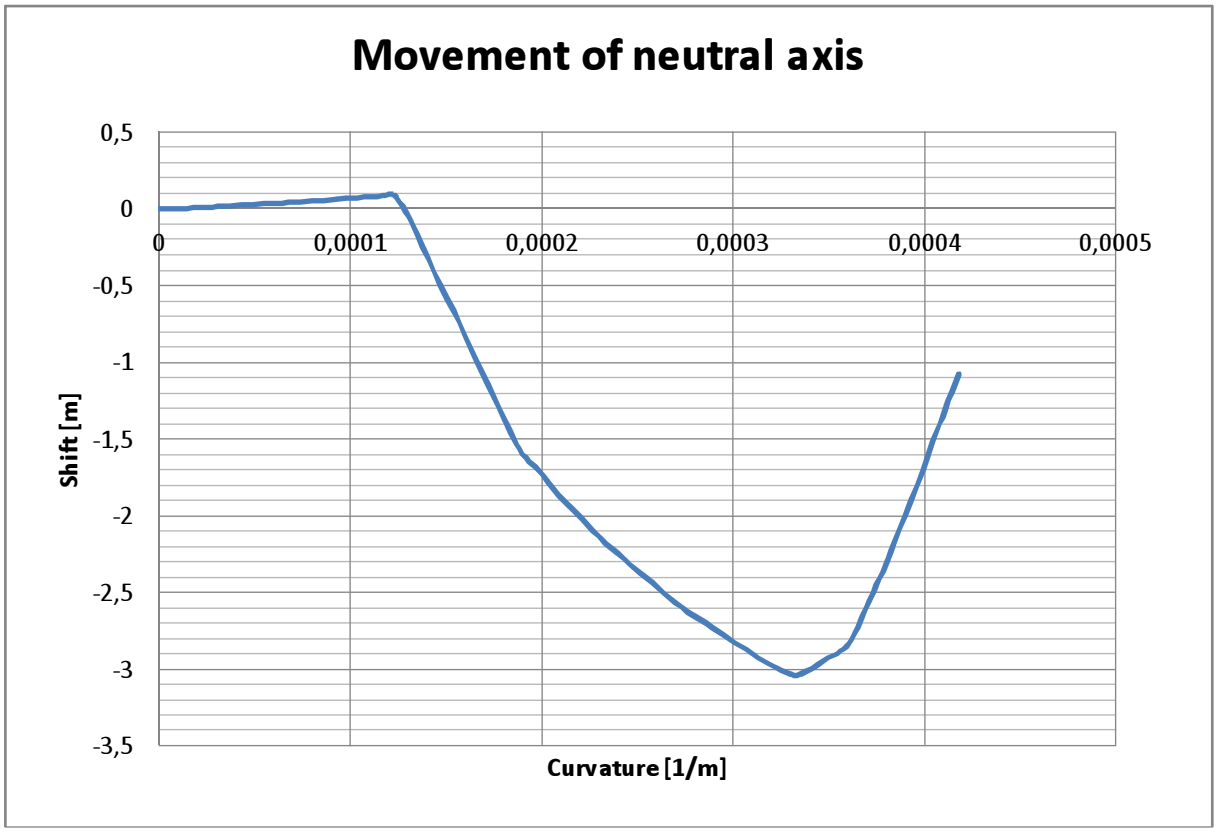

Figure 120 Movement of the neutral axis from the Poseidon model

5.3 Comparison of the results for the bulk carrier

The comparison of the progressive collapse curves for the model with imperfections and obtained in Poseidon software is shown in the Fig.121.

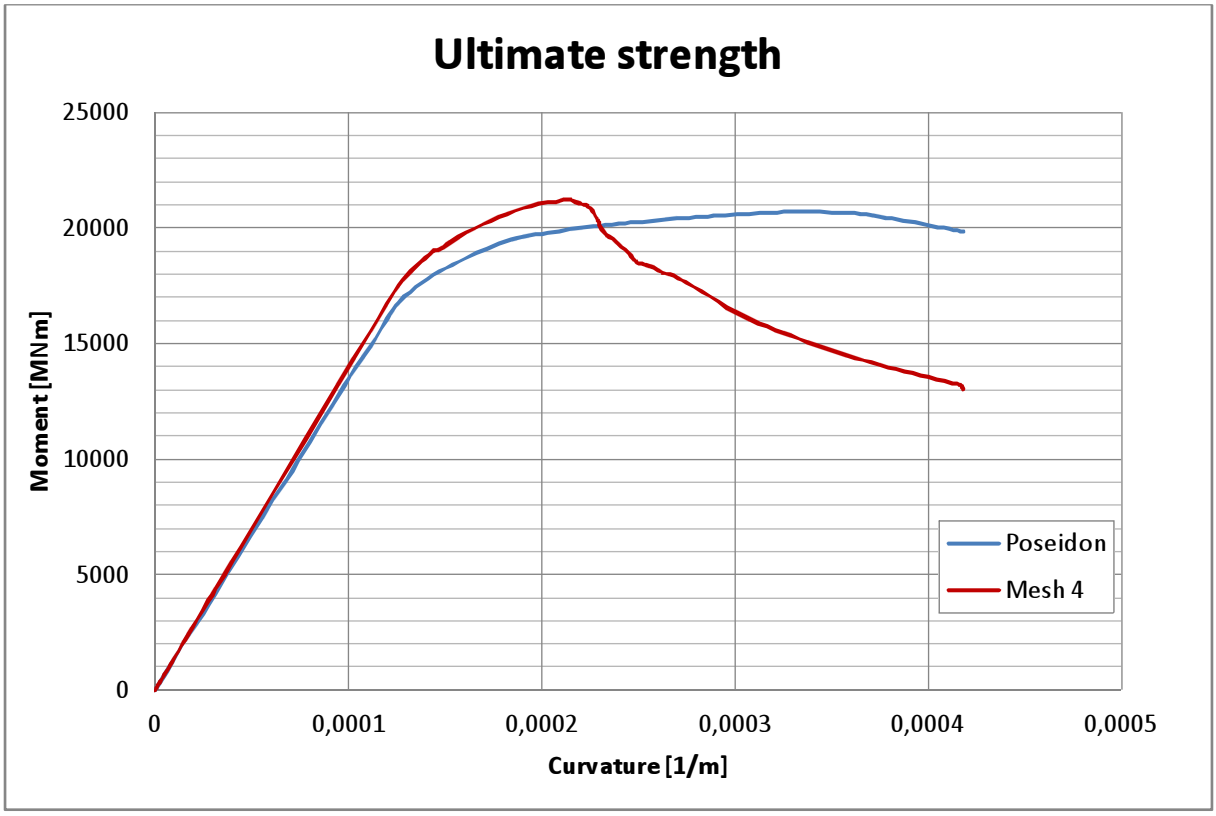

Figure 121 Comparison of the progressive collapse curves from the FE analysis and Poseidon software

The comparison between the values of the ultimate moment is shown below.

Table 11 Comparison of the results for direct FE analysis and model with imperfections

	Maximum moment [MNm]	Difference [%]
Mesh 4 (imperfections)	21180	-
Model Poseidon	20670	-2,41

Therefore the results for the pure vertical bending moment acting on the ship are more conservative for the Smith's method used in the Poseidon software.

6. CONTAINER SHIP – POSEIDON SOFTWARE

6.1 Container ship Poseidon model

In case of container ship the procedure was similar as with bulk carrier. The model in Poseidon was given and the check was done to ensure that the model is equal with one done for FE analysis. The picture of the container ship cross section in Poseidon is shown below.

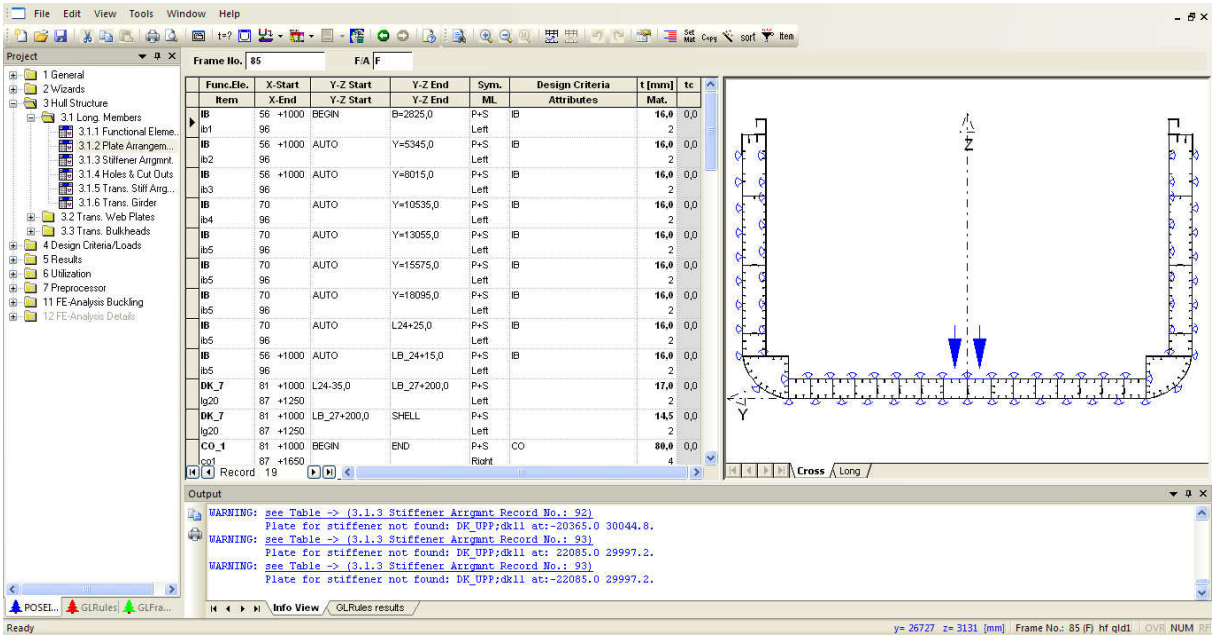

Figure 122 Container ship section view in Poseidon software

6.2 Results from Poseidon

The results for the ultimate bending moment capacity where calculated for the chosen section of the hull. The picture of the section is shown below. The plate-stiffeners elements as well as hard corners are presented.

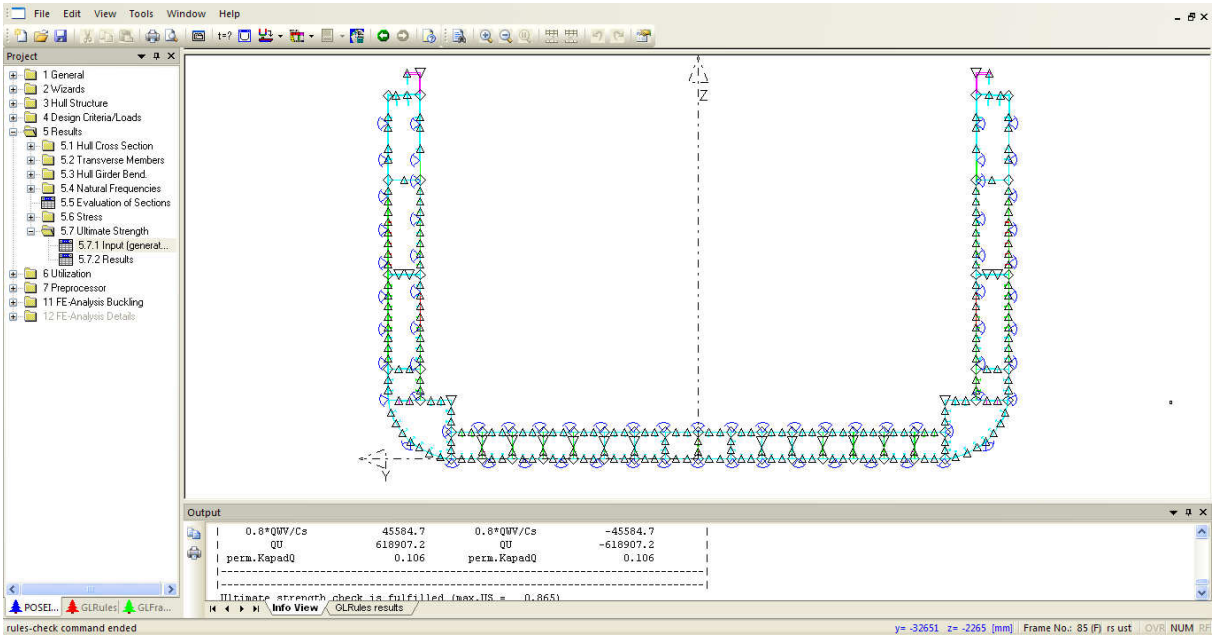

Figure 123 Container ship sectional view for computation of results in Poseidon software

The graph of the progressive collapse analysis in the Poseidon software is shown below.

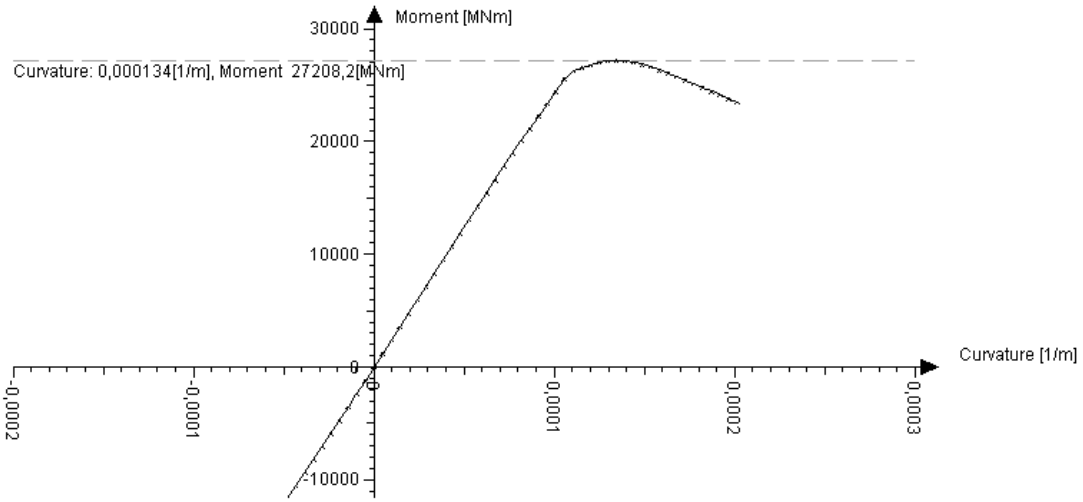

Figure 124 Progressive collapse curve in Poseidon software

The value of the ultimate moment reached in the hogging condition is 27210 MNm.

Movement of neutral axis

The increase of the acting moment and stresses in construction was followed by the movement of the neutral axis. The shift of the neutral axis is showed in the graph below.

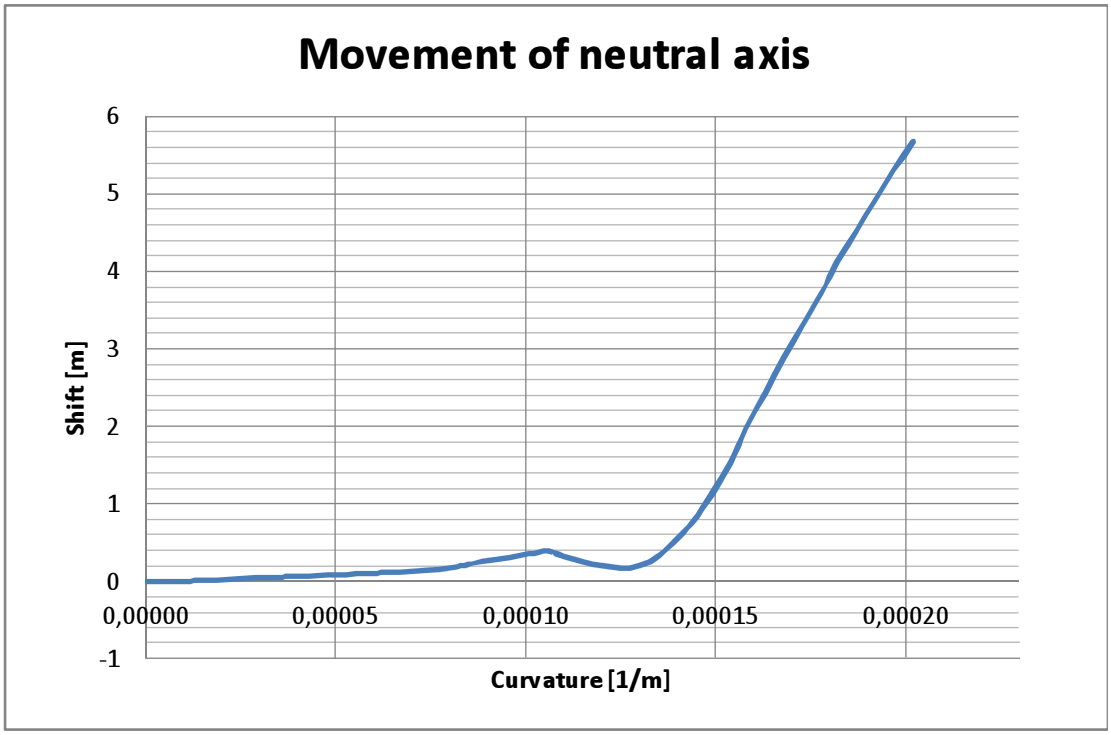

Figure 125 Movement of the neutral axis from the Poseidon model

6.3 Comparison of results with imperfections and Poseidon

The comparison of the progressive collapse curves obtained for the container ship FE model and in the Poseidon software is shown below.

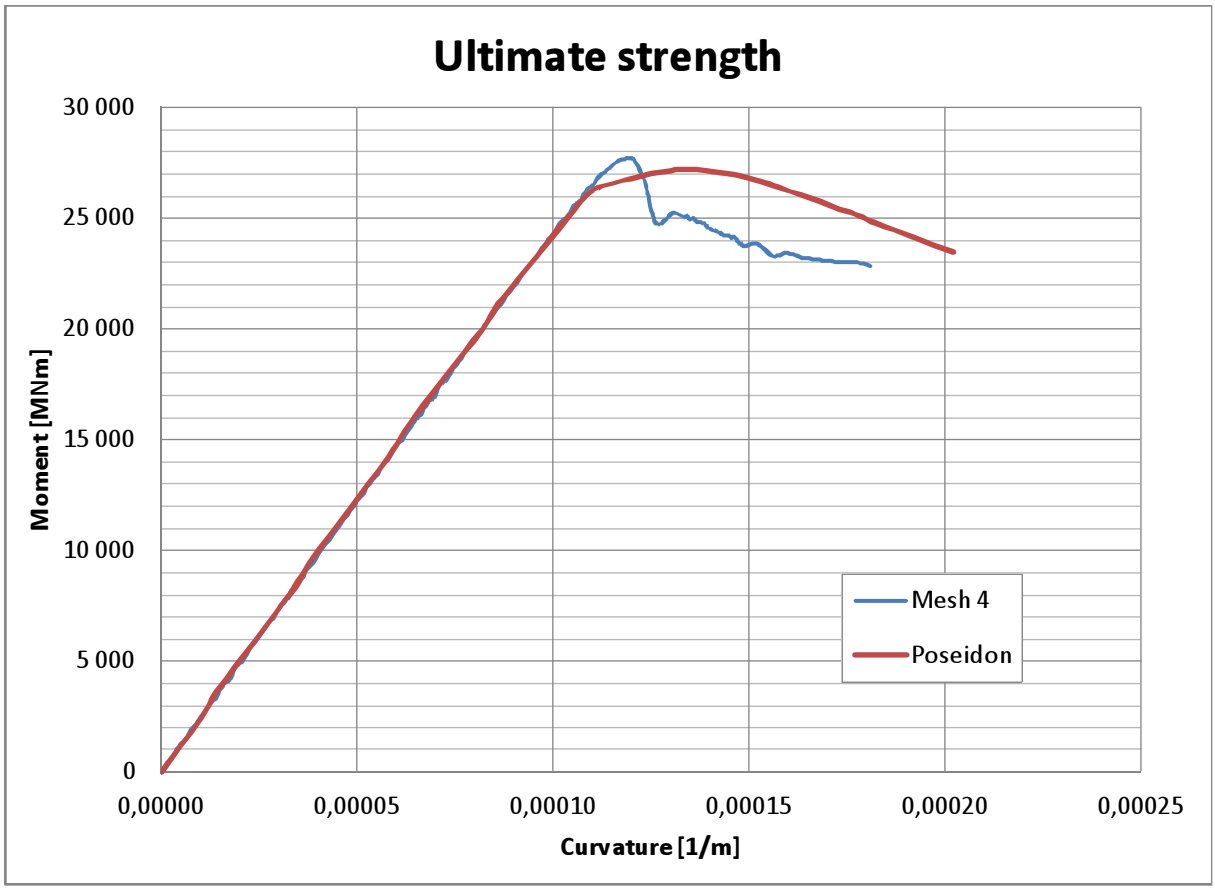

Figure 126 Comparison of the progressive collapse curves from the direct FE analysis and Poseidon software

The comparison between the values of the ultimate moment is shown below.

Table 12 Comparison of the results for direct FE analysis and from Poseidon software

	Maximum moment [MNm]	Difference [%]
Model (imperfections)	27710	-
Model Poseidon	27210	-1,80

Therefore the results for the pure vertical bending moment acting on the ship are more conservative for the Smith's method used in the Poseidon software.

7. CONCLUSIONS

The progressive collapse analysis for both bulk carrier and container ship was performed. The software is more and more user friendly and computers are more powerful than before. However, it still requires time to prepare a finite element model and to run nonlinear analysis of such complexity as global ultimate strength of a ship.

Additional care should be taken when modelling details of the geometry and especially with the mesh generation which can affect final results or have impact on the stability of the calculations.

For the pure vertical bending moment acting on the ship the comparison between the direct FE analysis and method given by the rules was done. The obtained results show hull bending capacity calculated be the FE method higher than obtained in the Poseidon software. Calculations proved that both bulk carrier and container ship have sufficient safety level in terms of ultimate strength.

The influence of included imperfections shows reduction of the calculated hull bending capacity by around 3%. However this value may be changing for different pattern or assumed amplitude of the imperfections.

The structural design of the hulls are according with the Common Structure Rules. Therefore it was shown that the actual hull bending capacity assessed with the nonlinear finite element analysis proves to have bigger ultimate strength capacity which ensures its safety.

For the local loads included due to the alternate loading condition the analyzed hull collapsed only for the highest considered wave height which has very small probability of occurrence. It needs to be noticed that the loads applied on construction have already included the safety margin of $\gamma = 1,2$. However local loads and especially bottom bending can significantly reduce the global bending capacity.

It can be stated that the Smith's method implemented in the rules gives sufficiently accurate results. Even though it is relatively old it can be successfully used to predict hull bending moment capacity for the pure vertical bending moment acting on the hull.

Although obtained results are proving the accuracy of existing methods, final estimation of hull bending capacity is still dependant on many assumptions. For better prediction of real ultimate moment capacity more detailed modeling and meshing can be used, requiring more calculation capacity and time necessary for analysis. Finally better insight in the influence of imperfections in the further analysis of the subject could be desired.

LIST OF FIGURES

LIST OF TABLES

REFERENCES

Journal article	J.K.Paik, A.Mansour, 1995 "A simple formulation for predicting the ultimate strength of ships" *Journal of Marine Science and Technology*, 52-62.
	M.K.Rahmann, M.Chowdhury, 1996 "Estimation of Ultimate Longitudinal Bending Moment of Ships and Hull Girders" *Journal of Ship Research*, 40(3), 244-257.
Book	Owen F.Hughes "*Ship structural design*" New Jersey: SNAME
	J.K.Paik, A.K.Thayamballi, 2002 "*Ultimate Limit State Design of Steel Plated Structures*" John Wiley & Sons.
	Y.Okumoto, 2008 "*Design of Ship Hull Structures*" Springer.
	Y.Bai, 2003 "*Marine Structural Design*" Elsevier.
	A.Mansour, D.Liu, 2008 "*Strength of Ships and Ocean Structures*" New Jersey: SNAME
Chapter	Philippe Rigo, Enrico Rizzuto, 2002 Analysis and Design of Ship Structure. In:"*Ship Design and Construction"* SNAME, 18.1 – 18.77
	Schellin et al. 2010. Load Generation For Finite Element Analysis. In: Paik et al. "*Ship structural analysis and design*" 4.61–4.71
Classification society rules	Rules of Germanischer Lloyd 2012 Sea going ships – Hull Structures
	Common Structural Rules for Bulk Carriers